Serviceability of a Cantilever Grandstand under Dynamic Crowd Loading

J.J. Knibbe

MSc Thesis

Civil Engineering

Track Structural Engineering

Serviceability of a Cantilever Grandstand under Dynamic Crowd Loading

by

J.J. Knibbe

to obtain the degree of Master of Science
at the Delft University of Technology,
to be defended publicly on December 19, 2023

Student number:	4824520	
Project duration:	February 13, 2023 – December 19, 2023	
Thesis committee:	dr. E. Lourens,	TU Delft, chair
	dr. F.P. van der Meer,	TU Delft
	prof. R.D.J.M. Steenbergen,	TNO, supervisor
	ir. R. de Vries,	TNO

TU Delft

Cover image: ”*We shall make them tremble!*,” A banner shown by Feyenoord supporters before a match, referencing both a popular song about the club as well as the earthquakes in the region of the opponent, FC Groningen. From (FSV de Feijenoorder, 2018).

Preface

When I started considering topics for my Master Thesis, I know from the beginning that I wanted to research my ‘own’ topic, and not an ‘off-the-shelf’ assignment. Not that there is anything wrong with those, in fact, they are probably more relevant to the research group or company providing them than topics proposed by students themselves. But call it creative, ambitious, or maybe slightly naive, once I had the idea of researching the vibrations in the Feyenoord Stadium I could not let go of it.

Coming to TNO, specifically in Risk and Reliability group, added some focus to the topic: I was going to look at the effects of the vibrations on the reliability of the stadium. This way, I could also combine three domains I am especially interested in: modelling, dynamics, and uncertainty. It also gave me the opportunity to step outside the bubble of the university, get to know new people, and to start considering the steps to take after graduation.

While being able to research my own topic was a great motivator during the whole process, I think most of the problems that I encountered could be traced back to this as well. At times, it was difficult to find the right direction for the project. Not just at the beginning, when everything is supposed to be more open, but also during the later stages, even when I was already collecting results. I think I was also a bit headstrong at times, wanting to figure things out myself too much, and not always keeping my committee in the know. That said, writing a thesis is not something you should coast through, it should be something that you can look back on and know that you created something unique that you put your blood, sweat and tears into. I believe I managed to do just that, so while it wasn’t always easy, it was definitely worth it.

I would like to thank my committee for their help and advice. Frans and Eliz-Mari on the TU-side and Raphaël and Rein on the TNO-side were certainly vital to make this combination of FEM and R&R a success. I would also like to thank my parents, my friends and my TNO-colleagues for their support and ‘being there’.

Finally, I would like to dedicate this work to one of my cats, Aslan, who sadly passed away on October 2nd, 2023.

J.J. Knibbe
Delft, December 19, 2023

Abstract

This thesis presents a novel methodology to determine the reliability of cantilever grandstands under dynamic crowd loading. No method currently exists to evaluate this, despite the occurrence of significant vibrations in such structures, for example in the Feyenoord Stadium in Rotterdam. These vibrations can negatively affect both the safety and serviceability of such structures, so a method able to evaluate both is desirable.

The methodology consists of four components: a model of a grandstand, a model of the dynamic crowd load, a failure criterion, and a reliability analysis. Of these, the first and third component are case-specific, as a wide range of different grandstands and different criteria could be considered. In this thesis, the methodology is applied on a case study based on the Feyenoord Stadium, with a model of the trusses beneath the main grandstand of this stadium, and a criterion based on the intensity of the vibrations of the upper cantilever of this grandstand, a serviceability issue.

The second component represents the most novel aspect of the methodology: a model describing the dynamic crowd load, defined in the frequency domain, and generally applicable regardless of the structure being considered. The core of this model is a parameterisation of the amplitude spectrum of the load applied by a group of jumping spectators. The parameters describing the spectrum are considered as stochastic variables, with distributions fitted using samples from a state-of-the-art database of measured loads. As opposed to the first and third components, this load model should be generally applicable.

The parameters of the load model, together with other stochastic variables in the grandstand model, form the input of a Limit State Function. The output of this function determines whether the structure loaded by the crowd meets a certain criterion, and forms the basis of a reliability analysis together with the distribution of the stochastic variables. The probability of *not* meeting the criterion, the failure probability, is calculated through a number of reliability methods in the final component of the methodology. These methods should be generally applicable as well, though which methods fits the best could still depend on the case being considered.

This methodology was successfully applied on the case study, and a failure probability was found with two different methods. One of these, Crude Monte Carlo, allowed for a more fluid view of the concept of 'failure' when a serviceability criterion based on a subjective limit is considered. The other method, SDARS, returned a slightly larger failure probability, in a much shorter runtime than Monte Carlo. This method is therefore more fit for safety criteria with a small (expected) failure probability, for which Monte Carlo would require an unreasonably long runtime.

In addition, the wider applicability of the methodology has been investigated. An important requirement for this is flexibility with regards to the applied reliability methods. Two other methods, Directional Sampling and SDARS, were also attempted but did not yield usable results. This is caused by the manner in which phase angles are defined in the frequency-domain model. Random values are drawn, which causes noise to appear in the limit state function: a constant input does not lead to a constant output. Being able to use different reliability methods is an important requirement for applying the methodology in a wider variety of cases. In order to apply these methods, the phase angles need to be defined in a manner which does not introduce noise.

Another important requirement is the ability to consider different failure criteria. While the criterion applied in the case study could be evaluated in the frequency domain, many others will require the results to be transformed to the time domain. Applying this transformation to the frequency-domain results of the models currently does not yield usable results, which is likely also caused by the definition of the phase angles in the load.

In conclusion, while the methodology is applicable on the case study, the definition of the phase angles requires attention before it can be applied on other cases.

Contents

List of Figures

List of Tables

Nomenclature

Abbreviations

Table 1: Abbreviations used in this thesis

Abbreviation	Definition
ADI	Axis Directional Integration
CDF	Cumulative Density Function
CoV	Coefficient of Variation
CMC	Crude Monte Carlo
DARS	Directional Adaptive Response surface Sampling
DS	Directional Sampling
FE	Finite Element
FFT	Fast Fourier Transform
FORM	First-Order Reliability Method
HSI	Human-Structure Interaction
IFFT	Inverse Fast Fourier Transform
LSF	Limit State Function
MAC	Modal Assurance Criterion
NLSS	Nonlinear Least-squares
PDF	Probability Density Function
RMS	Root Mean Square
RS	Response Surface
SV	Stochastic Variable
VDV	Vibration Dose Value

Symbols

Table 2: Symbols used in this thesis

Symbol	Definition	Unit
a, b_i, c_i	Fitted parameters of a quadratic response Surface	Varying
a_0, a_1	Rayleigh damping parameters	Varying
$a_{rms}(t)$	Root Mean Square accelerations	$\mathrm{m/s^2}$
$a_{rms,\infty}(t)$	Infinite-T_s Root Mean Square accelerations, calculated in frequency domain	$\mathrm{m/s^2}$
$a_w(t)$	Frequency-weighted acceleration record	$\mathrm{m/s^2}$
$\tilde{\boldsymbol{a}}(f)$	Acceleration response	Vector of $\mathrm{m/s^2}$ (Complex-valued)
f	Frequency	Hz
f	Distance of sample points along axis in DARS	–
f_b	Base jumping frequency in the Ellis-Littler, Sim and Weijs load models	Hz
f_{target}	Target jumping frequency in the frequency-domain load model	Hz
$f_{\boldsymbol{X}}(\boldsymbol{x})$	Joint distribution of the SV's in $\boldsymbol{X}$	–
$f_{\boldsymbol{U}}(\boldsymbol{u})$	Joint distribution of the transformed SV's in $\boldsymbol{U}$	–
$\tilde{\boldsymbol{f}}_{crowd}(f)$	Dynamic crowd load defined in the frequency domain	Vector of N (Complex-valued)

Table 2: Symbols used in this thesis

Symbol	Definition	Unit
$\boldsymbol{f}_{st}$	Static load	Vector of N
g	Gravitational acceleration	$\mathrm{m/s^2}$
$g(\boldsymbol{X})$	Output of a LSF	Varying
k_p	Peak jump factor in the Sim load model	–
m	Mass	kg
r_n	Amplitude of the $\mathrm{n^{th}}$ harmonic in the load of a single spectator in the Ellis-Littler load model	–
$r_{n,p}$	Amplitude of the $\mathrm{n^{th}}$ in the load of a group of p spectators in the Ellis-Littler model	–
t_p	Load impulse duration in the Sim load model	s
$w_{left,k}$	Left width of peak k in the frequency-domain load model	Hz
$w_{right,k}$	Right width of peak k in the frequency-domain load model	Hz
$\ddot{x}(t)$	Measured acceleration of a jumping person	$\mathrm{m/s^s}$
A	Modal acceleration resulting from the Ellis-Littler non-rhytmic load model	$\mathrm{m/s^2}$
$\tilde{A}(f)$	Acceleration spectrum	$\mathrm{m/s^2}$ (Complex)
$\boldsymbol{C}$	Damping matrix	Matrix of varying
D	Modal displacement resulting from the Ellis-Littler non-rhytmic load model	$\mathrm{m/s^2}$
E_c	Young's Modulus of concrete	$\mathrm{N/mm^2}$
E_s	Young's Modulus of steel	$\mathrm{N/mm^2}$
$f_R(r)$	PDF of resistance value in an LSF	-
$F_S(s)$	CDF of sollicitation value in an LSF	-
$F(t)$	Dynamic crowd load in the time domain	N
$\tilde{F}(t)$	Jump factor in the time domain	–
$\tilde{F}_{sts}$	Component of the peak jump factor varying from person to person in the Weijs load model	–
$\tilde{F}_{ws}$	Component of the peak jump factor varying from jump to jump in the Weijs load model	–
F_{mean}	Mean load in the frequency-domain load model	N
G_s	Static weight of a single spectator	N
$G(x,y)$	Static weight of a group of spectators	$\mathrm{N/m^2}$
H_k	Height of a peak in the frequency-domain load model	N
K	Number of peaks in frequency-domain load model	–
$\boldsymbol{K}$	Stiffness matrix	Matrix of varying
$\boldsymbol{M}$	Mass matrix	Matrix of varying
P_f	Failure Probability	–
$P_k(f)$	Load peak k in the frequency-domain load model	N
R	Resistance in an LSF	Varying
S	Solicitation in an LSF	Varying
T_b	Base jumping period in the Ellis-Littler, Sim and Weijs load models	s
T	Length of time signal	s
T_{event}	Event duration time for the VDV	s
T_s	Sample time for the RMS accelerations	s
$\boldsymbol{U}$	Input vector of SV's for a LSF, transformed to standard-normal space	Vector of varying
VDV	Vibration Dose Value	$\frac{\mathrm{m}}{\mathrm{s}^{7/4}}$
$V(P_f)$	CoV of the failure probability	–
$W(f)$	Frequency weighting factor	–

Table 2: Symbols used in this thesis

Symbol	Definition	Unit
$\boldsymbol{X}$	Input vector of SV's for a general LSF	Vector of varying
$\boldsymbol{X}_{model}$	Input vector of SV's used for the FE model used in the LSF of this thesis	Vector of varying
$\boldsymbol{X}_{resistance}$	Input vector of SV's used for resistance variables not used in the LSF of this thesis	Vector of varying
Z	Output of a LSF	Varying
α	Contact Ratio of dynamic crowd loads in the Sim and Weijs load models	–
α_i	Sensitivity Factors in a FORM analysis	–
β	Reliability index	–
ϵ_{phase}	Random noise in the LSF due to phase differences in the load	$\mathrm{m/s^2}$
$\boldsymbol{\theta}$	Direction in polar coordinates in U-space	Vector of –
λ	Distance from the origin in polar coordinates in U-space	–
λ_0	Distance from the origin to the limit state U-space	–
λ_i	Sample distance from the origin to the limit state U-space, used in DS	–
λ_{LSF}	Sample distance from the origin to the limit state U-space, found using the LSF, used in DARS	–
λ_{RS}	Sample distance from the origin to the limit state U-space, found using the RS, used in DARS	–
$\Delta\lambda_{add}$	Threshold for using the LSF or the RS in DARS	–
λ_{min}	Smallest value of λ found in DARS	–
μ	Mean of an SV	Varying
σ	Standard deviation of an SV	Varying
ϕ	Phase of one jump in the Weijs load model	rad
ϕ_n	Phase of the $\mathrm{n^{th}}$ in the dynamic load of a single spectator in the Ellis-Littler load model	rad
Φ	CDF of the standard normal distribution	Vector of –
$\boldsymbol{\phi}$	Mode shape	Vector of –
$\chi^2_N(.)$	Chi-squared distribution with N degrees of freedom	–
ω	angular frequency	$\mathrm{rad/s}$

1

Introduction

The Feyenoord Stadium in Rotterdam, known better locally as *De Kuip*, was the first football stadium of its kind in Europe when it opened in 1937. Its distinct oval shape, with 'levitating' concrete seating decks supported by slender trusses, ensures a good view of the pitch from all seats, and an intense and intimate atmosphere (Vereniging van Aandeelhouders Stadion Feijenoord, 2022). The spectator capacity has varied over the years, from over 60,000 in the 1950's to 47,500 after a renovation in 1994, which is still the current number. Throughout the last decades, multiple plans have been developed to either demolish the stadium and construct a new one at the same or a nearby location, or to renovate it again while adding a significant number of seats. As recently as 2022, a plan involving a new stadium on the banks of the Nieuwe Maas river was cancelled, and Feyenoord director Dennis te Kloese has indicated that the club intends to play their matches in De Kuip for at least ten more years (Vinke, 2022).

Figure 1.1: A sold-out crowd in the Feyenoord Stadium, from (Feyenoord, 2017a)

Among football fans, the Feyenoord Stadium is known for its atmosphere, with the frontmost spectators located close to the field and those behind them forming a continuous wall of people cheering on the players, their sound reflected from the bottom of the upper tier. The stadium also has been used to host music concerts, many of which are fondly remembered by visitors for their ambience and the acoustics of the venue (RTV Rijnmond, 2023).

One of the most notorious aspects of the stadium and its atmosphere is the vibration of especially the upper cantilever due to jumping crowds. The natural frequency of the stadium is a realistic rhythm for humans to jump to, and also a conventional tempo of pop songs. This means resonance is likely to occur, amplifying these vibrations. During concerts, the displacement at the tip of the upper cantilever is measured by TNO, and protocols exist to lower the sound level or shut off video feeds when certain thresholds are crossed (NEMO Kennislink, 2008). This is not done during football matches, even though the stadium hosts these much more often than concerts, and noticeable vibrations do occur as well (NOS, 2017). While some consider this phenomenon to be part of the 'culture' of visiting football matches and concerts, others may find them uncomfortable, negatively affecting their enjoyment of the event they are visiting, and its venue in particular.

1.1. Problem Description and Research Question

After the collapse of a grandstand element at De Goffert, a stadium in Nijmegen (Rutten et al., 2022), the reliability of football stadiums has come under more scrutiny in the Netherlands, with one club even reducing the capacity of a specific section (NOS, 2023). At the Feyenoord Stadium, the vibrations could influence the safety of the structure in the long term, through fatigue in the steel trusses or cracks in the concrete seating decks. Research from TNO suggests that there are currently no significant concerns about the structural integrity of the stadium, however. On the other hand, as mentioned, the comfort of the spectators present in the stadium could be affected by the vibrations, bringing the serviceability of the stadium into question. Being comfortable or not at a certain level of vibrations is subjective, and the targeted reliability indices for serviceability requirements are generally lower than for safety requirements (Jonkman et al., 2017), so at first glance safety seems like a greater concern. However, the vibrations can still play a large role in how the stadium is viewed by the public, which can in turn effect the discourse surrounding its future, a difficult subject not only for Feyenoord itself, but also within local politics (RTV Rijnmond, 2022). Because of this, serviceability appears to be the bigger concern for the Feyenoord stadium than safety at this moment.

Norms regarding the safety and serviceability of grandstands (The Institution of Structural Engineers, 2008) do exist, with the latter often being the main focus, but they do not give enough guidance to perform a reliability analysis. Usually, they contain some recommendations for limits on measured vibrations, but little in the way of predicting them. Instead, they recommend intervening when the vibration limits are exceeded during an event, as is done at the Feyenoord Stadium, but this is complicated to organise and not applicable for all types of events (for example, a football match cannot be 'turned down' like the volume at a concert). So, there is a need to determine the reliability of grandstands *a priori*, taking account of the uncertainty in both the structure and the load.

This can be achieved by combining a model of a grandstand with a model of dynamic crowd loads, with quantified uncertainty in both. The response of this modelling 'train' is then also uncertain, and can thus be used to perform a reliability analysis. While (finite element) models of stadiums have been made, their use is limited to determining their dynamic properties (Santos et al., 2018), and not the response to the load of a jumping crowd. And while models of such loads also exist, the uncertainty in them has not been quantified in a way that can be applied in a reliability analysis. This thesis therefore aims to construct this train, and so to form a methodology for determining the reliability of a cantilever grandstand under dynamic crowd loading. The application will be limited to serviceability for now, with the Feyenoord Stadium used as a case study, but the method should be applicable to safety problems and other structures as well. This leads to the following primary research question:

How can the serviceability of a cantilever grandstand under dynamic crowd loading be determined?

To answer this question, the following steps are followed, forming the core components of the methodology:

1. Construct a model of the cantilever grandstands
2. Create a model of crowd loads and apply it to the grandstand model
3. Determine a failure criterion based on the response of the grandstand
4. Calculate the failure probability of this criterion

The first and third steps are specific to the case study, which is introduced in the next section. In general, different stadiums or failure criteria could be considered in different cases, which require their own models and different response values to be considered. The second and fourth step should be generally applicable, also for other grandstands loaded by jumping crowds and for other failure criteria, including those based on safety. While the problem considered in the case study only concerns serviceability, as does the main research question (and title) of this thesis, it is emphasised that the methodology should be widely applicable in the future. Whether this is feasible is therefore also investigated at the end of this thesis.

1.2. Case Study: The Feyenoord Stadium

As mentioned, the Feyenoord Stadium in Rotterdam is used as a case study for this thesis. Figure 1.2 shows the inside of the stadium without spectators The main structure consists of the two tiers of concrete seating decks forming an oval, bowl-like shape around the field. These decks are supported by steel trusses placed on concrete foundation blocks. Both tiers have a significant cantilever at the side facing the field, with the front rows of seats placed upon them. The cantilever of the upper tier (also referred to as the 'second ring') is the largest of the two, and overlaps the back rows of the lower tier ('first ring'). The concrete decks are curved to form the oval; this curvature is most pronounced near the corners of the field, and nearly zero around the middle of the long sides of the field. An additional layer of shallow, demountable grandstands is situated in the space between the field and the grandstands formed by the curvature. These seats was added in the 1994 renovation, during which the cantilever roof covering the two rings was also constructed, and one side of the lower tier was opened to add business amenities.

Figure 1.2: The two oval tiers of the grandstand in the Feyenoord Stadium, the lower demountable section and the roof of the stadium, from (Feyenoord, 2017b)

The lower seats, cantilever grandstands and cantilever roof are three separate structures. As the serviceability concerns stem from the vibrations of the upper cantilever of the grandstand, this thesis will focus on that part of the stadium, specifically the trusses supporting the concrete deck. A diagram of these trusses is given in Figure 1.3, with the location where the most significant vibrations are expected to occur indicated: the front tip of the upper cantilever. This is also where TNO measures the displacements during concerts.

The shape of the truss could be described as two ‘arms’ connected to a ‘spine.’ The lower arm covers two spans and one cantilever: the back span is supported by a typical N-shaped pattern, and the front span and cantilever by a beam with a varying profile, increasing in height towards the frontmost support column. The cantilever of the lower arm has a length of approximately 6.9 meters, and overhangs an area containing spectator facilities.

The back part of the upper seating deck runs over the top of the spine, and the front part is supported by the upper arm, with a cantilever of 9.7 meters, and overhangs a number of rows on the lower tier. The pattern of the members in this arm is similar to a Fink truss (Dominik, 2023). The spine connecting to both arms has an N-shaped (or Z-shaped) structure in its lower half, which ends abruptly at the height of the bottom chord of the upper arm. This creates some open space for balconies containing public amenities for the spectators on the upper deck, which are located slightly above this height.

Appendix A contains a more detailed exploration of the stadium, including the trusses, and a number of pictures taken by the author.

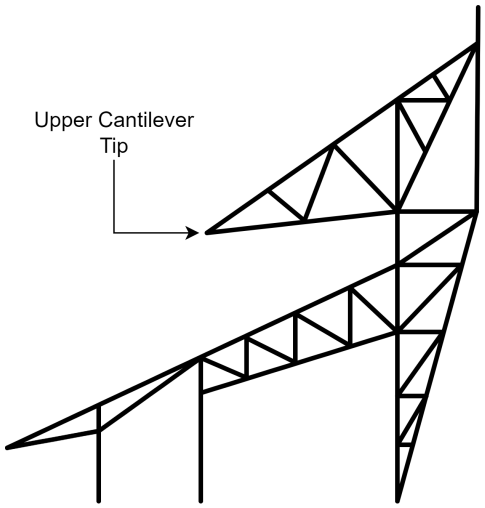

Figure 1.3: Diagram of a truss in the stadium, with the critical location for vibrations indicated

1.3. Report Structure

This thesis consists of six chapters and two appendices. After this introduction, Chapter 2 contains a literature study, forming a theoretical background to the methodology, which is described in Chapter 3. This chapter covers the entire ‘train’, from the crowd and stadium models to the failure criterion and reliability analyses. Chapter 4 then contains the results of this methodology, applied on the case study, and an interpretation of these result with respect to the Feyenoord stadium and the chosen failure criterion specifically. Then, in Chapter 5, the potential wider use of the methodology is discussed, determining which issues could arise and what could be adjusted to avoid these. This is done by critically examining two steps within the ‘train’ which did not influence the case study, but will be important when applying it on other cases. The level of conservatism in the methodology is also discussed in this chapter. Finally, chapter 6 ends the main body of the thesis by drawing conclusions based on the results and discussion, and providing recommendations.

The two appendices contain the background of the two models described in the methodology. As mentioned, appendix A contains an ‘exploration’ of the Feyenoord Stadium by the author, both through publicly available sources and the pictures taken by the author himself. Appendix B describes the process of constructing a dynamic crowd load model in frequency domain, which is quite novel, so worth adding to this report.

2

Literature Study

This Literature Study provides a theoretical background to the methodology for assessing the reliability of a cantilever grandstand under dynamic crowd loading. The consulted literature includes papers, norms and academic literature such as lecture notes.

The structure of this chapter follows the four components outlined in the introduction, albeit in a slightly different order. The first section presents existing crowd load models which have been developed over the last few decades. Next, Finite Element models of grandstands found in literature are examined, which focus on the dynamic behaviour of such structures through their modes and natural frequencies. The topic of Human-Structure Interaction is also briefly mentioned. Then, the reliability of grandstand structures is covered, focusing on serviceability criteria, followed by different methods to quantify this reliability. The Literature Study is concluded with a synthesis, where the knowledge gathered in the literature study is used to specify the approach to the aforementioned steps in the methodology. This section serves as a bridge towards the next chapter, where the methodology itself is presented.

2.1. Dynamic Crowd Loads

Within the scope of this thesis, 'Dynamic Crowd Loading' is the load generated by crowds jumping, dancing or bobbing (bouncing without leaving the ground) on a grandstand structure, with jumping assumed to be the activity causing the most critical loads. A distinction can be made between Rhythmic and Non-Rhythmic Loading, as done by (Ellis and Littler, 2004b). The former is typically encountered at pop concerts, with the crowd moving along to the music in a synchronised manner. The latter is associated with crowds at sporting events reacting to the event in a chaotic and uncoordinated manner. This distinction is not absolute, and a crowd load can change from one type to another in a short time span. For example, some football clubs play a 'goaltune' after a goal is scored, resulting in the initial Non-Rhythmic cheers from the crows transforming into Rhythmic movement to the beat of the music. Nevertheless, both types will be treated separately in this section.

2.1.1. Rhytmic Loading

In the frequency domain, these loads can be characterized as having clear peaks at the jumping frequency and its integer multiples, as if it were a Fourier series. There is some spread around these peaks due to not all spectators jumping at exactly the same frequency. An example of acceleration measurements in a stadium due to rhythmic loading is given in Figure 2.1. This crowd is jumping at (approximately) 2.2 Hz, but peaks are visible at 4.4 Hz and 6.6 Hz too. Of course, the jumping frequency itself is often 'imposed' on the crowd through music or other stimuli, and the height of the peaks will depend on the composition and behaviour of the crowd itself, and the dynamic properties of the structure. The master thesis of (Weijs, 2023) proposes a probabilistic model for rhythmic loads. The following paragraph is an abridged version of this work, leading to a description of its load model.

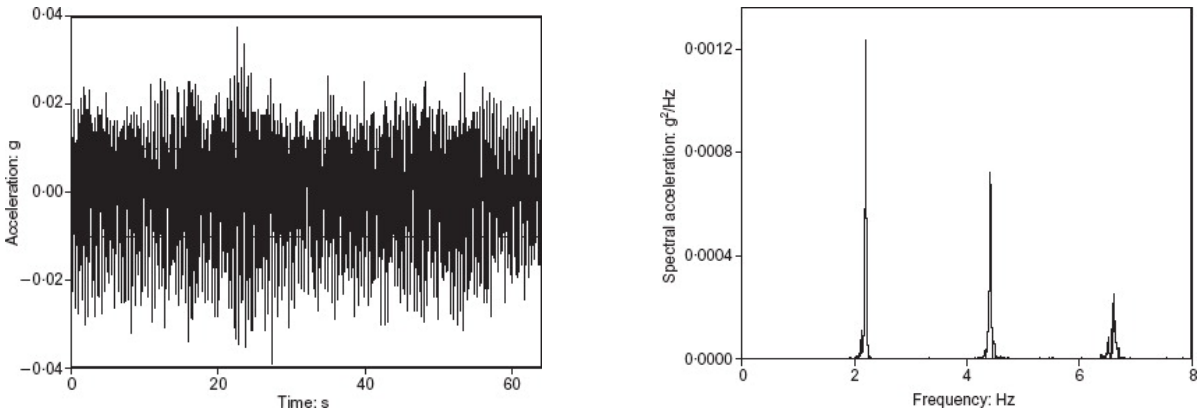

(a) Time Domain (b) Frequency Domain

Figure 2.1: Typical plots of the acceleration response of a grandstand to Rhythmic Crowd Loading, from (Ellis and Littler, 2004b)

Based on earlier work by (Bachmann et al., 1995), Ellis and Littler proposed the following simple model for Rhythmic Crowd Loading coming from a single person, as a point load (Ellis and Littler, 2004b):

$$F(t) = G_s\left(1.0 + \sum_{n=1}^{\infty} r_n \sin(2\pi n f_b t + \phi_n)\right) \tag{2.1}$$

Where G_s is the weight of the person and f_b is the base jumping frequency of the load, which can vary from 1.0 to 2.8 Hz for jumping according to (Ginty et al., 2001). The amplitude r_n and ϕ_n of the n^{th} harmonic could indeed be regarded as forming the Fourier series of the load signal. Usually, the summation of harmonics is truncated to three components.

For a crowd, the own weight is replaced by the density of the crowd $G(x, y)$, varying in space, and the amplitudes vary with the number of persons in the crowd p:

$$F(t) = G(x, y)\left(1.0 + \sum_{n=1}^{\infty} r_{n,p} \sin(2\pi n f_b t + \phi_n)\right) \tag{2.2}$$

These loads are often formulated in terms of a normalised force or jump factor $\tilde{F}(t)$, corresponding to the value between brackets in equations 2.1 and 2.2:

$$\tilde{F}(t) = \frac{F(t)}{G} \tag{2.3}$$

In other words, the jump factor is the amplification of the own weight G of the jumping crowd. Typical peak values of the jump factor vary between 2.3 and 4.7 according to (Weijs, 2023). An example of the jump factor generated in the Ellis load model is given in Figure 2.2.

Other load models were proposed by (Sim et al., 2008), using different shapes to approximate an impulse load generated by a single jumping person. The shape that best fit the measured load was found to be a squared cosine function, applied for one half period, followed by a delay until the next jump:

$$\tilde{F}(t) = k_p \cos^2\left(\frac{\pi t}{t_p}\right) \text{for } t \in [-t_p/2, t_p/2],\ 0 \text{ otherwise} \tag{2.4}$$

Where k_p is the impact factor, or amplitude of the impulse, equal to the maximum of $\tilde{F}(t)$. Outside of the impulse duration t_p, the jump factor is equal to zero. This means the static weight of the crowd is not taken into account by this model, and needs to be considered as a separate load case. This is not the case in the Ellis and Littler model, where the weight of the crowd taken into account by the factor 1.0 in Equations 2.1 and 2.2 (though seemingly not in Figure 2.2). Whether or not the static weight of the crowd is taken into account in the load model needs to be considered in the application of these models.

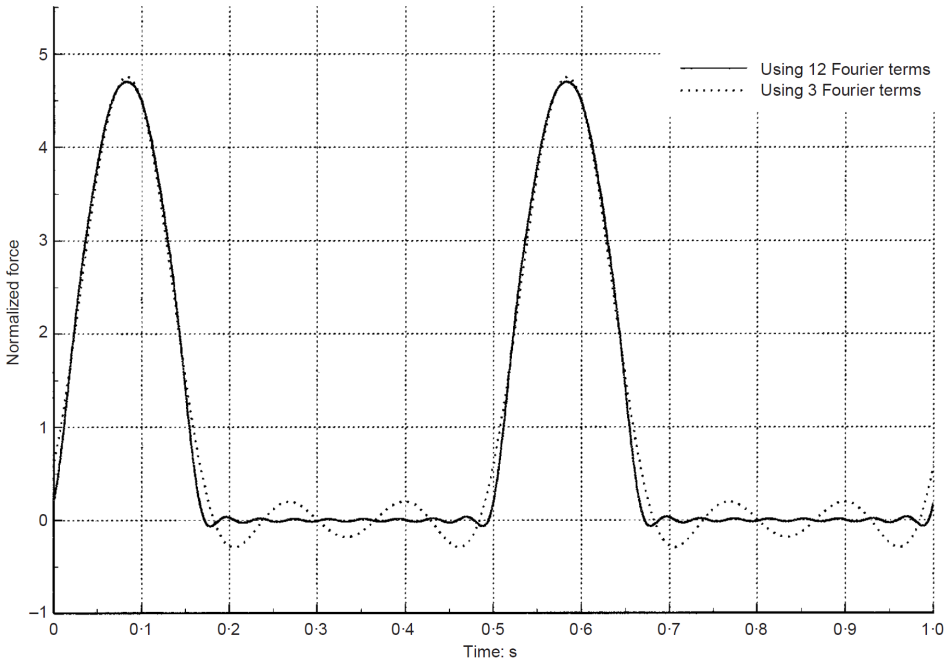

Figure 2.2: The shape of the jump factor from the model proposed by (Ellis and Littler, 2004b)

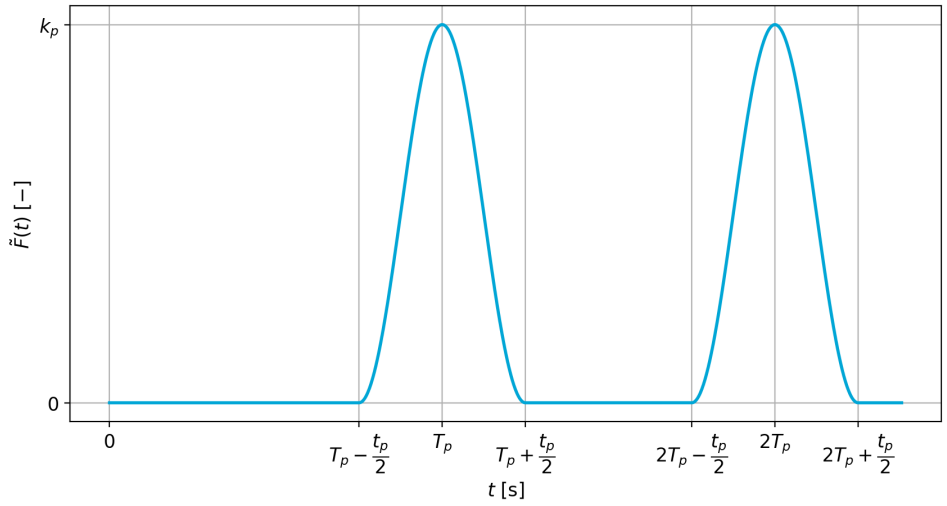

Figure 2.3: The shape of the jump factor from the model proposed by (Sim et al., 2008)

The ratio between the impulse duration t_p in the Sim model and the total period of the jump T_b $(= 1/f_b)$ is defined as the contact ratio α:

$$\alpha = \frac{t_p}{T_b} \tag{2.5}$$

This value, as well as several parameters concerning the phase delay between the music and jumps, are uncertain and were fitted to β-distributions. Figure 2.3 contains an example of two jumps simulated using this model (with constant values for t_p and k_p). Sim's model served as a base for that of (Weijs, 2023), which defines a single jump - without static load - as:

$$\tilde{F}(t) = \left(\tilde{F}_{sts} + \tilde{F}_{ws}\right) \sin^2\left(\frac{\pi t}{\alpha T_b} + \phi\right) \tag{2.6}$$

The impact factor k_p is replaced by two stochastic variables, describing the variation in the peak jump factor from person to person ($\tilde{F}_{sts}$, series-to-series) and from jump to jump ($\tilde{F}_{ws}$, within-series). A phase difference ϕ is also added. Together with α and T_b, a single jump is described by five stochastic variables. A load signal of a single spectator then consists of a series of simulated jumps, each with different realisations of these five variables. Two examples of such a jump are given in Figure 2.4. The distributions of these variables were determined using data from an open-access dataset (Xiong and Chen, 2021), and they contain correlation between the variables for one jump, between the jumps of one spectator, and between spectators in a group. This means the individual load signals of a group of spectators need to be simulated simultaneously, which made generating load signals representing such groups a rather complicated process.

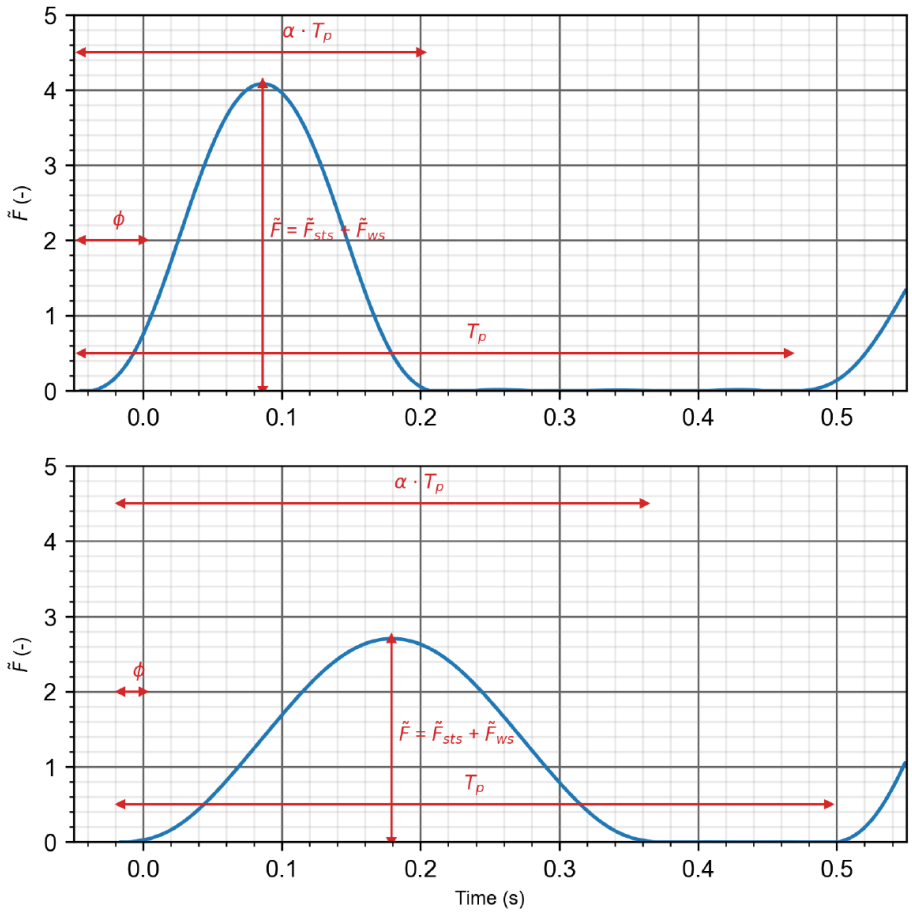

Figure 2.4: Two realizations of a single jump from the load model proposed by (Weijs, 2023)

Weijs included these correlations to take account of coordination between spectators. In literature, a coordination factor ρ is often defined by dividing the largest peak value in the amplitude spectrum of the group load $|F_{crowd}(f)|$ by the sum of the amplitudes of the N individual loads at their jumping frequencies $f_{b,i}$:

$$\rho = \frac{\max\left|F_{crowd}(f)\right|}{\sum_{i=1}^{N}\left|F_i(f_{b,i})\right|} \tag{2.7}$$

Equation 2.7 is formulated here in terms of load F and not jump factor $\tilde{F}$ (as is done in literature), since the latter is scaled by different weights for every spectator and would result in an unintuitive formulation.

The coordination factor can take values between 0 and 1, the latter implying perfect coordination. A study from (Chen et al., 2019) found that this value decreases from nearly 1.0 for small groups to just under 0.8 for more than 20 persons, at a jumping frequency of 1.8 Hz, and 0.6 for higher frequencies. Another paper by (Georgiou et al., 2015) found lower values, between 0.2 and 0.5 depending on the frequency, with the best coordination occurring at 2 Hz. Finally, by comparing results from (Ellis and Ji, 2004) with those from (Ebrahimpour and Sack, 1989), Weijs also found values between 0.32 and 0.67. Clearly, it is difficult to reproduce consistent results for the coordination factor.

Weijs does not use ρ as a reduction factor explicitly in his model. As every jump is simulated separately with correlations between spectators, the crowd 'synchronizes itself' to some degree. By transforming the resulting load signal of a crowd to the frequency domain, Weijs could calculate the coordination factor *a posteriori*. This resulted in a value of ρ between 0.52 and 0.68.

Weijs' approach results in a narrowband spectrum of the group load, with some spread around the peaks at the jumping frequency as would be expected from figure 2.1. Comparing the summed synthetic signal of a group of 93 spectators generated by this model with the sum of the same number of records sampled from the experimental dataset it is based on does reveal some differences (See Figure 2.5, where 'Synthetic data' refers to data generated by the load model). In the time domain, the synthetic signal has a more regular amplitude than the experimentally measured load. This could indicate that some transient effects have not been taken into account, like fatigue of the jumping persons, or a decrease in jumping intensity after 'settling' on a rhythm. In the frequency domain, the synthetic peaks appear too low and too narrow compared to those coming from the dataset, and they are located at slightly less than the 'target' 2 Hz. This indicates Weijs' model underestimates both the intensity at which the crowd is jumping, and the variance in jumping frequency.

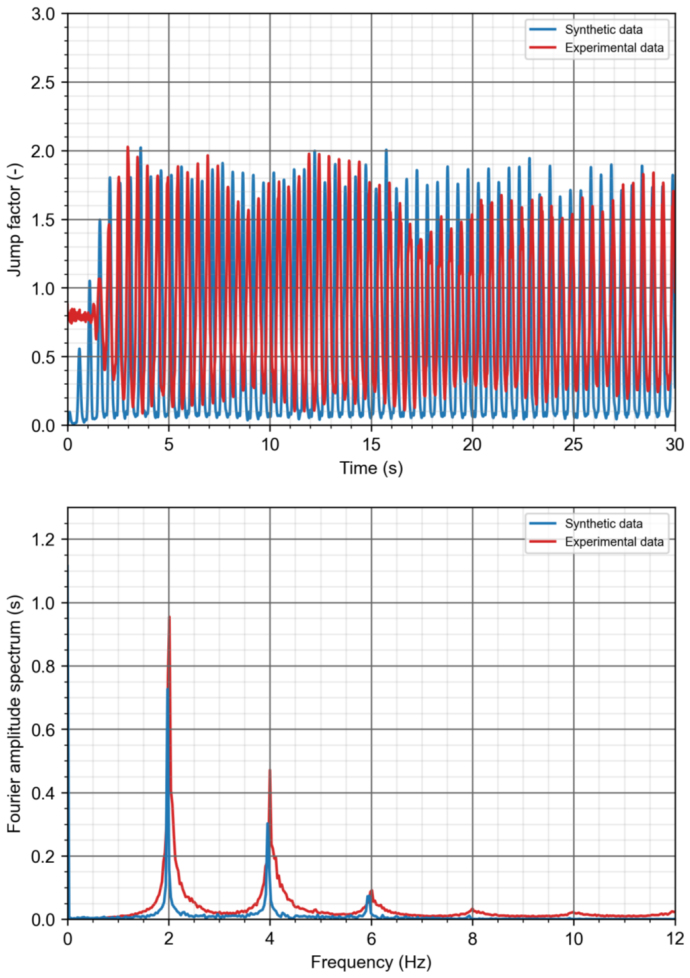

Figure 2.5: Comparison of a load generated by the Weijs load model of and the measurements it was based on. Both loads are sums of 93 seperate signals, from (Weijs, 2023)

Considering the harmonic nature of the load models, the shape of the experimental data from (Xiong and Chen, 2021) in frequency domain, and the difference with the results of Weijs' model, perhaps a new load model could be defined directly in the frequency domain. Such an approach cannot easily capture the transient effects Weijs appears to have missed, but it could result in a more realistic spectrum. In fact, defining new models for human-induced loads was one of the goals of publishing the dataset, so this forms an interesting task for this thesis to fulfill.

2.1.2. Non-Rhythmic Loading

Non-Rhytmic crowd loading occurs when spectators react to a certain event (e.g. a goal being scored), without a rhythm to guide them. Measuring these types of loads experimentally is difficult, because such events cannot be easily replicated in a controlled environment where measurements could be performed. The response to this type of load typically has a much broader spectrum than the response to rhythmic loading, as can be seen in figure 2.6. Clear peaks are still visible in this spectrum, corresponding to natural frequencies of the system. According to (Ellis and Littler, 2004b), Non-Rhythmic loading can be viewed as an impulse-like load occurring incidentally during the event, causing free vibrations in the structure, which explains the peaks at natural frequencies. Literature on this load is much more limited than on rhythmic loading, as it is generally considered less severe (Ellis and Littler, 2004b). Still, a short description of a load model will be given.

Next to their rhythmic loading model, Ellis and Littler also propose a model for non-rhythmic loading, based on their assumption of free vibrations. They assume that the entire static weight of the crowd causes a displacement which can be expressed in the mode shapes of the structure:

$$D = mg\boldsymbol{\phi}/k \tag{2.8}$$

Where m is the mass of the crowd, and k is the modal stiffness associated with the mode with shape $\boldsymbol{\phi}$. When the crowd responds to an event, they assume all spectators jump at once, removing their weight from the structure. This causes an instantaneous acceleration in the same mode shapes:

$$A = mg\omega^2\boldsymbol{\phi}/k \tag{2.9}$$

Where ω is the frequency associated with the mode. This model does not give a value for a load, but rather the peak acceleration response for each mode. One would expect a minus sign in equation 2.9, though for the absolute value this does not matter. The total peak response then depends on which modes are taken into account. The displacement is dominated by the first, low-frequency modes, and the accelerations by the high-frequency ones. When evaluating the serviceability of structure such as grandstands, accelerations play an important role, and their frequency affects their perceptibly. This will be covered in more detail in the section on reliability.

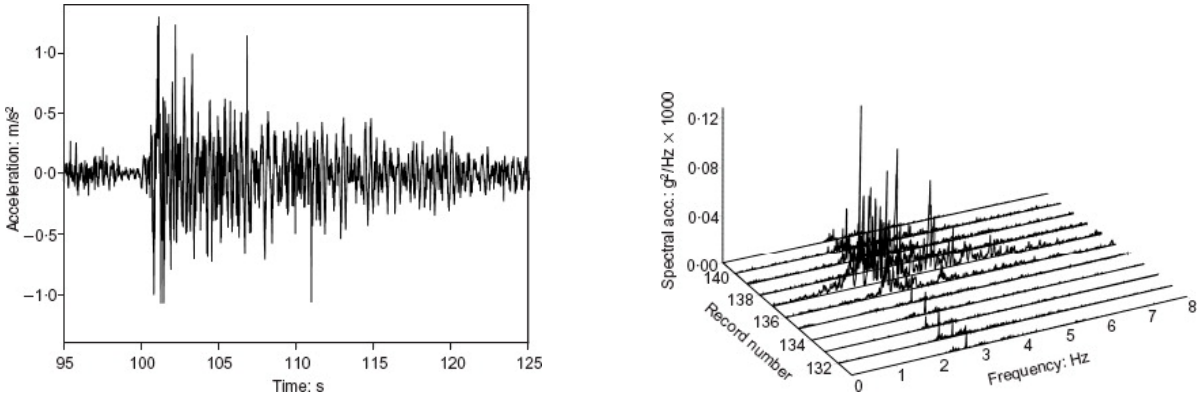

(a) Time Domain (record 137)

(b) Frequency Domain (*waterfall diagram)*

Figure 2.6: Typical plots of the response of a grandstand to Non-Rhythmic Crowd Loading, from (Ellis and Littler, 2004b)

The idealisation of the entire crowd jumping simultaneously assumes a large degree of coordination, which goes against the chaotic nature one would expect from this type of loading. Furthermore, the static displacement of a structure is not generally in the same shape as the modes, though the first mode could be a good approximation depending on the boundary conditions. Perhaps a better model would be similar to those for rhythmic loading, but with a continuous range of base frequencies and shorter contact ratios. Such a model could activate the modes of a structure if the natural frequencies are covered by the frequency range, and general responses (including displacements or stresses) could be considered instead of just accelerations. Further literature on non-rhythmic crowd loading is sparse, however, as these loads are seen as less dangerous than the rhythmic counterparts, while being harder to model (Ellis and Littler, 2004b) and measure. This thesis will therefore focus on rhythmic crowd loads.

2.2. Models of Grandstands

This section focuses on Finite Element (FE) models of grandstand structures, and briefly covers Human-Structure Interaction as well. Multiple papers have been found that use in-situ measurements of a grandstand to update an FE model to better represent the real structure, specifically its dynamic components (natural frequencies and modes calculated through mass, stiffness and damping matrices). Such measurements are not available for this thesis, but these models are interesting nonetheless as they could serve as an inspiration for a model of the Feyenoord Stadium. No literature has been found that uses an FE model in combination with a reliability analysis or a dynamic crowd load model, so this thesis provides something novel in this area.

2.2.1. Models from Literature

Natural frequencies and mode shapes of structures such as grandstands can be determined experimentally using in-situ measurements of the structure (Lourens, 2021). When the load applied on the structure during this experiment is also measured, for example by using a shaker, this is called Experimental Modal Analysis (EMA). When the load is not known, such as when ambient wind load or actual live load is applied, the process is called Operational Modal Analysis (OMA). It stands to reason that measurements for OMA are easier to perform, but some assumptions have to be made about the unknown load. Most critically, in the case of stadiums, is that the load should contain a broad range of frequencies and be able to excite all modes that need to be identified. Ideally, it should be described by a white-noise spectrum (Lourens, 2021) and be applied over the entire structure. Looking at the spectra of the response to crowd load in figures 2.6 and especially 2.1, the first condition is not met. For wind loads, a white noise spectrum might be a more realistic assumption, but the second condition is not met due to most stadiums having a roof over the stands, shielding part of it from wind.

A paper by (Santos et al., 2018) attempted to solve this by using a artificial, non-rhythmic live load generated by a group of volunteers walking around randomly. While this still does not load the entire structure, it does at least at least apply on the most relevant part (the seating deck), and can reasonably be assumed to have a broad spectrum. Perhaps the load generated by spectators finding their seats before an event, or leaving them afterwards, is also a good fit for OMA.

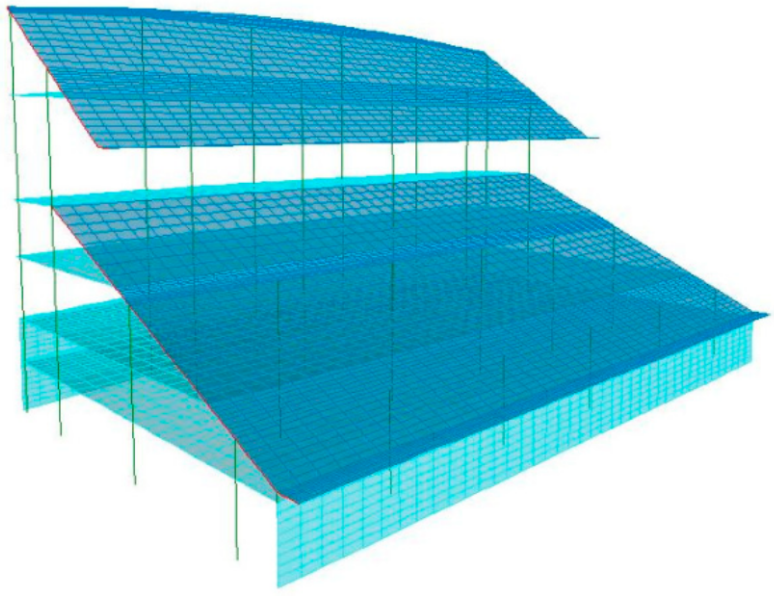

Figure 2.7: Finite Element model of a grandstand, from (Santos et al., 2018)

The FE model created as part of this paper is shown in Figure 2.7. It uses shell elements for the seating deck, and truss elements for the supporting structure, both representing reinforced concrete. The experimentally determined modal characteristics were then used to update this model, such that its calculated modal properties correspond with those found by OMA. During this process, the connections between different structural components were found to have a significant influence on the frequencies and mode shapes. Furthermore, the additional mass of non-structural components, as well as the constraints they can provide, were also an important source of uncertainty in the dynamic behaviour of the structure. This study did not take any nonlinear effects into account, as these would violate the assumptions behind modal analysis. Human-Structure Interaction (HSI), covered briefly at the end of this section, was also not considered in the model explicitly. As the number of volunteers used to generate load is not mentioned, it is also unclear how significant the effects of HSI could have been.

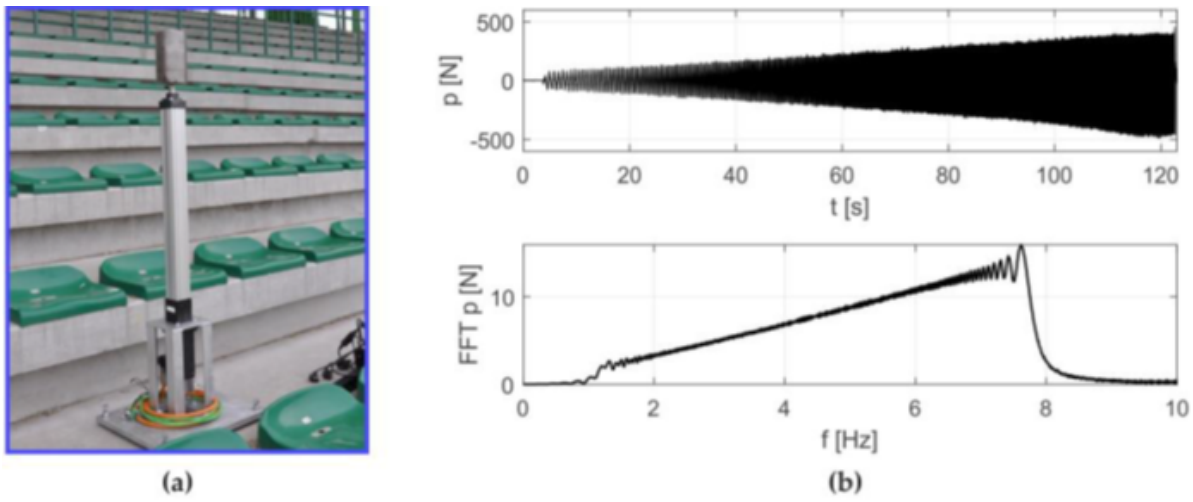

Figure 2.8: Force actuator (left) and its applied force in time and frequency domain (right), from (Grebowski et al., 2019)

A similar study was performed by (Grebowski et al., 2019), this time applying EMA on a grandstand at a racing track. The load was applied by actuators 'sweeping' through different frequencies, see figure 2.8. This structure had several closely-spaced natural frequencies, caused by the repeating shape of the stand. This resulted in a 'beating' phenomenon when the structure is rhythmically loaded. All of these sectors were modelled using only beam elements, including the seating deck. Non-structural elements were modelled as additional masses. The reinforced concrete was modelled as a homogeneous material, and the model updating was limited to reducing the elastic modulus of concrete used for the girders beneath the deck, to take account of cracked concrete and activation of the tensile strength of the reinforcement.

Another study by (Magalhães et al., 2008) focused on the roof of a stadium structure instead of the seating deck. While this is not what this thesis focuses on, the paper does contain some aspects the other two papers lack. First, this study uses two reference points in its measurements to determine two sets of 'experimental' modes. By using a Modal Assurance Criterion (MAC), these sets could be compared and their accuracy determined before using them to update the FE model. Second, it included some nonlinear effects in its FE model without violating the assumptions behind modal analysis. The modes are determined based on the tangent stiffness matrix, which is calculated using the deformed geometry after applying static loads. This way, second-order effects caused by the self-weight are are taken into account. This approach achieved a very good correspondence to the modes determined by OMA, where the dynamic excitation was provided by wind load.

2.2.2. Human-Structure Interaction

A complicating factor in the behaviour of grandstand structures is the effect of Human-Structure Interaction (HSI). This is the phenomenon where the occupants of a structure change its (dynamic) properties. Especially for slender structures, the added mass of a dense crowd can be of the same order of magnitude as that of the structure itself. The literature found does not cover this topic in detail, though the OMA measurements by (Santos et al., 2018) do implicitly take account of HSI to some extent, as the load was generated by humans walking on the structure.

Generally, an occupied grandstand will have lower natural frequencies, different mode shapes and larger damping than the same structure when unoccupied (Ellis and Ji, 1997). The latter effect is beneficial, but the lower natural frequencies could pose a problem if the lowest value overlaps with one of the first harmonics of the jumping load.

To take account of HSI in the assessment of a grandstand structure, some guidelines propose modelling the crowd as single degree-of-freedom (SDOF) systems (The Institution of Structural Engineers, 2008) representing groups of spectators. The combined human-structure system is then excited by a pair of driving forces within the spring-dashpot interface between these crowd bodies and the structure, see Figure 2.9.

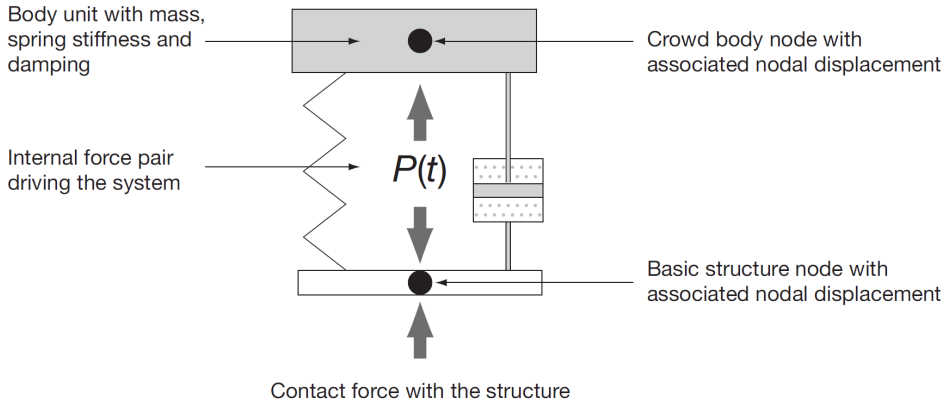

Figure 2.9: SDOF system representing a crowd on a grandstand, from (The Institution of Structural Engineers, 2008)

This approach has been verified on for simple model with three degrees of freedom in total (Pavic and Reynolds, 2008), but not on a full FE model of a grandstand. The closest the author could find was the thesis of (Appelman, 2022), which modelled a demountable event deck under dynamic crowd and applied HSI using crowd bodies, but with an initial velocity as excitation instead of the driving forces. Appelman did not find HSI to have a significant effect on the response of the structure, though it should be mentioned that the natural frequency of the event deck was much higher than what humans can achieve while jumping, so resonance did not play a role.

Applying HSI on an FE model where resonance does play a role could also be an interesting task for this thesis. However, combining this with a novel load model in frequency domain *and* a reliability analysis would increase the scope of the work beyond that of a Master thesis. So, as with most literature concerning grandstands, Human-Structure Interaction is ignored.

2.3. Reliability of Grandstand Structures

The Dutch Institute for normalisation provides norms for the design of spectator facilities, including grandstands, in NEN-EN 13200 (Stichting Koninklijk Nederlands Normalisatie Instituut, 2019b). These do not cover the reliability with regards to dynamic crowd loads, however. In fact, the chapter 'Loads and other dynamic actions' is just one sentence long, referring to the Eurocode 1. According to this more general norm, dynamic loads can be applied as a quasi-static load if resonance or other dynamic effects are negligible. This is not a safe assumption with regards to slender grandstand structures. For cantilever grandstands in general the base jumping frequency of a crowd, or its second or third integer multiple, could fall in the same range as the fundamental frequency of the structure (The Institution of Structural Engineers, 2008). This means a full dynamic analysis needs to be performed, but the NEN provides little guidance on how to do so (Stichting Koninklijk Nederlands Normalisatie Instituut, 2019a), and what criteria should then be used to determine the reliability. In the following section, guidelines from other countries will be described, focusing mostly on serviceability criteria as safety is not covered in detail by these codes.

2.3.1. Serviceability

Serviceability is inherently a much more subjective criterion than safety. What behaviour of the structure does or does not conform to expectations will differ from person to person. Some spectators may consider any noticeable vibration of a grandstand to be discomforting, while other may tolerate or even enjoy it. Fans of football clubs may even celebrate is as part of their specific subculture. So, while methods do exist to quantify the amount of vibration experienced, the limits imposed will always be somewhat arbitrary. Three foreign codes have been found that provide these methods. They all use accelerations of the structure to quantify its serviceability, though with different approaches to determine these limits:

- The Canadian Commission on Building and Fire Codes gives a general range of acceleration values (Canadian Commission on Building and Fire Codes, 2006)
- The International Organization for Standardization (or ISO) makes a distinction between comfort and panic criteria (International Organization for Standardization, 2007)
- The British Institution of Structural Engineers uses 4 design scenarios with different audience expectations in their guidance (The Institution of Structural Engineers, 2008, referred to as the UK Guidance for brevity)

The measure to quantify the 'intensity' of vibrations most often used in these codes is the root-mean-square of the acceleration (RMS), which is based on the perception of vibrations occurring at a specific moment:

$$a_{rms}(t) = \sqrt{\frac{1}{T_s}\int_{t}^{t+T_s} a_w^2(t)dt} \tag{2.10}$$

Where T_s is a sampling period, and $a_w(t)$ is an acceleration record. Before calculating the RMS value, weight-factors are applied on the acceleration record based on the frequency of the vibrations (hence the subscript). This weighting, which is similar to a band-pass filter, is applied because humans only perceive vibrations in a certain frequency range (Jones et al., 2011). A table of weighting factors is given in ISO 2631 (International Organization for Standardization, 2007), with different values for the vertical and horizontal directions. Another ISO-standard, 10137:2007 (International Organization for Standardization, 2007), recommends values for the sampling period T_s: 10 seconds for comfort criteria, and 1 second for panic. The shorter this period, the more $a_{rms}(t)$ becomes sensitive to short peaks in the acceleration signal. If T_s is taken as the length of the entire acceleration signal, the RMS is equal to the square root of the power of the signal. The unit of the RMS vibrations is the same as the original acceleration record, often expressed as a percentage or fraction of the gravitational acceleration g. The same holds for the limit values recommended by the norms, the UK guidance for example recommends a maximum of $0.2g = 1.962\ \mathrm{m/s^2}$ for the fourth design scenario, with the most active crowds.

An alternative method is the vibration dose value (VDV), advocated for by (Ellis and Littler, 2004a):

$$VDV = \sqrt[4]{\int_0^{T_{event}} a_w^4(t)dt} \tag{2.11}$$

The VDV is calculated using T_{event}, which is the entire duration of the event. This means the VDV is a cumulative value based on tolerance of total vibrations over a longer period. In other words, it will return a higher value for longer events, and will 'remember' recurring vibrations that the RMS method 'forgets' because they fall outside of the sampling period. The unit of this criterion is $\mathrm{m/s^{7/4}}$, which is less intuitive than accelerations. Because T_{event} is determined by the event length, there is also less flexibility to adjust the calculations to different scenarios or criteria. For this thesis, a failure criterion based on RMS accelerations will be used.

2.3.2. Safety

In general, serviceability (SLS) requirements seem to place stricter requirements on grandstand structures than safety (ULS) requirements. The norms found generally do not cover ULS requirements in detail, with only the UK guidance advising an extra check for stadiums where a global mode involving both the seating and support structure can be activated (The Institution of Structural Engineers, 2008). It appears that no ULS failures specific to grandstands are assumed to occur when the design already has to ensure that vibrations are sufficiently limited, and that general ULS requirements (e.g. stresses, stability) do not require special attention compared to other building types. Still, structural failures from dynamic crowd loads have occurred, notably the recent collapse of a beam element in the away section at De Goffert in Nijmegen (Rutten et al., 2022). Some time later, PSV Eindhoven reduced the capacity of the away section in the Philips Stadium to prevent a similar incident (NOS, 2023).

Royal Haskoning DHV found two causes for the collapse at De Goffert: the effective load applied by the jumping crowd was larger than the quasi-static load applied in codes, and the eccentricity of the load was not properly taken account of in design calculations (Koper and Kortenaar, 2022). So while resonance and mode shapes did not play a role here, even then the codes appear to be insufficient. Furthermore, (Weijs, 2023) found that the reinforcement in the collapsed element may have been placed too far from the bottom edge of the concrete, reducing the bending moment capacity. From these findings, it appears structural safety requirements for grandstands should be more comprehensive than they currently are.

Figure 2.10: The collapsed grandstand element at De Goffert, from (NOS, 2021)

Some other well-known stadium disasters were caused by overcrowding of the stands, crowd misbehaviour or mismanagement by the local authorities (The Stadium Guide, n.d.). Much of the research on crowd loads this thesis builds on was in fact performed in response to the Hillsborough Disaster of 1989, which resulted in the deaths of 97 spectators due to a crowd crush (Tikkanen, 2023). In such cases, the design of the grandstand structure could of course play a role, but not within the scope of this thesis. Other incidents involving a roof collapsing such as in Alkmaar (RTL Nieuws, 2019) and Enschede (Trompers, 2011) are also not covered.

2.4. Quantification of Reliability

In order to quantify the reliability of the stadium, the failure probability P_f needs to be determined. This is the probability that one or more criteria are not met, causing a 'failure' of the considered structure. Most failure criteria can be formulated in terms of a resistance R and a solicitation S. For example, S could be the stress occurring in a critical member of a steel structure, and R the strength of the material. Within the context of this thesis, S will be the RMS accelerations and R a limit value. Failure then occurs when $S > R$, while the structure is considered 'safe' (or serviceable) when $R > S$. The failure probability can then be formulated as follows:

$$P_f = P[S > R] \tag{2.12}$$

This section explains how the failure probabilty can be calculated.

2.4.1. Limit state functions

Failure criteria can often be expressed with a Limit State Function (LSF): $Z = R - S$, with $Z < 0$ indicating failure. This function can depend on multiple different variables (stiffness, dimensions, crowd density, etc.), some of which may be deterministic, and others stochastic. Some may affect S, others R, or possibly even both, depending on the problem being considered. If the stochastic variables (SV's) are collected in the vector $\boldsymbol{X}$, then the limit state becomes a function of this vector $g(\boldsymbol{X})$. The combinations of variables where $g(\boldsymbol{X}) = 0$ form the Limit State, which is visualised in Figure 2.11. The Limit State divides the space described by the SV's in $\boldsymbol{X}$ into a 'safe' region and a 'failure' region. It can have any arbitrary shape, and an analytical expression may not always be available, for example when S represents the output of a Finite Element model. In that case, the LSF becomes a 'black box'.
The failure probability P_f is now defined as the cumulative probability of a combination of values $\boldsymbol{X}$ occurring that lies on the failure-side of the limit state, where $g(\boldsymbol{X}) < 0$. Using the joint distribution $f_{\boldsymbol{X}}(\boldsymbol{x})$ of all variables in $\boldsymbol{X}$, this calculation can be expressed in the form of an integral:

$$P_f = P[g(\boldsymbol{X}) < 0] = \int_{g(\boldsymbol{X})<0} f_{\boldsymbol{X}}(\boldsymbol{x}) d\boldsymbol{x} \tag{2.13}$$

Evaluating this integral analytically can become very difficult, if not impossible, especially if a large amount of SV's are used, if the Limit State $g(\boldsymbol{X}) = 0$ has a complicated shape, or if the LSF is a black box. Multiple methods exist to determine the reliability without evaluating this integral by hand, referred to as Reliability Methods, which can generally be divided in Level I, II and III. The level is determined by the accuracy in which the distribution of the SV's is taken into account (Jonkman et al., 2017):

- Level I: Characteristic values with partial coefficients (safety factors) are applied for the variables in $\boldsymbol{X}$, and the LSF is evaluated once to determine whether these values result in failure or not.
- Level II: The means, standard deviations and correlations are taken into account. Assuming normal distributions, the failure probability is approximated.
- Level III: The complete joint distribution is used, and the failure probability is calculated by evaluating (or numerically approximating) the integral in some fashion.

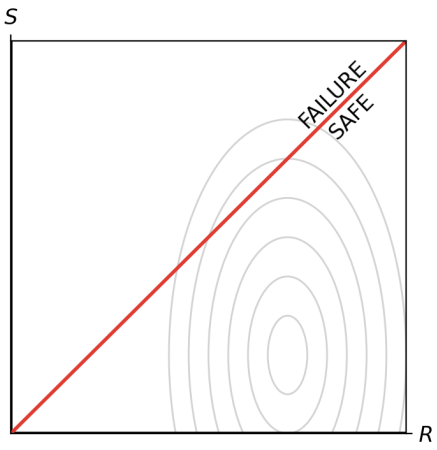

Figure 2.11: Example of a Limit State Function. The ellipses indicate lines of equal probability in the joint distribution $f_{\boldsymbol{X}}(\boldsymbol{x})$, and the red line indicates the limit state $Z = 0$

Level I methods are not considered for this thesis. Level II and Level III methods are covered in the following paragraphs.

2.4.2. Level II methods

A well-known level II method is FORM, First-Order Reliability Method. The aim of FORM is to find the point on the point on the Limit State $g(\boldsymbol{X}) = 0$, with the highest joint probability of the variables $\boldsymbol{X}$: the design point. This point is found using a linearisation of the LSF using its partial derivatives ($\partial g / \partial X_i$) in an initial approximation of the design point. Using this linearisation, a new approximate design point is determined, which is used for a subsequent linearisation. This iterative procedure results in a final design point, along with reliability index β and a set of sensitivity factors α_i, one for each SV.

The interpretation of these values requires transforming the SV's such that their joint distribution is described by the sum of standard normally distributed variables, contained in the vector $\boldsymbol{U}$. In this U-space, all points located at the a certain distance from the origin have the same joint probability $f_{\boldsymbol{U}}(\boldsymbol{u})$, indicated by the concentric circles in Figure 2.12. FORM can also be applied in the U-space directly, using the derivatives with respect to the transformed variables: $\partial g / \partial U_i$.

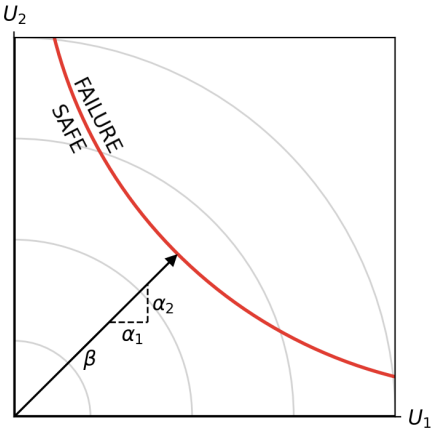

Figure 2.12: Interpretation of FORM in U-space. The concentric circles indicate lines of equal probability in the transformed joint distribution $f_{\boldsymbol{U}}(\boldsymbol{u})$

The results of FORM then determine the shortest vector from the origin to the Limit State in U-space. The direction of this vector is determined by the sensitivity factors α_i, and its length by the reliability index β. This is also visualised in Figure 2.12. The failure probability is then finally approximated using β and the CDF of the standard normal distribution Φ (Jonkman et al., 2017):

$$P_f = \Phi(-\beta) \tag{2.14}$$

Other level II methods, such as SORM (FORM with second-order gradients), are not considered.

2.4.3. Level III Methods

Level III methods calculate the failure probability directly using multiple evaluations of the LSF, either in U-space or in the untransformed X-space, in order to approximate the integral in Equation 2.13. Perhaps the most straightforward level III method is Crude Monte Carlo (CMC), where random sample values for $\boldsymbol{X}$ are drawn according to their joint distribution. The sign of the corresponding output values $g(\boldsymbol{X})$ then determines whether a sample lies in the domain of the integral in Equation 2.13 ($g(\boldsymbol{X}) < 0$). With enough samples, the distribution of the sampled values will resemble $f_{\boldsymbol{X}}(\boldsymbol{x})$. The failure probability is then calculated simply as the percentage of simulated values of $g(\boldsymbol{X})$ located in the failure domain (Jonkman et al., 2017). An example of a CMC analysis is given in Figure 2.13. Because CMC considers purely the input and output of the LSF, and does not require calculation of derivatives or points lying on the limit state, nor transformation to U-space, implementing it is rather straightforward even for complicated Limit State Functions. The downside is that the method requires a large number of evaluations of the LSF, which may involve running a Finite Element analysis or other lengthy calculation.

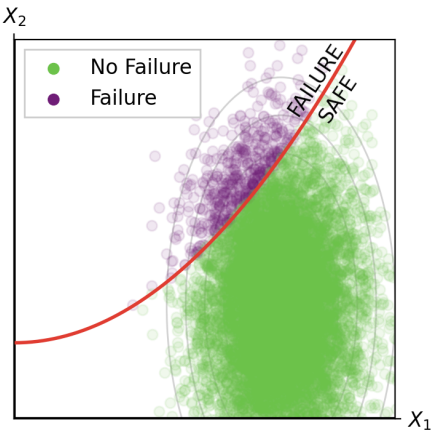

Figure 2.13: Example of a Crude Monte Carlo analysis in the untransformed X-space

An alternative to Monte Carlo is Directional Sampling (DS), which is performed in U-space with the variables in $\boldsymbol{U}$ transformed to polar coordinates. A point in U-space is then described by its distance from the origin, λ, and the direction from the origin to that point, a unit vector $\boldsymbol{\theta}$. The exact formulation of the failure probability from Equation 2.13 then becomes (Waarts, 2000):

$$P_f = \int \left(1 - \chi_N^2\left(\lambda_0^2\left(\boldsymbol{\theta}\right)\right)\right) d\boldsymbol{\theta} \tag{2.15}$$

Where $\lambda_0(\boldsymbol{\theta})$ is the length of the vector with direction $\boldsymbol{\theta}$ from the origin to the limit state. These points where $g(\lambda_0(\boldsymbol{\theta})\boldsymbol{\theta}) = 0$ are referred to as roots of the LSF. The probability of the variables along this direction exceeding a root (thus lying in the failure domain) is calculated with the chi-squared distribution χ_N^2, with N degrees of freedom corresponding to the number of variables in $\boldsymbol{U}$. When DS is applied, random values of $\boldsymbol{\theta}_i$ are drawn, through a uniform distribution. For each $\boldsymbol{\theta}_i$, the distance λ_i from the origin to the Limit State is found. This distance is used to calculate a sample probability for that direction P_i:

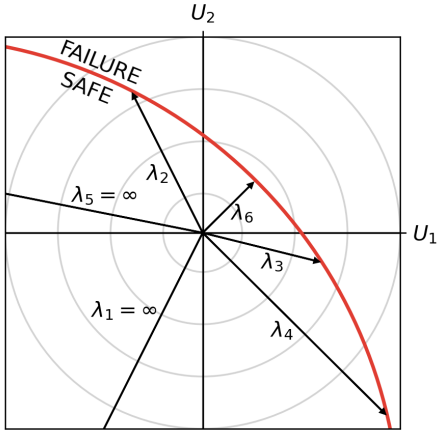

Figure 2.14: Example of Directional Sampling in U-space

$$P_i = \left(1 - \chi_N^2(\lambda_i^2)\right) \tag{2.16}$$

The failure probability P_f is then calculated by averaging the sample failure probabilities over all directions (Waarts, 2000).

For both Crude Monte Carlo and Directional Sampling, the accuracy of the result can be quantified by estimating the coefficient of variation (CoV) of the resulting failure probability, $V(P_f)$. This value depends on the approximated failure probability, and the number of samples of $\boldsymbol{X}$ or $\boldsymbol{\theta}$ used. The more samples used and the larger the estimated P_f, the smaller $V(P_f)$ will be for both methods, indicating a more accurate result. For very simple analytical Limit State Functions, DS requires less LSF evaluations than CMC to achieve the same $V(P_f)$, but this does not generally hold for more complicated shapes (TNO, 2017). It is clearly desirable to keep this number limited, as the time and computational resources required to perform a Reliability Analysis depend on this.

To reduce the number of LSF evaluations required, some reliability methods use a Response Surface $\hat{g}(\boldsymbol{X})$ (RS), constructed using a limited number of samples from $g(\boldsymbol{X})$. These act as a surrogate for the 'true' LSF, and have simple analytical expressions allowing them to be evaluated much faster, having a negligible effect on the total runtime.

For example, a quadratic response surface $\hat{g}(\boldsymbol{X})$ of an LSF with N variables could be formulated as:

$$\hat{g}(\boldsymbol{X}) = a + \sum_{n=1}^{N} b_i X_i + \sum_{n=1}^{N} c_i X_i^2 \tag{2.17}$$

Which would require at least $2N + 1$ samples of the LSF to be fitted. If more are used, a, b_i and c_i can be fitted using a least-squares approach. The downside of using a RS is that its accuracy influences the accuracy of the result, depending on the number of samples of the LSF and on whether the shape of the Response Surface resembles that of the LSF.

The dissertation of (Waarts, 2000) presents another method called Directional Adaptive Response surface Sampling, or DARS. This method uses adaptive response surfaces, in combination with directional sampling and axis directional integration (ADI). The latter is a method to find roots on the axes in U-space: the variables in $\boldsymbol{U}$ are individually increased or decreased until a root is found at some distance λ along each axis. These roots are used as sample points for a quadratic response surface, upon which directional sampling is performed. Alternatively, a set distance f and $-f$ from the origin along each axis (still in U-space) may be chosen for the sample points if a root cannot be found, or if ADI is not used.

For directions $\boldsymbol{\theta}_i$ where the Response Surface results in a small distance $\lambda_{i,RS}$ to the Limit State, the original LSF is used to determine a more accurate $\lambda_{i,LSF}$. The resulting root point $\lambda_{i,LSF}\boldsymbol{\theta}_i$ on the Limit State is used as an additional sample point update the RS. This way, the LSF samples used for fitting the RS are directed towards a point on the Limit State with a high probability, resulting in an accurate Response Surface around the most important region. The threshold for using the LSF instead of the RS is set by a parameter $\Delta\lambda_{add}$, and by the smallest distance λ_{min} found. If $\lambda_{i,RS}$ is smaller than $\lambda_{min} + \Delta\lambda_{add}$, the LSF is used to find $\lambda_{i,LSF}$ for that direction. This threshold is visualised as the dotted circle in Figure 2.15.

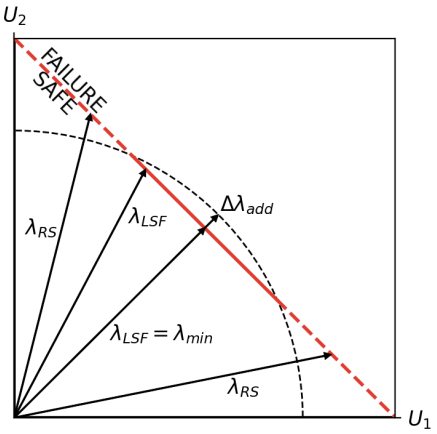

Figure 2.15: Example of DARS in U-space

For this thesis, evaluating the LSF will involve determining the response of an FE-model to dynamic loads. According to (Waarts, 2000), reliability problems involving FE models are a good use case for DARS, so this will be an interesting method to apply on this problem. FORM, on the other hand, does not perform well and even tends to fail, as an LSF resulting from an FE model tends to be erratic and contain multiple points on the limit state with high probability, aspects which complicate finding a single design point. Furthermore, determining the partial derivatives exactly is not possible for a 'black box' LSF, though they may be estimated numerically. On the other hand, FORM is generally a very efficient method in terms of the number of LSF evaluations, so an attempt will still be made to apply it. If the failure probability is large, Crude Monte Carlo or Directional Sampling may also be applied, as then the number of samples required to reach an acceptable $V(P_f)$ will be relatively limited.

2.5. Synthesis

This final section of the literature study serves as a bridge towards the methodology presented in the next chapter. Four topics were considered: models of crowd loads, models of grandstands, reliability of grandstands, and calculations of reliability, connecting to the four components mentioned in the introduction (in a different order):

1. Construct a model of the stadium's cantilever grandstands
2. Create a model of crowd loads and apply it to the grandstand model
3. Determine a failure criterion based on the response of the grandstand
4. Calculate the failure probability of this criterion

The aim of these four steps is, again, to form a methodology for determining the reliability of a cantilever grandstand under dynamic crowd loading. This methodology should be versatile, such that it can be used for both safety and serviceability considerations (with different failure criteria), for different grandstand structures, and with different reliability methods. The methodology will be applied through Python scripts, written by the author, which use a set of input variables to adjust the input of an FE model of a cantilever grandstand with dynamic crowd load applied on it. These scripts also run the model and post-process the results to evaluate a failure criterion. Essentially, a Limit State Function is evaluated with stochastic input variables $\boldsymbol{X}$ and output $g(\boldsymbol{X})$. The failure probability belonging to this LSF is then calculated, also through Python, using the distribution of the stochastic variables describing the variance in the load and structure. This calculation is performed through the Reliability Methods described in section 2.4. This 'train' is visualised in Figure 2.16 below.

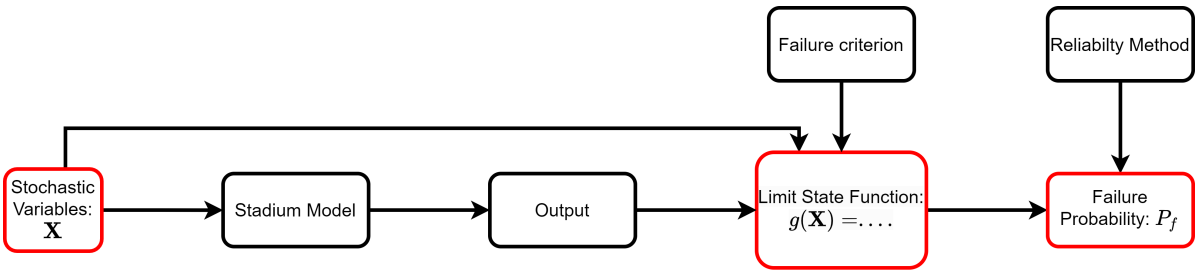

Figure 2.16: Diagram of the methodology or 'train' to be developed in the next chapter

The FE models found as part of this literature study did not have dynamic crowd loads applied on them, nor were they used for reliability analyses. This methodology will thus aim to combine these, in such a way that both the load and structure can be parameterised with stochastic variables, denoted by $\boldsymbol{X}$. To perform a reliability analysis, the response of the model to the crowd load will need to be evaluated many times, so it is desirable to keep the runtime of a single evaluation relatively short. How much time and computational resources are available of course depends on the problem being considered. Both are limited for this thesis, so for the case study only a specific part of the Feyenoord Stadium will be modelled: the trusses beneath the concrete seating decks, which contain the two cantilevers. In general cases, models with larger scopes could be used.

As the models from literature were specifically made to apply OMA, they are all linear. No measurement data is available for the Feyenoord Stadium, so OMA cannot be applied to calibrate the model used for the case study. Keeping the model linear would have other advantages, however, as the runtime will indeed be short if no Newton-Rhapson or other iteration scheme needs to be performed. This means no nonlinear effects can be applied in principle, though the cantilever roof model of (Magalhães et al., 2008) does present an interesting approach to take some second order-effects into account: The tangent stiffness matrix, calculated after applying the self-weight, is used for the modal analysis instead of the initial stiffness matrix, resulting in a good correspondence between the experimentally and numerically determined modes and natural frequencies.

While this paper investigated a roof over a grandstand rather than a grandstand itself, both types of structures are generally slender with large cantilevers, where second-order effects could play a significant role in the response. So, a similar approach will be followed in this methodology: the model will be linear, with the tangent stiffness matrix used to determine the response to the dynamic load. This means a static analysis needs to be performed to calculate this matrix before the response to the dynamic load can be determined, but the extra runtime this requires is not expected to be significant compared to the dynamic analysis.

Another advantage of using a linear model is that the response can be evaluated in both the time and frequency domains, with the latter likely requiring a shorter runtime, as the response of the structure for different frequencies can be evaluated in parallel. An Inverse Fast Fourier Transform (IFFT) can then be used to convert frequency-domain results back to time domain (though this will not be necessary for the failure criterion considered in the case study). In the time domain, the different time steps would need to be solved for in order, which would result in a significantly longer runtime. So, the response of the model will be evaluated in the frequency domain, which means the loads need to be defined in the frequency domain as well.

The load models found in the Literature Study are generally defined in the time domain, with the exception of that by Ellis and Littler, which uses a Fourier Series. A Fast Fourier Transform (FFT) could be applied on loads generated with these models before applying them on the FE model of the grandstand, but the harmonic nature of the loads loading lends itself to describing them in the frequency domain directly. So, a load model will be created that defines the Fourier transform of the load, characterised by a series of peaks, rather than the load itself in the time domain. To quantify the uncertainty in the load spectrum, samples from the (Xiong and Chen, 2021) database will be used. After all, this database was created with the explicit purpose of constructing new models for dynamic crowd loads, on both the time and frequency domain.

These samples, transformed to the frequency domain, could also be applied on the stadium model directly, without a specific definition of the spectra. A quasi-Crude Monte Carlo analysis could then be performed, evaluating the LSF with the responses to the sample loads. This might be sufficient for evaluating serviceability criteria, where (combinations of) sample loads causing 'failure' will occur relatively frequently. For safety criteria, however, extreme load cases need to be simulated, for which a parameterisation of the spectrum can be used. The spectrum is then described by a number of stochastic variables, forming a part of the input $\boldsymbol{X}$ of the LSF, with distributions based on samples of the dataset. Extreme cases can then be modelled with parameter values in the tails of their distributions.

Multiple Reliability Methods will be used, again to make the methodology more versatile: for serviceability criteria, with a large expected failure probability, Crude Monte Carlo may require a reasonable number of simulations to determine relatively large failure probabilities with sufficient accuracy. For safety problems, with smaller failure probabilities, DARS or FORM may be a better fit. These methods also require the load spectrum to be parameterised, as roots or gradients need to be expressed in the variables in $\boldsymbol{X}$. In this thesis, all methods will be applied on the serviceability criterion considered for the case study, but their performance will indicate whether they can be used for safety problems as well. The results of these methods are given in Chapter 4, where the interpretation with regards to the Feyenoord Stadium is also discussed. Chapter 5 then focuses on the general use of the methodology, which also includes an investigation of transforming the results of the model combination back to the time domain.

This approach is somewhat similar to the one applied in (Weijs, 2023) to calculate the reliability of an element in De Goffert. Instead of a linear stadium model with a frequency-domain load model, Weijs' thesis used a nonlinear model with one degree-of-freedom, and the time-domain load model described in Section 2.1. As every simulated jump of every individual spectator is described by five realisations of stochastic variables, the number of variables N in the vector $\boldsymbol{X}$ becomes rather large, in the order of 10^4. This makes determining roots or gradients of the LSF very difficult, meaning the only feasible Reliability Mehod to apply was Crude Mone Carlo. This load model can therefore not be used as part of the methodology developed for this thesis, as flexibility in Reliability Methods is likely needed for the wider applicability.

3

Methodology

This chapter contains the methodology developped to determine the reliability of a cantilever grandstand under dynamic crowd loading. The Feyenoord Stadium in Rotterdam is used as a case study, which has been described in the introduction. More details are given in Appendix A, along with a number of pictures taken by the author. The scope of the case study is limited to the trusses supporting the concrete seating decks, with the failure criterion based the vibration of the tip of the upper cantilever.

The first section of this chapter describes a Finite Element model representing such a truss, with special focus on the dynamic aspects. The software and scripts used to build and adjust the model are also briefly covered, as well as the stochastic variables that will be applied. The second section presents the frequency domain model for dynamic crowd loads created using the dataset from (Xiong and Chen, 2021), along with its application on the FE model and its stochastic variables. The process of creating this model is covered in more detail in Appendix B. The third section describes the considered failure criterion and its corresponding Limit State Function (LSF), which will be used for the reliability analysis, and the fourth section explains how this analysis is performed with the methods investigated in the literature study. Finally, the fifth section provides an overview of the methodology. As mentioned previously, the model of the grandstand and the considered failure cirterion are case-specific, while the load model and reliability analysis are generally applicable.

3.1. Finite Element Model

The Finite Element model used for the case study is shown in Figures 3.1 and 3.2. As said, this model represents a single truss in the Feyenoord Stadium, with the seating deck it supports placed on top of it. The profiles of the steel members have been estimated based on the pictures in Appendix A, and the concrete deck is simplified as having a wide rectangular cross-section, with another steel member directly below it, forming a combined cross-section. The tip of the upper cantilever has been marked in red in both figures.

The model uses quadratic (three-node) Timoshenko beam elements for all members, including the seating deck, with linear elastic material models. Most members are modelled by one such element, except some long members in the back of the spine, and the seating deck and the member below it. For the spine, this has been done to make the spacing between nodes somewhat more consistent in the upper part of the truss. For the decks, this is done to split them in a number 'load blocks' of approximately equal length, which are used to apply one of the two load cases.

These load cases are the static self-weight $\boldsymbol{f}_{st}$ and dynamic crowd load $\tilde{\boldsymbol{f}}_{crowd}(f)$, defined in the frequency domain. The latter is applied as distributed load on the seating deck of the trusses, where each load block can have a different value. How these values differ is explained in the next section, on the crowd load model. For all analyses, the static load is used to determine the tangent stiffness matrix, similarly to (Magalhães et al., 2008), which is then used in calculating the response to the dynamic load instead of the initial stiffness matrix. This means the set of equations to be solved is still linear, but they are defined using the shape of the truss when it is deformed under its own weight.

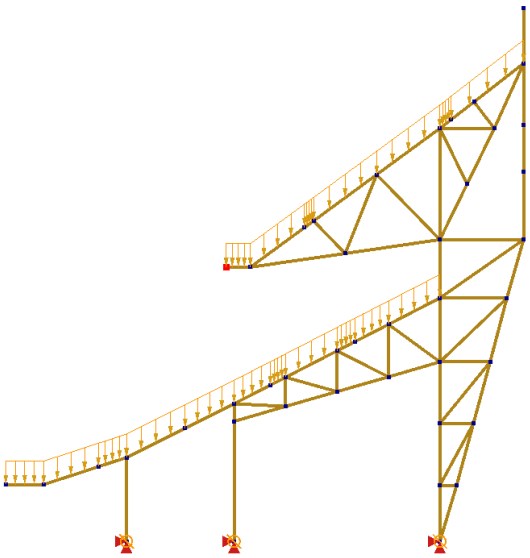

Figure 3.1: Geometry of the FE model representing a truss in the Feyenoord Stadium, with the tip of the upper cantilever highlighted in red

.

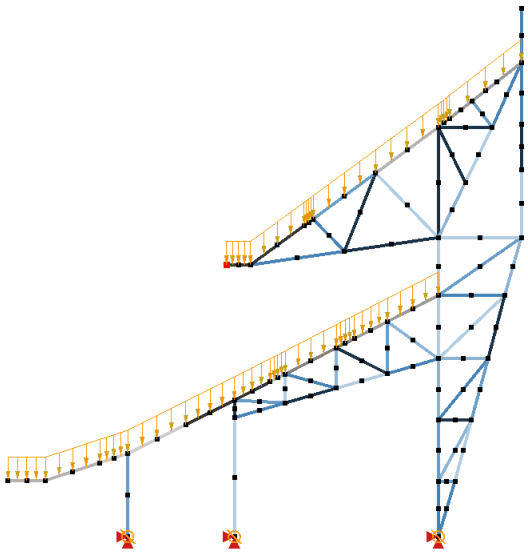

Figure 3.2: Mesh of the FE model, showing the elements and nodes

Some further assumptions and simplifications have been made. These include:

- Ignoring non-structural walls connecting the trusses to each other
- Ignoring the curvature of the concrete deck
- Ignoring small in between the trusses
- Modelling the geometry of the beam under the lower cantilever with a constant I-profile instead of a varying cross-section
- Assuming all connections are rigid, including the three supports at the bottom.

3.1.1. Dynamic Aspects

The first four mode shapes calculated by DIANA are given along with the corresponding natural frequencies in Figure 3.3. As mentioned, these are calculated using the tangent stiffness matrix resulting from applying the self-weight. The first natural frequency is nearly 2.0 Hz, which is chosen as the target jumping frequency f_{target} for the crowd loads. This means the considered load case will cause resonance, and a significant response can be expected. The corresponding mode sees the truss move mainly in the horizontal direction, though the vertical crowd load should be able to activate it, as the vertical displacement is nonzero. The second mode is located further at 4.6 Hz, and shows more vertical displacement, especially in the upper tier. These first two natural frequencies and modes match results found by TNO researchers, which inspires some confidence in the accuracy of this model (although these results were gathered before the 1994 renovation).

The third mode has a natural frequency of 5.2 Hz, even further from a multiple of f_{target}, and involves the lower cantilever vibrating up and down. Subsequent modes have natural frequencies of over 10 Hz, when the height of the peaks in the load spectrum will have become negligible.

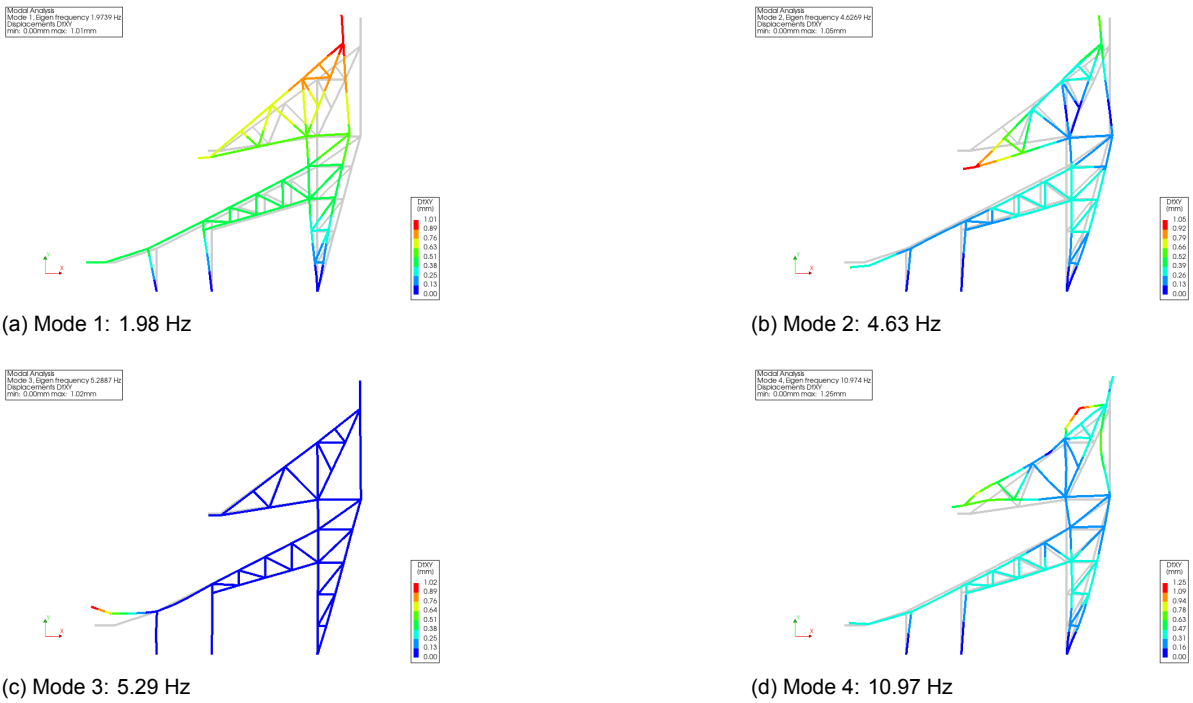

(a) Mode 1: 1.98 Hz

(b) Mode 2: 4.63 Hz

(c) Mode 3: 5.29 Hz

(d) Mode 4: 10.97 Hz

Figure 3.3: First four modes of the modelled truss. The colors indicate (relative) total displacements

Figure 3.4 shows the acceleration spectrum of the cantilever tip calculated when the amplitude spectrum of $\tilde{\boldsymbol{f}}_{crowd}(f)$ is set to white noise: a constant, arbitrary value. In other words, this is the acceleration response spectrum of the degrees of freedom of the node marked in Figures 3.1 and 3.2. At the first natural frequency, the response in the vertical and horizontal directions is similar. At the second frequency, the vertical response dominates, though both values are much larger than in the first mode. The tails of this peak also reach to multiples of f_{target}, 4 and 6 Hz, where peaks will appear in the crowd load spectrum. This means the second mode will likely dominate the total acceleration response, even if a slightly different target jumping frequency value had been chosen. The second mode having a larger response than the first is not unexpected considering the mode shapes and the vertical direction of the load, though the difference is amplified in the acceleration spectrum. High-frequency acceleration responses appear larger than displacements at the same frequency f, because the accelerations are calculated by multiplying the displacements with $(2\pi f)^2$.

These dynamic aspects have been determined with the stochastic parameters of the FE model, described in paragraph 3.1.3, set to their mean.

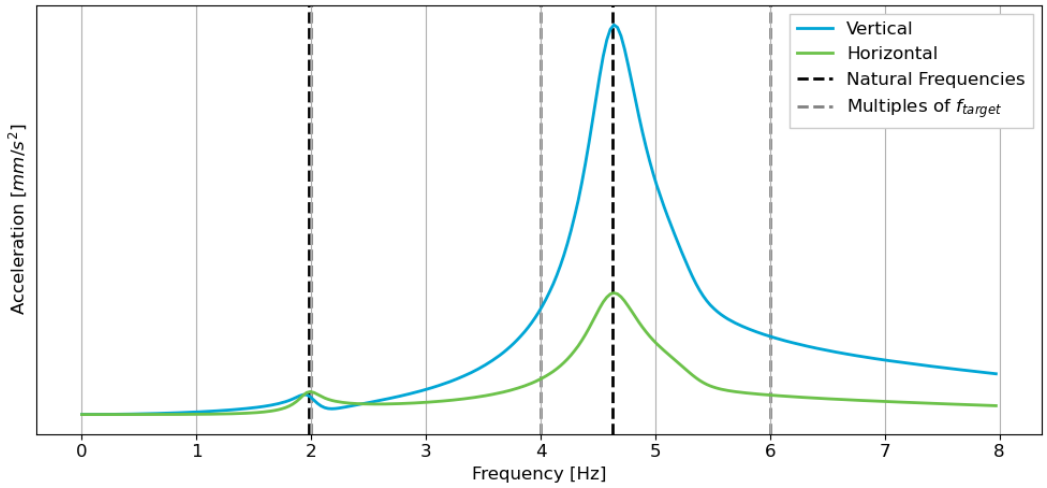

Figure 3.4: Acceleration response spectrum of the tip of the upper cantilever, generated by running the model with a white noise spectrum

3.1.2. Software and Scripts Used

To create and run the FE model, DIANA FEA v10.6 is used (Ferreira and Manie, 2022). This software has a graphical user interface, which has been used to set up the initial model, but adjusting and running it for the reliability analysis is done through Python. A script is used that can adjust the input file (or `.dat`-file) of the model, run it through a batch (`.bat`) and command (`.dcf`) file, and interpret the tabular (`.tb`) output file.

The `.dat`-file file contains all the geometrical, material and load parameters, which could be defined as or derived from the stochastic variables (SV's), covered later in this chapter. Numerical values can be inserted into this file by the script, forming the input of the model. The `.bat`-file, executed through the Python script as well, then contains the commands used to start DIANA, read the input file and perform the analysis described in the `.dcf`-file. Finally, after running the analysis, DIANA stores the desired results (accelerations in this case, but this could also be stresses, displacements or other outputs) in a `.tb`-file, which is post-processed by the script. This way, the model is parameterised, and different in- and output can be generated and stored automatically. Figure 3.5 shows a diagram of this set-up.

The software used for performing several of the reliability analyses is Probab, a toolkit written in Fortran used internally by TNO. For this case, the author used an interface in Python, which could be combined with the other script to set up the 'train' of defining distributions for input values and applying these on the model, solving and post-processing the model to determine the output, and repeating this process to perform the reliability analysis. The documentation of Probab contains a list of distributions that can be defined for stochastic variables, and a number of benchmark tests where different reliability methods have been applied on a number of analytical Limit State Functions (TNO, 2017).

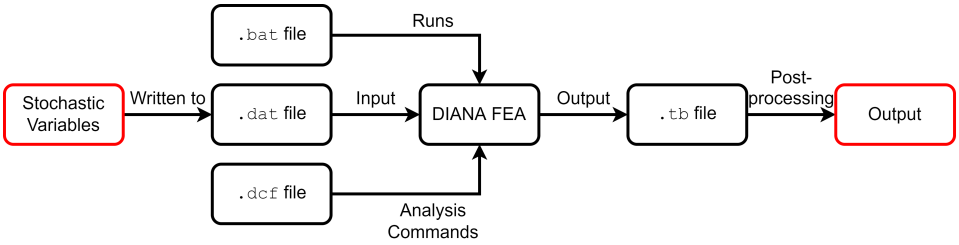

Figure 3.5: Diagram of files used to run the FE model with stochastic parameters as input

3.1.3. Stochastic Variables of the FE Model

In general, distributions for structure parameters are hard to find in literature. The matrices $\boldsymbol{M}$, $\boldsymbol{C}$ and $\boldsymbol{K}$ depend on the geometry of the mesh, the profiles of the members and the material parameters. The first two are rather complicated to adjust in the DIANA input file, and would require many variables, so these are taken as deterministic.

For the material parameters, usable distributions have been found for the Young's Moduli of concrete and steel, which influence the stiffness matrix $\boldsymbol{K}$. Gamma-distributions are used, from (Blondeel et al., 2018), who defined these with a shape parameter α and a *scale* parameter β: Probab defines this distribution with p as a shape parameter and b as a *rate* parameter, which is the inverse of β. A shift (nonzero lower bound) can also be applied, but this is assumed to be zero in this case. Table 3.1 shows the values of these parameters as applied in Probab, corrected for the units used in DIANA, and Figure 3.6 shows the density functions.

Table 3.1: Gamma-distributed structure parameters

parameter	unit	α (p)	$1/\beta$ (b)
E_s	N/mm^2	934.2	4.673×10^{-3}
E_c	N/mm^2	7.1633	2.388×10^{-4}

Other structure parameters that could be considered are the density of the materials, the Poisson ratios, and the damping. Literature on the uncertainty of the material densities is sparse. Generally, a steel density of 7850 kg/m^3 and concrete density of 2500 kg/m^3 is assumed in design codes (Eurocode Applied, 2017a, Eurocode Applied, 2017b). These two values are therefore taken as deterministic, which means $\boldsymbol{M}$ is deterministic as well. For the Poisson ratios 0.3 is assumed for steel and 0.2 for concrete, both deterministic.

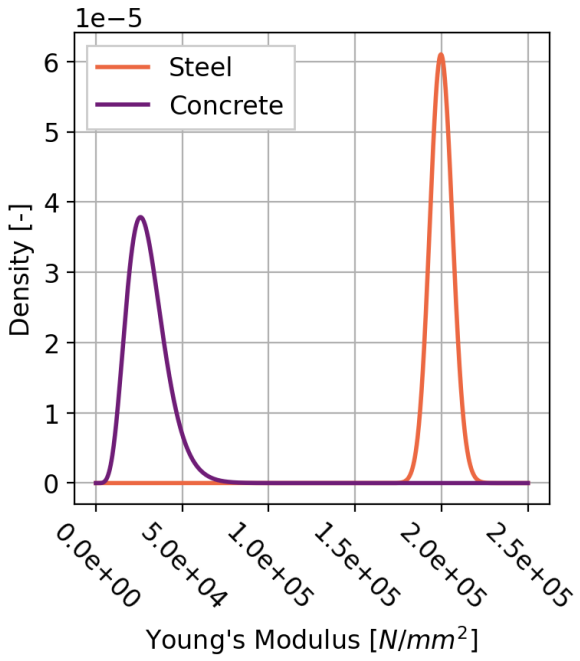

Figure 3.6: Distribution of Young's Moduli of the two materials used

3.1.4. Damping

The damping matrx $\boldsymbol{C}$ is defined using the Rayleigh method (Metrikine and Tsouvalas, 2022):

$$\boldsymbol{C} = a_0\boldsymbol{M} + a_1\boldsymbol{K} \tag{3.1}$$

Where the damping constants a_0 and a_1 are calculated based on the first two natural frequencies and damping ratios. Some of the papers on FE models of stadiums mentioned in the literature study contain estimated damping ratios, but the structures considered in these papers consist mostly of concrete instead of steel, including the supports of the seating decks. Therefore, these ratios are not considered to be applicable on the FE-model of the truss. Instead, the 'standard' 0.05 is assumed as a deterministic value for both modes. To reduce the runtime of the LSF, the damping constants are determined once using the mean values of the Young's Moduli, and the result is used for every evaluation of the LSF afterwards. This means the influence of the variability in the Young's Moduli on a_0 and a_1 is ignored.

3.2. Crowd Load Model

Solving the model in the frequency domain can be done much faster than in the time domain. While the steps in a time integration scheme need to be solved in-order, the response for each frequency can be solved in parallel. This means DIANA can calculate many more frequencies than time steps in the same amount of computational time. The challenge in solving the model in the frequency domain for a reliability analysis then lies in creating a model that takes the variance of the spectra of crowd loads into account. This can be achieved by describing the spectra with a number of stochastic variables (SV's), which then form the input of a limit state function (LSF), needed to calculate a failure probability P_f. This section presents such a model.

In the first section, a dataset containing experimentally measured crowd loads is described. Following that, the parametric model that approximates these loads in the frequency domain is presented. Appendix B contains more information on the creation of this model, including a comparison with two other options to apply crowd loads on the FE model. Next, the application of the load model on the FE model from the previous section is explained, followed by an overview of the stochastic variables forming the input of the load model. Finally, the model is validated by comparing the variance from spectra generated with the model to those sampled from the dataset, and comparing the acceleration response to a model load with the response to measured loads.

As mentioned in the synthesis, instead of using a parametric model, direct samples of the dataset could be used to describe the crowd load, but the variance within these samples then becomes hard to quantify. Only reliability methods that use random samples could then be applied, like Crude Monte Carlo, and applying extreme load cases would become difficult.

3.2.1. Dataset of Loads

Several measurement campaigns on crowd loading have been performed by (Xiong and Chen, 2021). The data of these experiments has been made public with the explicit purpose of developing new load models. This thesis uses the data of 'Experiment IV', where groups of 48 students were instructed to jump up and down, and the loads of every individual were measured. During these measurement sessions, one of several types of stimuli was used to instruct the students, including popular songs and metronomes. The forces transferred on the floor were not measured directly, but rather the acceleration $\ddot{x}(t)$ of the students was tracked using reflective markers placed around their upper torso, and converted to an applied normalized force as follows:

$$\tilde{F}(t) = \ddot{x}(t)/g + 1 \tag{3.2}$$

Where the 1 is added to account for the static weight, meaning the full force normalized by the participant's weight is recorded; the jump factor $\tilde{F}(t)$ including the static weight. The weight of every participant is also available, so converting between the jump factors and actual loads is trivial. The results were then low-pass filtered to remove components at 12 Hz or higher, and a handful of failed records were removed from the dataset. This approach is assumed to give accurate results, meaning the records can be used as-is and no further filtering is required.

Five measurement sessions were performed with a metronome set at 2 Hz (or 120 BPM), resulting in 204 usable records of individuals jumping at the desired value of f_{target}. The earlier study from (Chen et al., 2019) suggests that coordination effects are independent of group size when this size is larger than 20, so it is assumed that these effects did not differ from session to session, nor between the measurement environment and a lively grandstand. This means all 204 individual measurements are considered to be representative of spectators jumping on a grandstand in a crowd, and records can be sampled without regard for which session each record belongs to. Effectively, they are regarded as one big group.

So, to construct a 'sample spectrum' of the total load of group of jumping spectators, a number of records equal to the number of spectators in that group is selected randomly from the 204 records, then summed up and transformed to the frequency domain using the Fast Fourier Transform (FFT) with a scaling to keep the units of the original signal (Newton). Figure 3.7 shows such a sample load, in both the time and frequency domain. Note the peaks at 2, 4 and 6 Hz in the lower plot, their asymmetric tails, and the large mean value at $f = 0$ from the mean load.

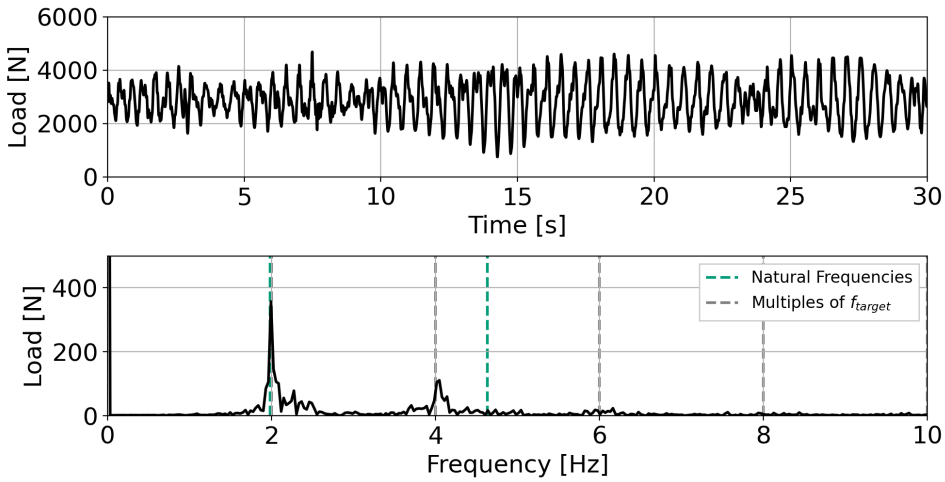

Figure 3.7: A sample of a group of 48 records from crowd load dataset in time and frequency domain, for a group of 48 spectators, with the natural frequencies of the truss and the multiples of f_{target} highlighted. The large value at $f = 0$ has been cropped for legibility

Figure 3.8 shows 1000 sample signals and spectra plotted over each other with transparency. This darker the color, the more the signals or spectra overlap each other. This shows a general, relatively smooth shape of the spectra, as well as the variance around this shape.

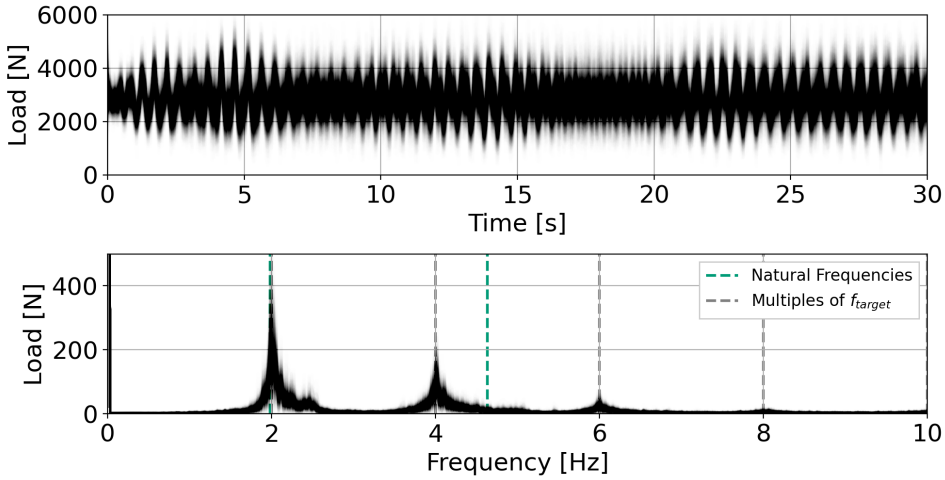

Figure 3.8: 1000 samples of 48 spectators, plotted with transparency to indicate variance

The values at $f = f_{target}$ (2 Hz) of the 1000 samples are plotted in a histogram in Figure 3.9, to further visualise the variance in the spectra. Based on samples such as shown in these two figures, a parameterised shape of the spectrum has been constructed. This shape forms the core of the load model, and is presented in the following paragraph.

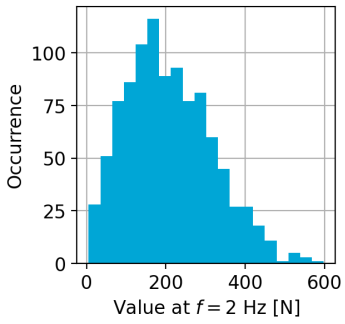

Figure 3.9: Histogram of the spectrum values at f_{target} in Figure 3.8

3.2.2. Parameterised Amplitude Spectrum

Three options to represent the load spectra stochastically were considered: one where the sampled spectra are used directly, one describing the complete spectrum in complex form, and one describing just the amplitude spectrum. The first option is of course the most representative of the actual loads, but very difficult to describe using stochastic variables, and as mentioned not able to represent extreme load cases. The second option is more usable, as the shape of the real and complex spectra can be parameterised and distributions can be determined for these parameters, though this was still rather difficult. The number of parameters was also quite large, much more so than for the third option, which was determined to be the most practical despite resulting in the least 'complete' description of the spectra. This option was finally chosen as the load model for this thesis, and is described in the following paragraphs. As mentioned, the complete process to arrive at this option is given in Appendix B.

In essence, the load model describes the amplitude spectrum of the crowd load, $|\tilde{f}_{crowd}(f)|$, ignoring phase angles within the load (for now). The spectrum is formulated as follows:

$$|\tilde{f}_{crowd}(f)| = \begin{cases} F_{mean} & \forall\, f = 0 \\ \sum_{k=1}^{K} P_k(f) & \forall\, f > 0 \end{cases} \tag{3.3}$$

Where F_{mean} is the mean of the load signal, which is inserted at $f = 0$. The K peaks of the spectrum are described by $P_k(f)$, where k is the number of the peak. The value of K then determines the length of the spectrum, and the largest frequency that needs to be considered. In literature, load models such as that of Ellis and Littler are generally truncated to three harmonics. Considering Figure 3.8, the height of the fourth peaks are indeed negligible compared to the first three, so K can be set to 3. The peaks themselves are formulated using a two-sided quadratic shape:

$$P_k(f) = \begin{cases} H_k \left(\frac{(f - k f_{target} + w_{left,k})}{w_{left,k}} \right)^2 & \forall\, f \in [k f_{target} - w_{left,k}, k f_{target}] \\ H_k \left(\frac{(f - k f_{target} - w_{right,k})}{w_{right,k}} \right)^2 & \forall\, f \in [k f_{target}, k f_{target} + w_{right,k}] \end{cases} \tag{3.4}$$

Here, H_k is the height of peak k, which is located at k times the target jumping frequency f_{target}, which is always 2 Hz for this thesis. The values of $w_{left,k}$ and $w_{right,k}$ determine the width of the left and right arm of the peak, allowing for an asymmetric shape. One peak is thus described by three parameters, so along with the mean value $3K + 1$ parameters are needed to describe the full spectrum. Figure 3.10 shows how the parameters describe the shape of a single peak, and Figure 3.11 shows an example of a load spectrum. The parameters are applied as stochastic variables (SV's) , and the distributions of these parameters are determined by repeatedly fitting a model spectrum to sample loads and recording the resulting values of the parameters. The results of this process are given in paragraph 3.2.4.

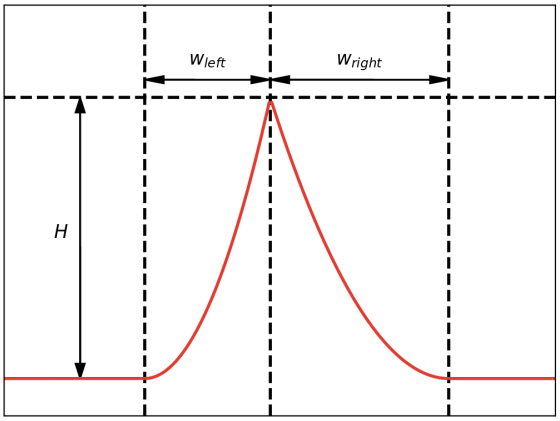

Figure 3.10: Diagram showing how a peak in the model load spectrum is described by three parameters

3.2.3. Applying the Load Model

DIANA allows a table of frequency-dependent multiplication factors to be applied on a load case. These factors can be defined as complex numbers with real and imaginary components, or as amplitudes and phase angles. A response spectrum can then be generated for arbitrary frequencies, with the multiplication factor being linearly interpolated if it is not specified in the table. The result of such an analysis can then also be stored as complex values or amplitude-phase pairs, regardless of how the load factors were defined.

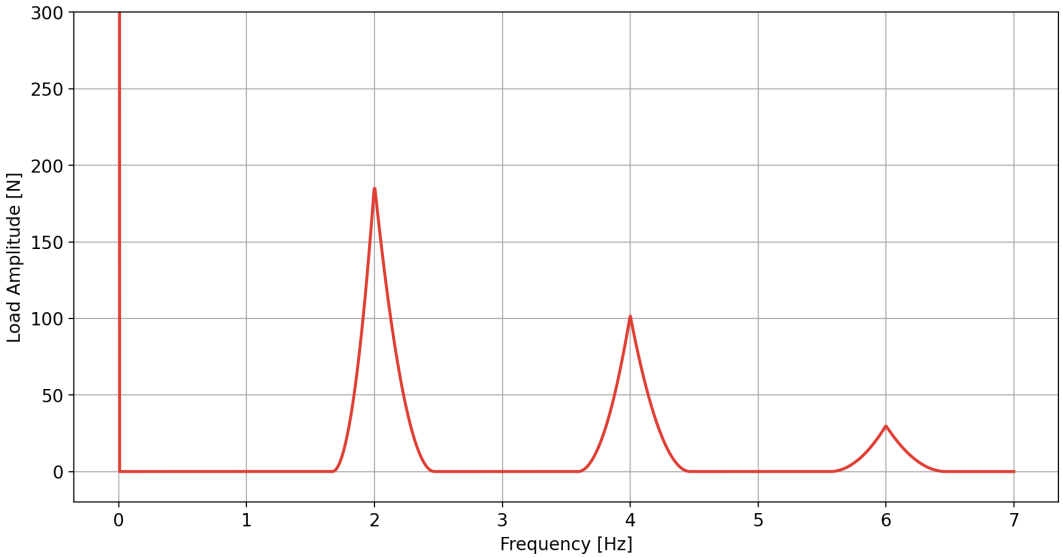

Figure 3.11: Example of a parameterised load spectrum with 3 peaks

The experiments for the dataset were performed in China, where the average weight is lower than in the Netherlands. Furthermore, of the 96 students participating, 54 were male and 42 female, while the most intense groups of spectators at a football match could be expected to consist mostly of males. This may differ at concerts, but a fully male crowd is assumed for simplicity. According to (WorldData, 2020), the average Chinese man weighs 73.5 kg, while the average Dutch man weighs 87.9 kg. For women, this is 62.2 kg versus 73.2 kg. The weighted average mass of the students then becomes 68.6 kg. Dividing the average mass of Dutch males by this number returns 1.28. So, a correction factor of 1.3 will be applied on the crowd loads. This can be done either on the measured loads, before constructing the spectra, or when applying the loads in the model. The latter approach is chosen so the data can be used as-is while constructing the frequency-domain load model, which aligns more with the purpose of the researchers who gathered the data. Of course, using data from crowds more representative of those in (western) football stadia would be preferable, but this is not available.

Aside from the amplitudes of the load spectrum, DIANA also requires phase angles as input. These are all zero by default, which would mean the entire crowd jumps in unison. There also be some spatial variability in real crowd loads, which cannot be modelled by a single spectrum. This is what the load blocks mentioned previously are used for. To model the spatial variability, a separate realisation of the load spectrum for each block was considered, but this would vastly increase the amount of stochastic variables. A large amount of stochastic variables means more evaluations of the limit state function are likely needed to perform a reliability analysis, which heavily affects the runtime. This approach also does not introduce any values for the phase angles. Instead, one realisation of the spectrum is used for each tier of the grandstand, and each load block will have its own phase angle. These phase angles will be randomised and drawn from a normal distribution with zero mean and a standard deviation of 0.2π, which is in accordance with the results of (Chen et al., 2019). New values are drawn every time the model runs, but their value is not part of the stochastic input variables. This means the response of the model will vary, even if the stochastic input is the same. This is considered as random noise of the response, and will be denoted by ε_{phase}. The magnitude of this noise is briefly investigated in the next section, as well as the runtime of the model.

The load model is thus applied as follows: For each tier, a realisation of the parameterised amplitude model is generated, representing 48 or 60 spectators for the lower and upper tier, respectively (that is, four or five rows of twelve spectators). This spectrum is multiplied by 1.3, and divided by the length of the load block along the seating deck to spread the load. The resulting amplitude values are written to the input files of DIANA. Finally, a phase angle is drawn for each load block and written to the input file as well.

3.2.4. Stochastic Variables of the Load Model

Distributions of the parameters in the crowd load model are estimated by fitting the load model 10,000 times on random draws from the dataset, then fitting distributions on the resulting 10,000 sets of load parameters. The correlations between these parameters were also determined, and the most significant value between two parameters is 0.3 (see also Figure B.10 in the Appendix). For simplicity, these correlations are ignored. As the mean of the dynamic load F_{mean} does not affect the accelerations, which will be used for the failure criterion described in the next section, this variable is skipped. This leads to 9 parameters being needed to described one realisation of the spectrum instead of 10.

Fitting the distributions was performed using SciPy, while the reliability analysis is performed in Probab, so attention needs to be paid to the definition of distributions in both implementations, specifically the parameters. For the lognormal distribution, which is used for all crowd load parameters, SciPy uses a 'shape parameter' `s`, defined as the standard deviation of the log-transformed variable. It also uses `loc` as a nonzero lower bound and `scale` as a scaling parameter, equivalent to the exponent of the mean of the log-transformed variable (SciPy, 2023b). Probab has multiple options, but the most intuitive uses the mean and standard deviation of the non-transformed variable, defined as m and s, along with a shift ε (TNO, 2017). The first two values are calculated by SciPy with its `mean` and `std` methods, while the shift can be copied from `loc`.

In Tables 3.2 and 3.3 below, the lognormal distribution parameters as given to Probab are given. Recall that the load spectra represent a certain number of rows of spectators summed up: four for the upper tier (48 spectators), and five for the lower tier (60 spectators). The sampling was performed separately for both numbers, resulting in two distributions for each load parameter, one for each tier.

Table 3.2: Lognormally Distributed Load Parameters for the upper tier with 4 rows (48 spectators) per load block

parameter	unit	μ (m)	σ (s)	ε
$H_{1,48}$	N	188.48	84.95	3.02
$H_{2,48}$	N	102.28	40.42	7.81
$H_{3,48}$	N	30.81	11.23	2.90
$w_{left,1,48}$	Hz	0.3299	0.1862	−0.1644
$w_{left,2,48}$	Hz	0.4075	0.2217	−0.5468
$w_{left,3,48}$	Hz	0.4401	0.2360	−0.9288
$w_{right,1,48}$	Hz	0.4728	0.2309	−2.2520
$w_{right,2,48}$	Hz	0.4872	0.2489	−2.6783
$w_{right,3,48}$	Hz	0.4867	0.2621	−1.3674

Table 3.3: Lognormally Distributed Load Parameters for the lower tier with 5 rows (60 spectators) per load block

parameter	unit	μ (m)	σ (s)	ε
$H_{1,60}$	N	220.56	97.64	−1.56
$H_{2,60}$	N	119.00	46.43	6.95
$H_{3,60}$	N	36.12	13.02	2.42
$w_{left,1,60}$	Hz	0.3286	0.1884	−0.1429
$w_{left,2,60}$	Hz	0.4049	0.2215	−0.5246
$w_{left,3,60}$	Hz	0.4366	0.2352	−0.8804
$w_{right,1,60}$	Hz	0.4745	0.2314	−2.6973
$w_{right,2,60}$	Hz	0.4858	0.2479	−2.6737
$w_{right,3,60}$	Hz	0.4852	0.2626	−1.2112

Figures 3.12 and 3.13 show the probability density functions of the model parameters for the upper tier. The coefficient of variation varies between 0.3 and 0.4 for the peak heights H, and tends to be over 0.5 for the widths w. Many of the lognormally distributed parameters have a negative shift, indicating a negative lower bound. In the PDF's of the peak widths especially, it is clear to see the left tails reaching into negative value. A negative peak width (or height) should not be possible in this load model, and these likely result from the rough fitting procedure described in Appendix B. However, the reliability analysis is expected to focus on the right tails of these distributions, as a higher or wider peak will cause a larger response, the effects of this will be limited. It is also interesting to note that the distributions for the right widths are all very similar, while they differ for the left widths, tending to larger values for later peaks.

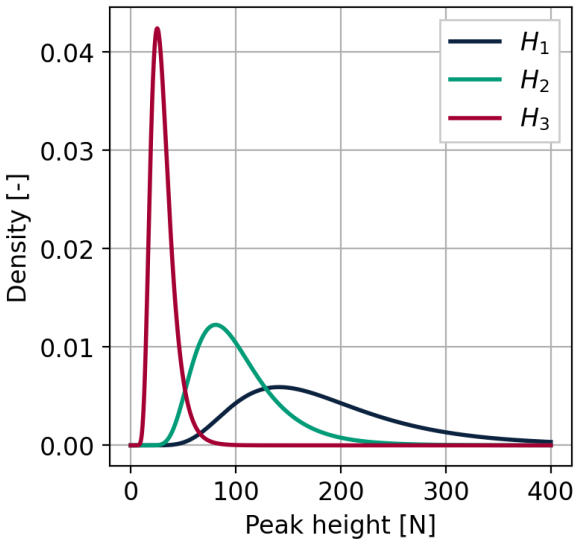

Figure 3.12: Distribution of the heights of the peaks in the load spectrum model for the upper tier

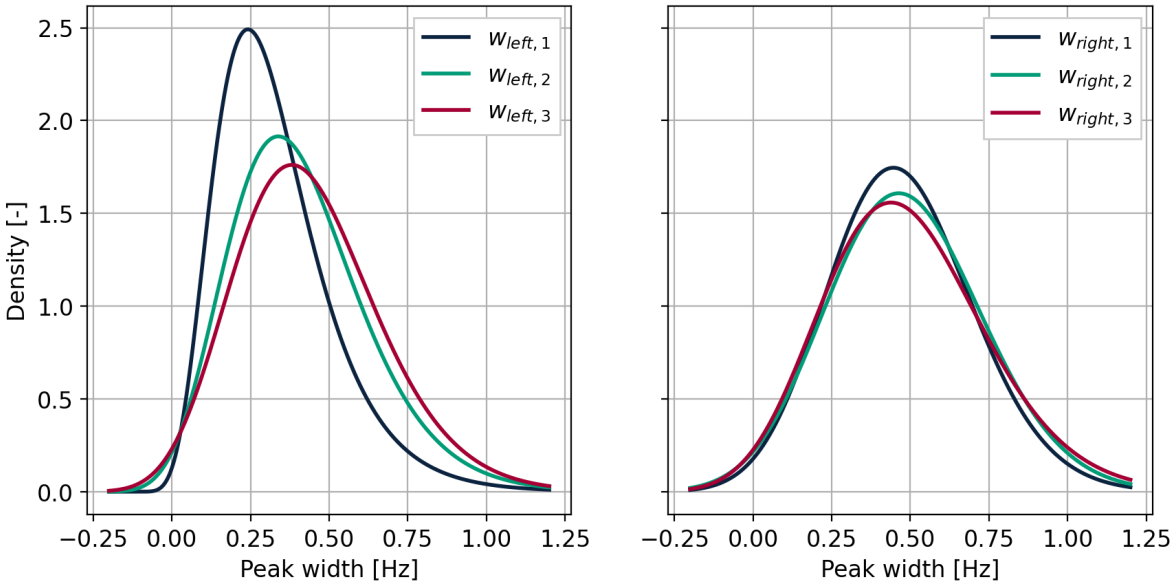

Figure 3.13: Distribution of the widths of the peaks in the load spectrum model for the upper tier

3.2.5. Validation

The following paragraph contains two figures which are used to validate the crowd load model. Figure 3.14 is similar to the lower half of Figure 3.8, with sample spectra plotted over each other to indicate the shape and variance of the loads in frequency domain. On top of that, the percentiles from a large number of samples of the load model are plotted, drawn according to their fitted distributions given in the previous paragraph. For every model sample, a value was drawn for each parameter according to its respective distribution, and the resulting spectrum was generated with a very fine frequency resolution. This indicates how the uncertainty in the load model 'covers' the variance in the sample loads.

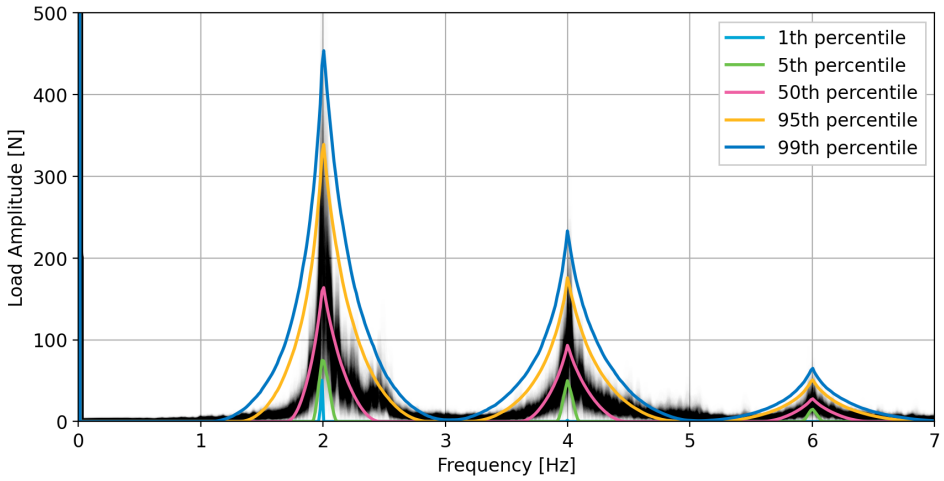

Figure 3.14: Sample load spectra from the dataset with percentiles of samples from the load model

The heights of the peaks at $f = 2, 4, 6$ match very well, with the 50^{th} percentile placed in the darkest part of the plot and the other percentiles forming an upper and lower bound. The peak widths appear to be somewhat too large, as the 95^{th} percentile in between the multiples of f_{target} lies outside the shaded area. This could be caused by the smooth, quadratic shape of the peak not matching the more erratic shape of the sample spectra.

Because slight negative correlations between peak heights and widths have been ignored (see the Appendix), the largest peaks are slightly too wide (and smaller peaks too narrow). To ease the set-up of the reliability analyses, the choice is made to continue without these correlations, even if taking them into account might result in a better representation of the sample data by the load model.

The lowest percentile is nearly invisible at $f = 2$ and $f = 4$. The distributions used to generate the model load spectrum samples, given in Tables 3.2 and 3.3, were determined based on repeatedly generating sample spectra and fitting the model. As mentioned, this resulted in distributions with negative lower bounds for some of the peak widths, as can be seen in Figure 3.13. If a value of w in the load model is negative, that side of the specific peak effectively disappears. This is not expected to significantly affect the reliability analysis, however. A wider peak will result in a larger response, so the right tails of the distributions are more important.

Figure 3.15 shows the vertical acceleration response of the tip of the upper cantilever in the FE-model to the crowd load model with all parameters set to their mean, plotted in blue. In green, the response to a sample load spectrum representative of the darkest area in Figure 3.14 is shown. Both the ‘model load’ and ‘sample load’ responses were calculated at the same frequencies.

At the first peak, the response to the model load is larger than the sample load. At the second peak, the two responses match reasonably well, though it is again clear that the model spectrum does not capture the more erratic shape of the sample spectrum, resulting in some gaps between the two responses. At the third peak, the response to the model load is also slightly larger than the response to the sample load.

Overall, these two figures indicate that the total response is likely somewhat larger when applying the crowd load model, compared to applying sample spectra directly. This means the load model is conservative, and will result in a slight overestimation of the failure probability P_f, which is deemed acceptable for this thesis. The model is considered to be validated, and usable for a reliability analysis considering safety or serviceability criteria.

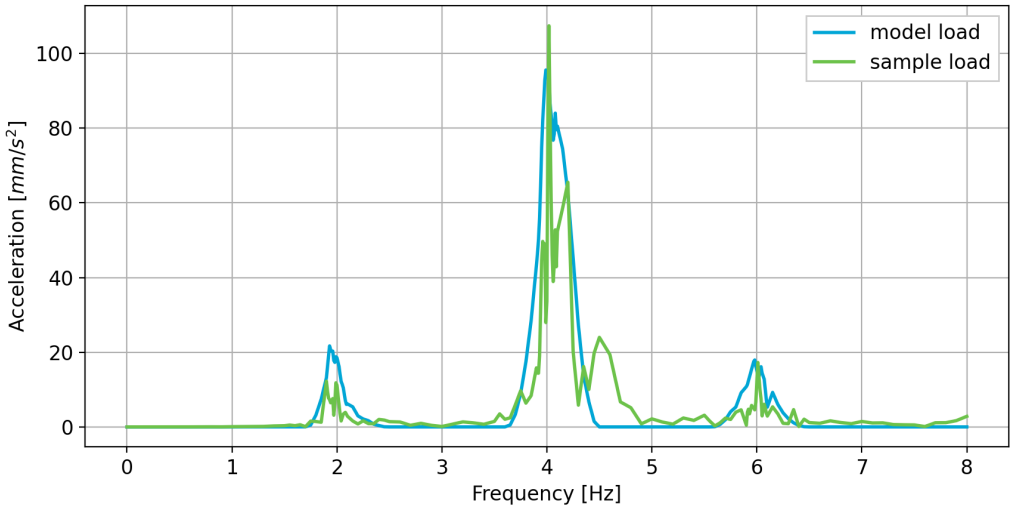

Figure 3.15: Response spectrum of the cantilever tip to a model and sample load spectrum

3.3. Limit State Function

This section describes the failure criterion applied for the case study. Failure criteria can in general be represented by a Limit State Function (LSF):

$$Z = R - S \tag{3.5}$$

Where R is the resistance and S is the solicitation, which is calculated based on the response of the model:

$$S = g(\boldsymbol{X}_{model}) + \varepsilon_{phase} \tag{3.6}$$

Here, $\boldsymbol{X}_{model}$ represents the stochastic input parameters of the model, presented in paragaphs 3.1.3 and 3.2.4. The function $g(.)$ represents the output, which has random noise ε_{phase} added to it due to the phase differences between the load blocks. The resistance R may in general also depend on stochastic parameters, which would be represented by $\boldsymbol{X}_{resistance}$, but this depends on the chosen failure criterion. For this thesis, the primary criterion concerns the Root-mean-square (RMS) of the acceleration, which may not exceed the norm value. This means S is the RMS of the acceleration, and R is the deterministic norm value, so $\boldsymbol{X}_{resistance}$ is not used. The calculation of the RMS value is explained in the following paragraph. After that, the magnitude of the noise ε_{phase} and runtime required to evaluate the LSF is briefly investigated. Many additional criteria could also be thought of, but are not considered in this thesis. A handful of these are shortly described in the last paragraph, along with the reasoning to not consider them.

3.3.1. Failure criterion: RMS accelerations

This serviceability criterion is based on (Jones et al., 2011), and concerns the vibrations of the tip of the upper tier. Multiple different measures for the vibrations 'felt' by spectators exist, but the most recommended one is based on the RMS acceleration, calculated as follows:

$$a_{rms}(t) = \sqrt{\frac{1}{T_s}\int_{t}^{t+T_s} a_w^2(t)dt} \tag{3.7}$$

Where $a_w(t)$ is a frequency-weighted acceleration record and T is a sample time. When T_s is taken as the entire length of the acceleration record, the RMS corresponds to the square root of the power of this signal. Through Parseval's theorem, the power can be calculated in the frequency domain, by taking

the integral of the square of the amplitude spectrum. Effectively, the acceleration is then assumed to be a periodic function of infinite length ($T_s = \infty$):

$$a_{rms,\infty} = \sqrt{\int_0^\infty \left(W(f)|\tilde{A}(f)|\right)^2 df} \tag{3.8}$$

The function $W(f)$ represents the frequency-weighting factors, which are taken from a table in ISO 2631, the norm for human exposure to vibrations (International Organization for Standardization, 1997) and linearly interpolated. Figure 3.16 shows these factors. $\tilde{A}(f)$ is the acceleration response spectrum of the specific location and direction being considered.

Taking the sample time T_s as infinite is not in accordance with the norms, which recommend $T_s = 1$ seconds for panic, and $T_s = 10$ seconds for comfort, resulting in a rolling value $a_{rms}(t)$. The shorter T_s, the more this value is sensitive to short peaks in the acceleration record. When T_s is infinite, the acceleration record is considered as a periodic signal with infinite length, and the power of this signal then quantifies its intensity. The actual length of the acceleration record is then arbitrary, as the time-domain signal itself is never considered anyhow. This calculation is similar to how the variance of a Gaussian Process is calculated, where the variance spectrum is integrated over the frequencies to determine the variance of the signal (Vrouwenvelder, 2022).

This approach does allow for the evaluation of the LSF to be performed entirely in the frequency domain, meaning no inverse Fourier Transform is required, and the frequencies at which the response is evaluated can be chosen freely. It also removes one source of subjectivity in the failure criterion, as no decision needs to be made on the value of T_s. Any phase differences in the response also do not influence the calculations this way. For these reasons, the infinite-T_s approach is chosen, despite its deviance from the norms.

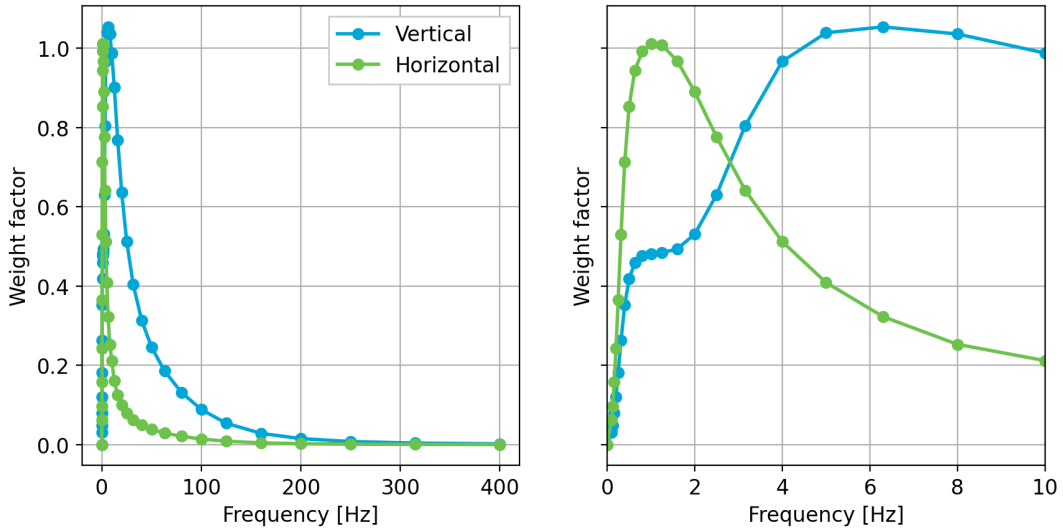

Figure 3.16: Frequency-weight factors for accelerations. Left: full table from ISO 2631 (International Organization for Standardization, 1997). Right: zoomed in to the relevant frequency range

The acceleration response spectrum for every DOF in the model, $\tilde{\boldsymbol{a}}(f)$, is calculated by DIANA as follows:

$$\tilde{\boldsymbol{a}}(f) = -(2\pi f)^2[-4\pi^2 f^2 \boldsymbol{M} + 2\pi f i \boldsymbol{C} + \boldsymbol{K}]^{-1}\tilde{\boldsymbol{f}}_{crowd}(f) \tag{3.9}$$

This is formulated in terms of f, and not ω, as that is what DIANA uses in its documentation (Ferreira and Manie, 2022). For the considered failure criterion, the horizontal and vertical accelerations of the tip of the upper cantilever are used, which are two specific values of $\tilde{A}(f)$ to be extracted from $\tilde{\boldsymbol{a}}(f)$. This post-processing is performed by the Python script. The static load does not influence the accelerations,

and neither does the mean of the crowd load (F_{mean} at $f = 0$). To evaluate the integral in Equation 3.8 numerically, a fine frequency resolution (0.01 Hz) is used around the peaks of the load spectrum - 2, 4 and 6 Hz - and a coarser one between them, where the response is expected to be lower (this is another advantage of not requiring an inverse Fourier transform). An example of a resulting vertical response spectrum has been given in section 3.2.5. The full response spectrum is then approximated using linear interpolation, from which the RMS can be calculated through Equation 3.8, effectively using the trapezoidal rule for the integral.

According to ISO 2631, the vertical and horizontal directions should be combined as follows for serviceability requirements:

$$a_{rms,total} = \sqrt{a^2_{rms,vertical} + a^2_{rms,horizontal}} \tag{3.10}$$

Which is the final value of S for this criterion.

As mentioned, serviceability requirements are generally somewhat subjective. ISO 2631 defines limits for the RMS accelerations experienced by passengers in public transport, but explicitly states that expectations will differ depending on the application and that these values cannot be viewed as general limits. The UK standard mentioned in the Literature Study is focused specifically on grandstands, and uses multiple different scenarios with different types of crowds (The Institution of Structural Engineers, 2008). For 'extreme events' with 'vigorous participation' of the spectators, it recommends 20% of the gravitational acceleration g as a limit, which is 1.962 m/s^2. This deterministic limit is taken as R.

3.3.2. LSF noise and runtime

Figure 3.17 contains a histogram of the total RMS value resulting from evaluating the LSF (the value of S) after running it 500 times, with the mean values of all SV's as input (the distributions of the SV's are described in the next section). This plot indicates the noise ε_{phase} caused by the phase differences applied in the load model. The mean of the 500 results is 1.73 $\mathrm{m/s^2}$, the standard deviation is 0.039 $\mathrm{m/s^2}$, and the coefficient of variation is 0.022, with an asymmetric distribution. This mean is already quite close to the norm value used for R, which means the failure probability could become quite large. If the magnitude of the noise remains the same when other values of the SV's are applied, and the variance caused by the SV's in $\boldsymbol{X}_{model}$ is much larger than that caused by ε_{phase}, the resulting failure probability will not be influenced much by the noise, though its presence could make the application of several of the reliability methods more difficult.

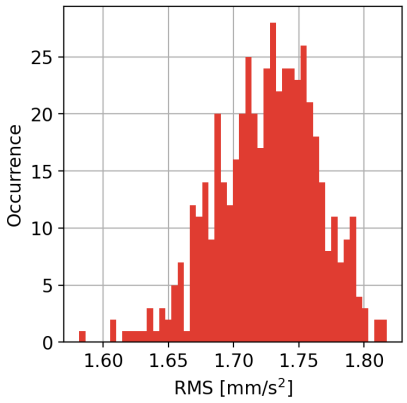

Figure 3.17: RMS results obtained by running the LSF 500 times with SV's set to their mean

During the 500 evaluations of the LSF for the previous figure, the time required for each one has also been recorded, and is displayed in Figure 3.18. With a mean runtime of 13 seconds, the LSF can be evaluated approximately 275 times per hour, and just over 2000 times in a working day accounting for set-up time. In the documentation of Probab (TNO, 2017), analyses using DARS typically take tens of LSF evaluations for simple, analytical Limit State Functions. When more than one design point is present, this increases to a few hundreds. If the LSF of this thesis behaves similarly, the runtime required for the DARS reliability analysis will be quite reasonable. For Monte Carlo, the runtime may be prohibitive, depending on the resulting P_f and the desired $V(P_f)$.

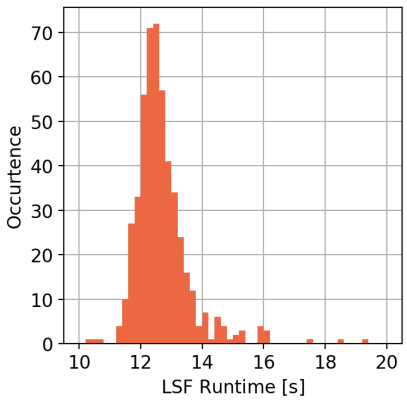

Figure 3.18: Runtimes recorded when running the LSF 500 times with SV's set to their mean

3.3.3. Alternative Criteria

This paragraph lists a handful of alternative criteria which could be considered as well. For each, the values of S and R are shortly explained, and a reason not to use them is given. One problem all of them share is that the value of S would need to be determined in the time domain. Since this requires an inverse FFT, the frequencies at which the model is solved would need to be equally spaced, increasing the runtime by repeatedly solving for a (near) zero $|\tilde{\boldsymbol{f}}_{crowd}(f)|$. The phase differences in the response then also play a role, which they do not for the infinite-T_s RMS accelerations.

Steel Yielding: This criterion was considered at first, but an RMS-based one turned out to be easier to perform, and more in accordance with literature. Failure would be defined as the steel yielding due to the Von Mises-stress (S) reaching the yield strength of the steel (R), causing plastic deformations (de Borst and Sluys, 2015). The yield strength could be described as a stochastic variable, meaning $\boldsymbol{X}_{resistance}$ would contain one value. Furthermore, the location where the maximum stress occurs is not known beforehand, which complicates the post-processing required compared to an SLS criterion where the cantilever tip is assumed to be critical. Together with the time domain-transformation, this criterion would thus be much more difficult to apply, which is why the RMS accelerations were chosen instead.

Stability: S would be the normal force in the members, and R the estimated buckling load of the same members, again leading to more complicated post-processing. From a linear buckling analysis (van der Meer, 2021) using a unit distributed load, performed to indicate the how large buckling loads would be in relation to the dynamic crowd loads, it appears buckling can occur when a distributed load of around 800 N/mm^2 is applied on the seating deck. The largest load value in the entire dataset, multiplied by the number of spectators carried by one truss (492) and spread over the length of both decks results in 16 N/mm^2, one-fiftieth of the buckling load. This very rough analysis does not take the self-weight or dynamic effects into account, yet it is still assumed that buckling of the structure is not a significant concern. Also, determining buckling lengths, imperfections and the like would require significant effort, especially if they were to be described stochastically in $\boldsymbol{X}_{resistance}$.

Switch from tension to compression: A simplified approach to buckling would be to assume failure when a member that is under tension due to self-weight becomes compressed when the dynamic load is applied. The value of S would then be the negative of the stress value in such a member, while R would simply be zero (effectively, the LSF is equal to the stress value, $Z = S$). When the structure is analysed in the time domain, by directly sampling load records from the dataset and spreading these out over the load blocks, it appears that the stresses caused by the dynamic crowd load are much smaller than those caused by the self-weight and the static ($f = 0$) component of the crowd load. This indicates that the probability of this failure criterion occurring is very small, and together with the buckling analysis suggests that response values specific to dynamic load (velocities and accelerations) are more critical in this case.

Displacements: S would be the maximum displacement of the cantilever tip, and R a limit value. No norms specific to grandstands were found for this limit, while the RMS criterion already corresponds closely to literature (albeit with an infinite T_s), so the displacements were not further considered. That said, this criterion does correspond to the measurements TNO performs at the Feyenoord Stadium, which could have made for an interesting comparison to real-world results, if the measurement data was available.

Velocities: The same holds as for displacements.

Collapse of the seating deck: This would be similar to the criterion used by (Weijs, 2023). However, it would be very difficult to model with only a planar model of a truss. The moment capacity of the concrete deck could be used as R, with possible uncertainties in $\boldsymbol{X}_{resistance}$, but this would heavily depend on the unknown characteristics of the concrete, like its profile, strength class and reinforcement. The value of S would then be the bending moment in the span of the seating deck between trusses, which simply is not within the scope of the grandstand model used for the case study. So, this is considered out-of-scope for this thesis.

3.4. Reliability Analysis

This section describes the reliability analyses that are performed, which provide the main part of the results in the next chapter. The first and most straightforward method, Crude Monte Carlo, has been implemented in Python by the author. The other three, SDARS, Directional Sampling and FORM, are applied through Probab.

3.4.1. Author-programmed: Crude Monte Carlo

The first Reliability Analysis to be performed uses a Crude Monte Carlo, through another Python-script written by the author. Values of all stochastic parameters are drawn according to their distributions described in the previous section. For each set of values, the LSF is evaluated, and the percentage of draws resulting in failure is taken as the failure probability. The CMC routine programmed by the author stores the input and output of every LSF evaluations, allowing for a more in-depth analysis of the results. It is also flexible in terms of performing the analysis, being able to run 'sessions' of a set number of evaluations or a maximum runtime, then combining the results of all sessions into a single result.

3.4.2. Probab: SDARS, DS, FORM

The other three Reliability methods to be applied are SDARS, Directional Sampling and FORM. While Probab itself is programmed in Fortran, the author was able to access a Python interface, and adjusted this to use the other Python scripts to evaluate the LSF, and to automatically store the settings and results of the analyses performed, provided they yield a result.

The first method, SDARS, is an evolution of DARS developed within TNO, which allows a start vector to be supplied as input. This start vector should indicate a design point in U-space, allowing the method to find the most important region of the limit state immediately. As a design point is not known beforehand for this case, this option is not used, meaning the difference between DARS and SDARS becomes negligible.

Following advice gathered within TNO, Axis Directional Integration (ADI) was not used, as experience has shown that this does not improve the results while requiring more expensive LSF evaluations. This makes sense, as the roots found by ADI are only used to fit the initial response surface, and will generally be replaced by points in the important region of the limit state anyhow.

Multiple SDARS analyses are performed, with f set to the recommended value of 3 and λ_{add} varying. The coefficient of variation $V(P_f)$ to be reached before stopping the analysis is set at 0.05.

The second method to be applied through Probab is Directional Sampling (DS), the crude method (S)DARS is based on. A large number of LSF evaluations is expected for this method, and Probab does not allow the analysis to be performed in sessions like the author-written CMC routine does. Because of this, $V(P_f)$ is set to 0.1, and the maximum runtime of the analysis is fixed to one working day (8 hours). If, after this time, no result is obtained, the analysis is terminated.

The final method to be applied is FORM, though this will most likely not be able to find a design point. The noise ε_{phase} makes it difficult to compute a numerical derivative, as a (nearly) identical input $\boldsymbol{X}_{model}$ can result in two different values of Z. Figure 3.19 shows what problem this causes: the blue line represents a one-dimensional LSF, with the dashed lines indicating random noise. With two evaluations of the function without noise (the green dots), a tangent can be determined that returns a reasonable approximation of the root (square markers) of the function. When the function contains noise, evaluations at the same locations (orange) can result in a tangent in a random direction, yielding an erroneous root.

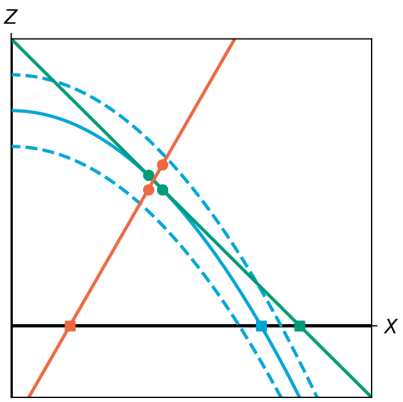

Figure 3.19: Example of how a noisy function complicates using numerical derivatives

3.5. Overview of the methodology

Figure 3.20 contains an overview of the 'train' that forms the methodology of this thesis. The blue arrows represent steps programmed by the author through Python. The input of the Limit State Function is formed by the stochastic variables in $\boldsymbol{X}_{model}$. Of these, the distributions for the two material parameters are taken from literature. The eighteen crowd load parameters (nine for each tier) are based on repeated samples of the crowd load database, upon which the crowd load model is fitted.

Every time the LSF is evaluated, the crowd load parameters set the shape of the load spectrum which is written to the DIANA input file, along with the material parameters. The response of the FE model is then evaluated by running DIANA through the batch file, with the analysis commands in the command file. The results, stored in a tabular output file, are post-processed to find the RMS accelerations, which is the solicitation S in the LSF. Subtracting this value from the deterministic value of R, the limit of $0.2g$ found in literature, then completes the evaluation and returns a value of Z. Together with the distributions of the stochastic variables $f_{\boldsymbol{X}}(\boldsymbol{x})$, these LSF evaluations are used in one of the reliability analyses to arrive at a final result: a failure probability P_f.

Constructing this 'train' by connecting the different components through Python scripts required a significant yet worthwhile effort from the author. As mentioned in the introduction, the grandstand model and failure criterion (and LSF) are case-dependent, while the load model and reliability analysis should be generally applicable. In principle, different grandstand models or criteria could be considered by replacing the corresponding components in the 'train', leading to a different LSF, allowing the methodology to be applied for other cases. For example, an inverse Fourier transform may be added as part of the post-processing, or a different response or location may be considered in the `dcf`-file. In fact, even structures loaded by jumping crowds other than grandstands could be considered, like dance floors. Of course, the FE model may also be constructed in different software with different programming languages used for the script, and different material parameters used as stochastic input. While this would require somewhat more programming effort, the overall shape of the flowchart in Figure 3.20 would remain the same. The input would still be formed by stochastic variables which adjust the model and load, and the output of the model would be post-processed to evaluate the LSF.

The load model and reliability analysis, the second and fourth steps mentioned in the introduction, should be generally applicable. The load model can in principle be used for any case, possibly with different load blocks and a different value of f_{target}. Which reliability method is best used could differ, depending on the specific problem. If a serviceability criterion with a larger expected failure probability is considered, and the runtime of the model is reasonable, Crude Monte Carlo might be very usable. For smaller failure probabilities and 'heavier' models, a more advanced method like (S)DARS might be preferable to limit the number of LSF evaluations.

In the next chapter, the results of the reliability train as it is applied in this thesis are given. After that, its general applicability is discussed.

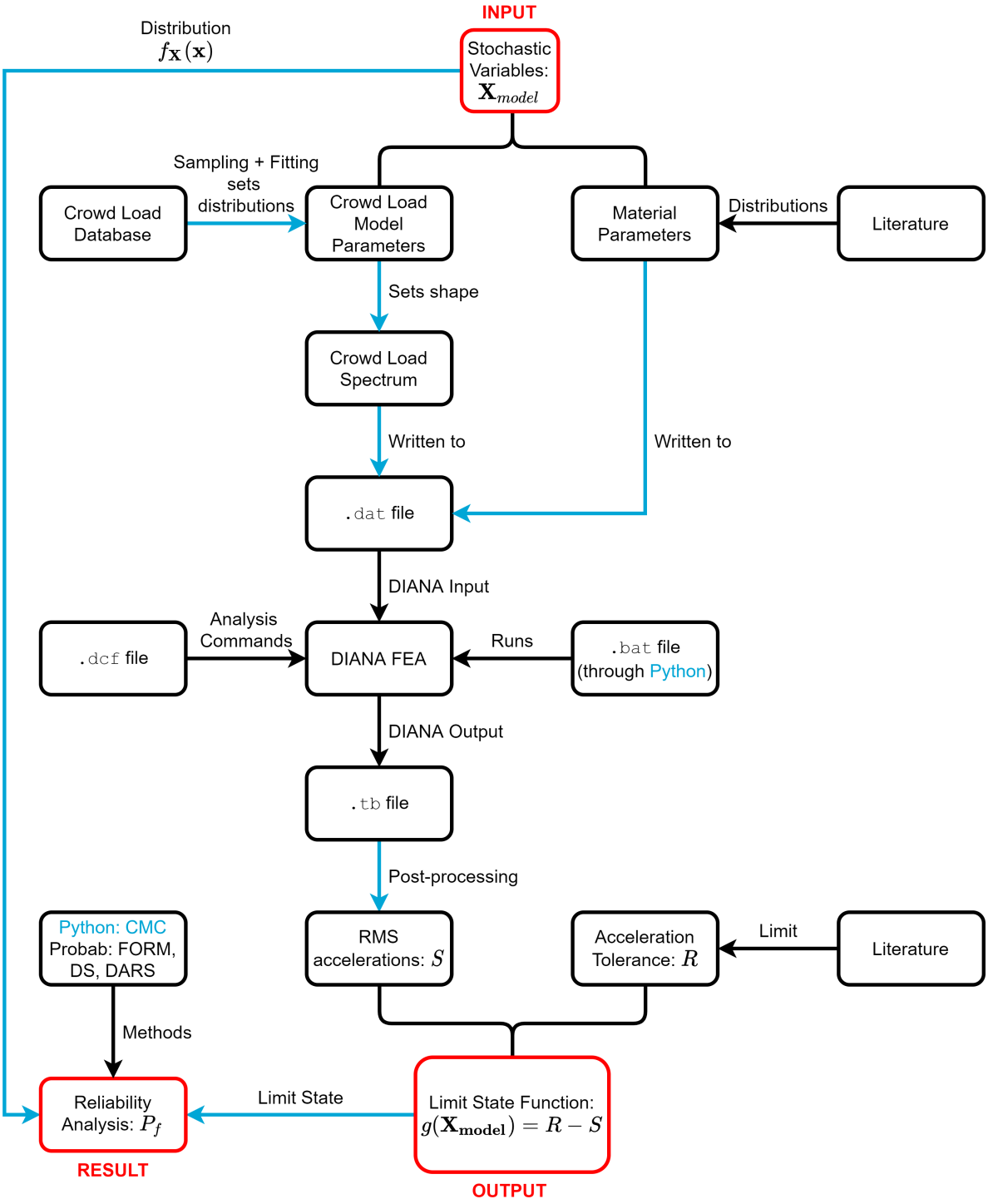

Figure 3.20: Overview of the methodology

4

Case Study Results and Interpretation

The first section of this chapter contains the output of the reliability train presented in the previous chapter, forming the results of the case study. Of the four reliability methods applied, Crude Monte Carlo and SDARS yielded usable results, while Directional Sampling and (as predicted) FORM did not. Why this and what could be done to remedy this will be discussed in the next chapter, which focuses on the general applicability of the methodology.

It should be noted that, while the main result of a reliability calculation is usually referred to as a failure probability P_f, the term 'failure' is rather harsh when a serviceability criterion is concerned, as the structure does not 'fail' in the sense of a collapse occurring. A better term might be the 'limit exceedance probability', still represented by P_f. This term leads to a more fluid interpretation of the CMC results, which will be the focus of the second section of this chapter.

4.1. Reliability Analysis Results

4.1.1. Crude Monte Carlo

Figure 4.1 shows the results of the Crude Monte Carlo analysis, in the form of a histogram. The horizontal axis represents the RMS (S) values resulting from the simulations with random draws of $\boldsymbol{X}$, and the vertical axis the number of times values falling within a certain range occurred.

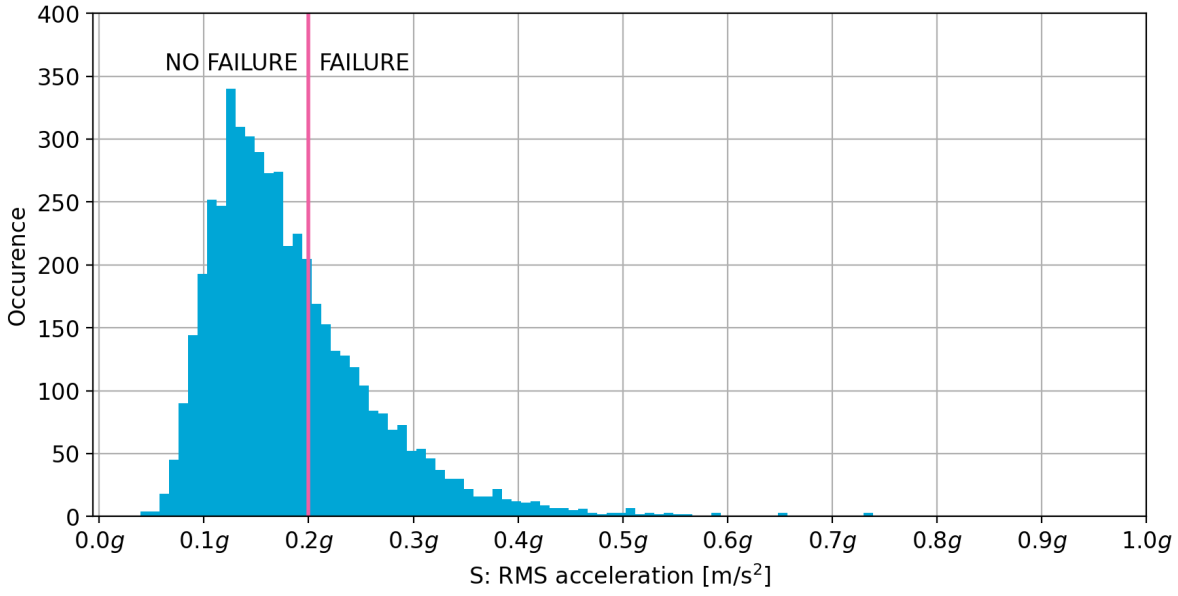

Figure 4.1: Results of the Crude Monte Carlo analysis

The histogram is cut in two sides by the deterministic limit value $0.2g$ (R). Of the 5000 simulations performed, 1632 resulted in an RMS value larger than the limit, which means the limit exceedance probability is found to be **0.3264**.

Aside from the limit exceedance probability P_f, two other measures can be determined based on these results (Jonkman et al., 2017). The first is the reliability index β, calculated through the inverse of the CDF of the standard normal distribution, Φ:

$$\beta = -\Phi^{-1}(P_f) \tag{4.1}$$

For a P_f of 0.3264, β is equal to **0.450**.

The second measure is the coefficient of variation of the limit exceedance probability, $V(P_f)$, which can be estimated using:

$$V(P_f) = \frac{1}{\sqrt{NP_f}} \tag{4.2}$$

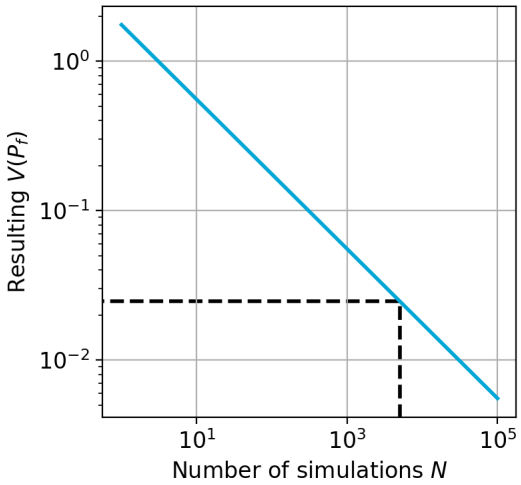

Figure 4.2: CoV of P_f obtained when N simulations result in a P_f of 0.3264. For a smaller P_f, the line would move to the right. The dotted lines indicate the values corresponding to the CMC analysis

With N the number of simulations. This results in a coefficient of variation of **0.0248**. Figure 4.2 shows the relation between $V(P_f)$ and the number of simulations for the limit exceedance probability found through CMC. With $N \approx 1000$, a reasonable $V(P_f)$ of 0.05 could also have been reached. The extra simulations performed allow a more fluid view of the exceedance probability to be formed, however, which will be investigated in section 4.2.

4.1.2. SDARS

Table 4.1 below shows the results of the SDARS reliability analyses. For every analysis, ADI was disabled, and f was set to the recommended value of 3 (Waarts, 2000). The value of $V(P_f)$ to be reached before stopping the analysis was set to 0.05. The value of λ_{add} was varied, and the resulting limit exceedance probability P_f and reliability index β are given for every analysis. Furthermore, the number of evaluations of the LSF and Response Surface are given, along with the runtime.

Table 4.1: Results of the SDARS Reliability Analysis

λ_{add}	P_f	β	LSF evaluations	RS evaluations	Runtime (h:mm:ss)
0.0	**0.428**	**0.182**	123	2377	0:26:11
0.1	**0.444**	**0.140**	161	2921	0:35:41
0.2	**0.400**	**0.252**	186	2503	0:39:35
0.3	**0.408**	**0.233**	316	9724	1:19:36
0.4	**0.420**	**0.202**	425	13460	1:43:56
0.5	**0.417**	**0.209**	519	17083	1:50:21

The limit exceedance probabilities found by SDARS are significantly larger than the value found by Crude Monte Carlo. The number of LSF evaluations needed increases with λ_{add} and was generally much less than the 5000 used for the Monte Carlo analysis, though the resulting values of P_f have a larger $V(P_f)$. As mentioned, to find a P_f of 0.3264 with a $V(P_f)$ of 0.05 with CMC, around 1000 simulations are needed. For the larger values as found by SDARS, around 1000 simulations would suffice, still twice as much as the longest SDARS analysis.

4.1.3. Directional Sampling and FORM

As mentioned, the Directional Sampling analysis would be terminated if it could not find a result within one working day, which was the case. So, no result is available for DS. Also no result is available for FORM, though this was expected. Probab does not store intermediate results, so the number of directions sampled through DS or the number of design point iterations performed in FORM is not known.

4.2. Interpretation of the Crude Monte Carlo results

With the author-written CMC code, able to store the RMS acceleration for every simulation, a different perspective on the serviceability criterion can be formed. Instead of considering a single value for the exceedance probability, based on a single limit, it can be considered as a function of the limit: $P_f(R)$. Figure 4.3 shows this exceedance probability: for every RMS value simulated through CMC, the percentage of simulations exceeding that value is plotted. This is equivalent to the resulting P_f of a CMC analysis that would have used that RMS value as R. Additionally, $V(P_f)$ is calculated for every value of R, and used to indicate the accuracy of the estimated exceedance probability. For $R > 0.4g$, $V(P_F)$ becomes larger than 0.1, though this could be reduced by running more simulations. This shows the reliability train is able to calculate smaller probabilities with CMC in a reasonable amount of time, even values in the order of 10^{-2}, with reasonable accuracy. As an indication, running the 5000 simulations forming Figures 4.1 and 4.3 took around 18 hours, on a laptop with a mid-range processor. The six SDARS analyses were performed in a single working day, on the same laptop.

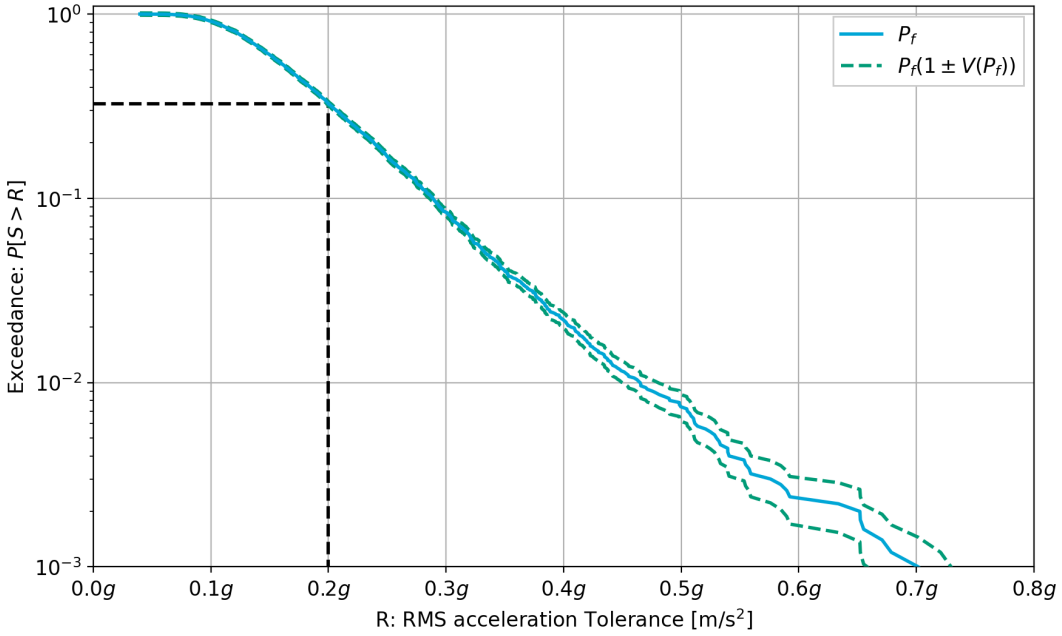

Figure 4.3: Exceedance probability of RMS values calculated from the CMC results, in semilog scale and with coefficient of variation indicated

The feeling of comfort is subjective, so a single limit value will always be somewhat arbitrary and likely on the conservative side. A more complete view of the serviceability with regards to the RMS vibrations could be gathered if the vibration tolerance of individual spectators was known. Combining this with the exceedance probability of vibrations shown in Figure 4.3 could then predict if a spectator will feel uncomfortable during an event where a dynamic crowd load is expected to occur. To illustrate this, an example calculation is performed using an arbitrary distribution of the tolerance: A normal distribution with mean $0.3g$ and standard deviation $0.05g$. The probability density function of R is then defined as $f_R(r)$, and the exceedance probability function of S can be defined as $1 - F_S(s)$. Both of these functions are shown in Figure 4.4.

When S and R in the Limit State Functions have a defined PDF or CDF (from which the exceedance is calculated) like in this example, the integral in equation 2.13 can be re-written as a convolution integral over the resistance r (Jonkman et al., 2017):

$$P_f = \int_{-\infty}^{+\infty} (1 - F_S(r))\, f_R(r) dr \tag{4.3}$$

This integral can be evaluated numerically, which leads to a failure probability P_f of 0.107, and a reliability index β of 1.24, which is closer to a target reliability index of 1.5 for serviceability criteria, found

in literature (Jonkman et al., 2017). No conclusions can be drawn as the definition of R was defined arbitrarily, but this example does show how a more fluid view of a serviceability criteria can be applied when distributions of the solicitation and resistance (or tolerance) are known.

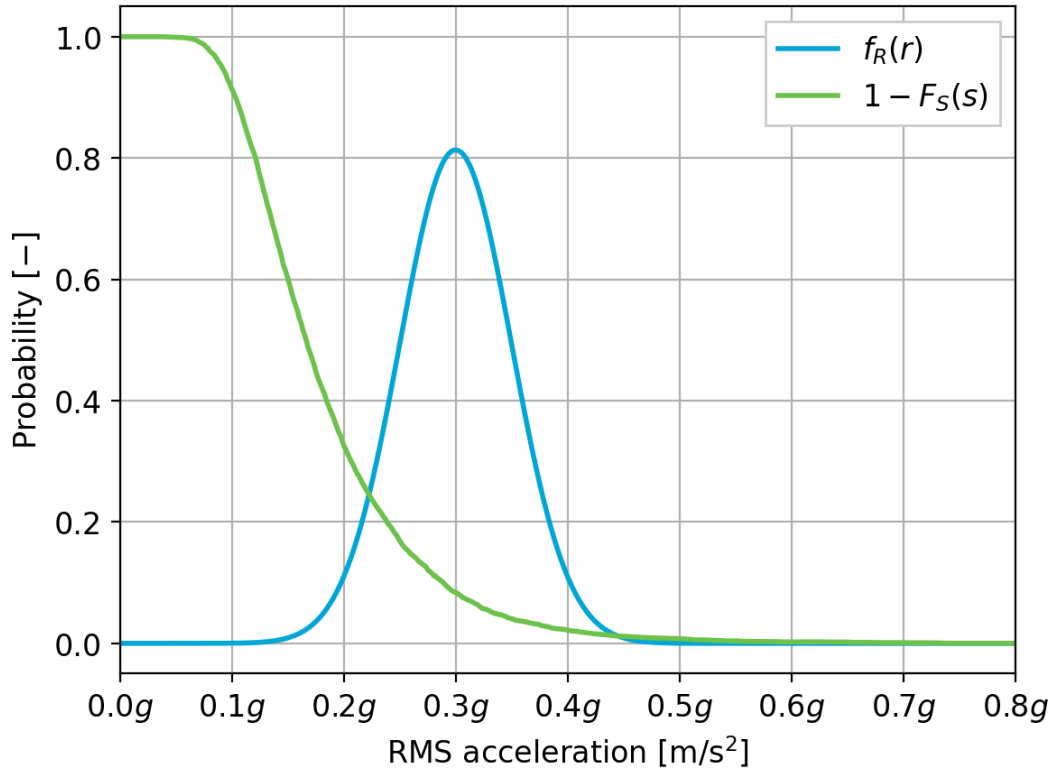

Figure 4.4: Probability density of RMS tolerance R and exceedance probability of RMS value S. The horizontal axis represents realisations of both values, r and s

While the RMS acceleration is a good measure for the intensity of vibrations experienced by the crowd according to literature, spectators themselves may not find it very intuitive. Quantifying the tolerance of individuals with this measure would therefore be rather difficult, especially when the circumstances of a concert are taken into account. Even a spectator with a generally low vibration tolerance will have different expectations during an concert compared to, for example, the train ride to and from the venue. One approach specific to the Feyenoord Stadium could be to monitor the comfort of the spectators (through a questionnaire, a mobile app or other means) at an event where TNO already performs measurements of the upper cantilever. This way, an ‘empirical vibration tolerance distribution’ could be constructed by determining how many spectators indicate discomfort at a certain value of the RMS. This would require measuring accelerations in addition to displacements, though is recommendable anyhow, as accelerations are generally used as a measure for serviceability towards vibrations, and are more practical to measure due to the sensors not needing a reference point.

This concludes the results and interpretation of the case study. The next chapter focuses on the general applicability of the methodology.

5

Discussion of the General Applicability of the Methodology

The purpose of this thesis was to develop a methodology to determine the reliability of a cantilever grandstand under dynamic crowd loading. For the case study, only a serviceability criterion has been applied, calculated in a manner that deviates somewhat from the norms. This chapter investigates whether the methodology could also be used for general cases in future studies, including safety criteria as well. These will generally require evaluating the response of the model in thetime domain (see paragraph 3.3.3), and are expected to result in much smaller failure probabilities, meaning Crude Monte Carlo would likely require too many LSF evaluations to be feasible. So, two specific aspects are covered: transforming the frequency-domain results to the time domain, and the use of reliability methods other than CMC. Additionally, a number of conservative decisions made in the methodology are mentioned.

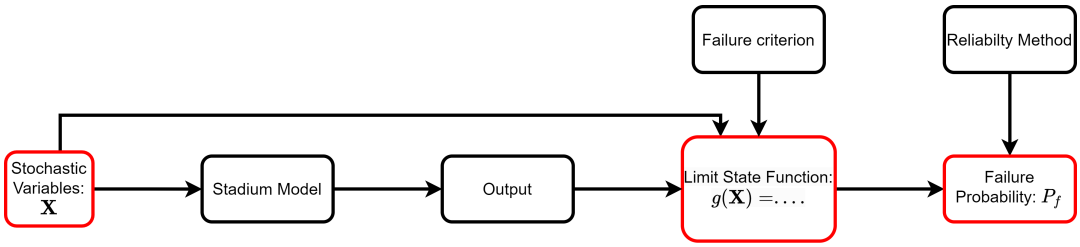

Figure 5.1: Generalised diagram of the methodology

To generalise the methodology, it should also be able to consider other grandstand models (or other structures loaded by jumping crowds), potentially made in other software. It is assumed that these models would function the same as the DIANA model used for the case study, with stochastic input variables in $\boldsymbol{X}_{model}$ setting different aspects of the structure and load, and the output being used to evaluate a Limit State Function. For safety problems especially, the distributions of these variables need to be defined analytically. They are required for the reliability methods more advanced than CMC which will likely be used, for example to transform the variables to U-space. Some of the SV's could be part of the LSF but have no influence the FE model (e.g. the yield strength if the model itself is linear), so these 'skip' the FE model itself and are stored in $\boldsymbol{X}_{resistance}$. This generalised methodology is visualised in Figure 5.1 (which is identical to Figure 2.16).

The load model is assumed to remain the same in principle, with a number of the input variables in $\boldsymbol{X}_{model}$ setting the shape of the amplitude spectrum: the crowd load parameters. Other variables in $\boldsymbol{X}_{model}$, the structure parameters, could for example be Young's Moduli, densities or dimensions of profiles. In essence, generalising the blocks forming the left part of Figure 5.1 comes down to being able to set-up the stadium model, and the routines to adjust it according to $\boldsymbol{X}$ through Python or other means. This is assumed to be possible for any case, and thus not further discussed here.

5.1. Versatility of Transforming Results to the Time Domain

For the following comparison, the vertical acceleration in time domain is considered. The response to a model load spectrum is compared to that resulting from a sample spectrum. In essence, Figure 3.15 is transformed to the time domain. This is done by running the model in frequency domain first, then applying the Inverse Fast Fourier Transform (IFFT), a step that was previously avoided by computing the RMS directly from the acceleration amplitude spectrum. This requires the frequencies for which the response is calculated to be equally spaced, making the analysis less efficient, as using a finer frequency resolution around the peaks of the load spectrum is no longer possible. Instead, a constant frequency resolution f_0 is used, which also sets the length T of the time signal resulting from the IFFT: $T = 1/f_0$. The value of T should correspond to the duration of the dynamic load, which could depend on the failure criterion being considered. In this case, the length of the signals in the (Xiong and Chen, 2021) database is used for convenience: 32.16 seconds, with a sampling rate of 100 Hz. For different response values belonging to different failure criteria, like displacements or stresses, a similar procedure could be followed.

The resulting acceleration signals are given in the Figure 5.2. The model load resulted in a time signal with very large values near $t = 0$ and $t = T$, shown in the top half. This was adjusted with a Hamming window, used to smooth jumps at the beginning and end of signals (SciPy, 2023c). The bottom half contains the result when applying a sample spectra, where windowing does not improve the result.

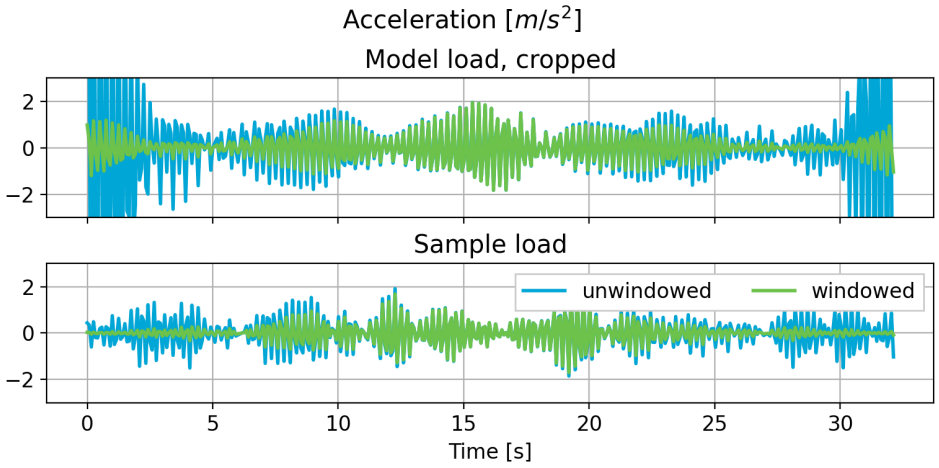

Figure 5.2: Acceleration response to a model and sample load in time domain

The windowed acceleration signal from the model load looks reasonably similar to the unwindowed results from the sample load, though the amplitudes are somewhat larger, and the shape of the signal is more regular. As mentioned in paragraph 3.2.5, is not unexpected that the crowd load model leads to a slight overestimation of the response amplitudes, due to the quadratic peak shape not capturing the erratic shape of the sample spectra. This could have a larger effect on a failure criterion considering the maximum of the response, compared to the RMS accelerations, though the latter is also sensitive to peaks when a short sample time T_s would be used instead of the frequency-domain calculation, as will be shown shortly. This overestimation could be reduced with a different peak shape, and a better fitting procedure, while still using a parameterised shape of the spectrum. Capturing the erratic shape of the spectra will be difficult without increasing the number of stochastic variables, however, so overestimations may have to be accepted.

The cause of the large values in the result from the load model, and not the sample load, is not as clear. A possible cause could lie in the phase differences, which are fully represented for every spectator in the sample load, but were applied in a rough manner in the model load. Drawing a random phase angles for each load block assumes all 48 or 60 spectators in that block are jumping perfectly synchronised with each other, which is unrealistic. Smaller load blocks may be more realistic, and possibly different realisations of the amplitude spectrum for each block could be used, at the cost of increasing the number of stochastic variables.

Another cause could be transient effects appearing from a large force applied at $t = 0$ on the seating deck, as the shape of a decaying vibration at the start is reminiscent of the response of a mass-spring system to an impulse load (Tsouvalas, 2020). The signal resulting from an IFFT is periodic, so the values near the end of the signal would then 'stretch' to match the values at the start. However, in the sample loads, the value at $t = 0$ is nonzero, due to the static weight of the spectators, but this does not cause such a transient effect. This suggests the phase angles are a more likely explanation for the odd shape of the time domain results.

Instead of defining a load spectrum and applying the IFFT, the loads could also be transformed to the time domain first, then applied on the grandstand model. This would require significantly more runtime, while yielding the same result as calculating in the frequency domain for a linear model. Nonlinear models could then also be used, however, which allows a wider variety of safety criteria to be considered. Defining the load in frequency domain while sacrificing one of the main benefits of doing so seems unintuitive, so for criteria requiring nonlinear effects, a time-domain load model might be preferable. Alternatively, a time-domain model could be transformed using the non-inverse FFT, and then the calculations performed in frequency domain. As the thesis of (Weijs, 2023) shows, it is possible to describe jumping crowd loads stochastically in the time domain, but this requires an unreasonable amount of stochastic variables. For linear models, the frequency-domain model still seems promising, though some adjustments are needed before it can be used for general cases.

To further investigate the difference between performing calculations in the time and frequency domain, the calculation of the RMS acceleration in both is compared. Figure 5.3 below shows the same unwindowed signal as the lower half of Figure 5.2: the acceleration response to a sample load in the time domain. Alongside, the time-domain RMS value as calculated through Equation 3.7 for different values of T_s is shown, as well as the value frequency-domain value from Equation 3.8. The response to a sample load is considered to focus purely on the calculation of the RMS value, and not the crowd load model.

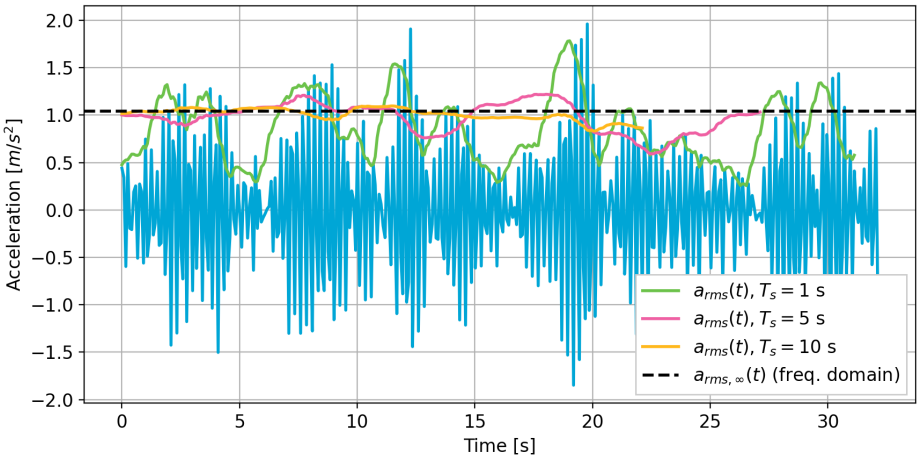

Figure 5.3: RMS values calculated in time and frequency domain, using the response to a sample load. The time domain values are calculated 'forwards', from t to $t + T_s$. No value is given if the sample period eclipses the length of the signal.

Clearly, the shorter the sample time T_s, the more sensitive $a_{rms}(t)$ becomes to peaks in the acceleration signal. As T_s decreases, $a_{rms}(t)$ becomes more constant. At a sampling time of ten seconds, less than one-third of the total signal duration, the time-domain result is already nearly identical to the frequency-domain result. So, there is good correspondence between the calculations in time and frequency domain, as long as short peaks in the response do not influence the considered failure criterion significantly. This is likely the case for many serviceability requirements, though moreso for ones based on the feeling of discomfort as opposed to panic. For safety requirements based on, for example, stresses or strains, the peak value will play a n important role. This means a time domain calculation would need to be performed to properly evaluate the criterion.

5.2. Versatility of Other Reliability Methods

The reason FORM did not work was already covered in the methodology: the noise due to the phase differences makes it impossible to determine partial derivatives numerically. The noise likely also influences the root finding procedure in both Directional Sampling and SDARS. With an LSF containing random noise, the Limit State could be imagined as a 'soft' area instead of a 'hard' line, and any combination of variables $\boldsymbol{X}$ in this area may or may not result in $Z = 0$. This means roots can lie anywhere in this area, too, so λ_0 can differ even for the same $\boldsymbol{\theta}$ (See also Figure 3.19, where the root of the LSF could lie anywhere between the dotted lines). This noise could also affect the algorithm used to find the root numerically, increasing the number of LSF evaluations required. This may explain why Directional Sampling did not yield a result after an entire day of running: finding enough roots to reach the desired $V(P_f)$ simply took too long. Probab does not keep track of the number of directions sampled, nor the number of evaluations needed to find a root, so a better investigation of the performance of this reliability method would require a more flexible implementation of this reliability method.

The evolved version of DS, SDARS, did yield useable results. The failure probabilities were noticeably larger than the CMC result, though still in the same order of magnitude (that said, a larger order of magnitude is not possible for such a large failure probability). The Probab documentation shows that SDARS does not always return the same failure probability as CMC, depending on the shape of the Limit State (TNO, 2017), so a perfect match was not expected anyhow. A possible explanation could be that the quadratic response surface does not capture the shape the shape of the limit state well, such that the roots λ_{RS} near but not in the important region are too small. However, one would then expect the difference between the SDARS and CMC result to become smaller when a larger λ_{add} is used, as more roots are then found with the LSF instead of the RS, but this is not the case. Another cause could be, again, the noise in the LSF. It seems unintuitive that this would cause a consistent overestimation of the sample probabilities P_i, though this could potentially be caused by the combination of a noisy LSF and the specific root finding algorithm used by SDARS. If Directional Sampling had yielded results, a comparison with SDARS could have shed more light on these differences.

Comparing the different SDARS analyses to each other, the values of P_f are reasonably consistent, and the number of LSF evaluations predictably increases with a larger value of λ_{add}. As the limit state is located rather close to the origin in U-space, a small λ_{add} causes much more roots to be evaluated with the LSF, which is why no value larger than 0.5 was used. Because Probab also does not track the number of roots for SDARS, however, the exact influence of λ_{add} is difficult to determine. The number of Response Surface evaluations also increases when a larger λ_{add} is used, which is not as expected. A possible explanation could be that all roots found using the RS are re-evaluated every time the response surface is updated, which happens more often with a larger λ_{add}. This is not something mentioned explicitly in (Waarts, 2000), though it could be an addition to SDARS specifically, and not part of the original DARS method. It is a logical approach as the RS becomes more accurate in the most important direction as more roots λ_{LSF} are found using the LSF, and the most accurate version should of course be used to determine the final set of roots λ_{RS} to calculate the failure probability. The number of RS evaluations this results in may seem wasteful, but these take a negligible amount of time compared to evaluations of the LSF, meaning the extra runtime required is likely insignificant.

Other methods exist that have not been applied for the case study. Some are an evolution of methods that have been used (CMC with importance sampling, for example, or FORM with a response surface), which may be worthwhile to apply on different cases. These are not covered here, though it seems reasonable to assume that most will also be affected by the noise caused by the phase angles.

These phase angles clearly appear to be the most important factor to improve the methodology before it can be more widely applied. To consider the results in the time domain, they need to be defined in a way that better represents the variability between spectators, and to facilitate the use of other reliability methods, they cannot introduce noise. This means they need to be either deterministic, or part of the stochastic input in $\boldsymbol{X}_{model}$. At the very least, if randomly drawn values are used, they need to be drawn *once* at the beginning of the reliability analysis, and then kept constant for every LSF evaluation within that analysis.

5.3. Conservatism in the Methodology

During the construction of the methodology, a number of conservative choices have been made. This means the failure (or limit exceedance) probability is likely to be somewhat overestimated, erring on the side of safety. Of course, this is preferable to a non-conservative approach, where P_f is underestimated and a structure may appear safer than it truly is. On the other hand, an over-conservative approach could result in needless concerns and waste of resources to address them. So, if this methodology is to be used in the future, it is important to be aware of which aspects are conservative, and if adjustments could potentially be made to them, so a number of these aspects are described here.

Every spectator is jumping at a metronome beat: The load model spectrum of a load block is based on a number of samples from jumping individuals, equal to the number of spectators represented by that load block. This implies every spectator is jumping, which may not generally be the case. If a part of the crowd is more passive, of course the dynamic load would be smaller, and so would the response. The sample data was also gathered from individuals jumping with a metronome present, which may be easier to follow than the beat of a song during a concert, let alone a chant during a football match. In general, the participation and coordination of the spectators will differ depending on the event they are attending.

Overestimating the spectra: As mentioned in section 3.2.5, the fitted model load spectra overestimate the sample spectra somewhat, mostly due to the difference in shape between the two. The repeated fitting procedure may also play a role in this, as well as ignoring the correlations between the fitted parameters. This overestimation is more pronounced near the upper percentiles of the spectra, so it may have a larger effect when safety criteria are considered, as the limit state will then be located around the tails of the distribution. As such, the fitting of the model parameter distributions to sample distributions is something that might be worthwhile to improve.

Ignoring Human-Structure Interaction: Including HSI would have likely reduced the response as well (Weijs, 2023), as human bodies add more damping to the mechanical system. It could also have reduced the natural frequencies by adding more mass, but this is case-specific. In theory, this phenomenon could be included in the future by adding the SDOF systems mentioned in the UK Guidance (The Institution of Structural Engineers, 2008), but this would likely require a significant adjustment of the load model.

Only considering one location: For serviceability criteria specifically, the responses experienced by a spectator depends heavily on their location in the grandstand. Those located on the cantilever part of the grandstand will likely experience larger displacements and accelerations than those sitting above a support column. Even when exceedance probabilities of S and individual tolerances of spectators are considered, as suggested in the previous chapter, the 'individual solicitations' will vary, and most will be lower than the value calculated for a critical location such as the tip of a grandstand.

It is difficult to estimate which one of these four factors has the most influence on the resulting failure probability. For wider use of the methodology, all of them could be adjusted in principle. The overestimation of the load spectra springs out, however, as another significant adjustment can be made here if more data becomes available. Currently, the distributions of the load model parameters are based on measurements a relatively small group of Chinese students (Xiong and Chen, 2021), with a correction factor of 1.3 applied to bring them more in line with (male) Dutch spectators. It would be better to fit the model on data representative of the crowd being modeled, with no correction factor needed, but this is currently not available. If it ever is, and the parameters are re-fitted, an opportunity also presents itself to adjust the load model and make it less conservative.

6

Conclusions and Recommendations

This chapter ends the main body of this thesis by drawing conclusions and providing recommendations, both presented as bullet points. First, conclusions are drawn for the methodology as it has been applied in this thesis, followed by its general applicability. Specific conclusions for the case study are also drawn. Then, recommendations are made, mostly for possible improvements to the methodology, and a handful of suggestions for the serviceability of the Feyenoord Stadium.

6.1. Conclusions

On the use of the methodology in this thesis:

- The methodology presented in this thesis is able to determine failure (or limit exceedance) probability for a serviceability criterion based on the response of a cantilever grandstand loaded by a jumping crowd, provided that the criterion can be evaluated in the frequency domain
- It is possible to adjust, post-process and run an FE-model, allowing a Limit State Function (LSF) to be evaluated and a reliability analysis to be performed, using the Python scripts written by the author
- With a Crude Monte Carlo (CMC) analysis, a failure (or limit exceedance) probability of the order of magnitude 10^{-2} and larger can be found with a number of LSF evaluations requiring 2 to 3 working days of runtime, if one LSF evaluation takes 10 to 16 seconds
- With an SDARS analysis, a failure (or limit exceedance) probability of the same order of magnitude can also be found, though the resulting value is somewhat larger than the Crude Monte Carlo result
- An SDARS analysis requires a much shorter runtime, ranging from 0.5 to 2 hours depending on the chosen λ_{add}

On the wider application of the methodology:

- Other Limit State Functions, representing different (models of) grandstands and failure criteria, can be set up with similar scripts as used in this thesis
- In order to evaluate safety criteria, the considered frequency domain response generally needs to be transformed to the time domain
- The current approach to the phase angles does not lead to usable time domain results
- The current approach of dividing the crowd into load blocks and drawing a random phase angle for every block does not suffice, and needs to be adjusted before the model can be applied on general cases

- Other reliability methods, like FORM and Directional Sampling, can currently not be used due to the noise in the LSF caused by the phase differences

On the interpretation of the results with respect to the case study:

- When spectators in the Feyenoord Stadium are jumping at a frequency near the first natural frequency of the stadium's trusses (2 Hz), the probability of the Root Mean Square (RMS) accelerations exceeding the $0.2g$ limit from (The Institution of Structural Engineers, 2008) is in the order of magnitude of 0.33
- As a single limit is somewhat arbitrary, the exceedance probability of a range of limit values can also be considered, providing a less rigid view of the serviceability criterion
- The author-written Crude Monte Carlo code provides the flexibility to determine this exceedance probability as a function of the limit value
- The exceedance probability decreases approximately exponentially with the RMS limit value, for limit values between $0.2g$ and $0.4g$
- To obtain a more complete view of the serviceability of the structure, the tolerance of the spectators to vibrations also needs to be taken into account

6.2. Recommendations

For improving the definition of the phase angles in the load model:

- The approach to determine the phase angles in the load model should be adjusted before the methodology can be applied for other cases
- The model phase angles should represent the variability in phase differences encountered in measured loads, in order to consider the response of a grandstand in time domain
- The model phases should be either deterministic or defined through stochastic variables in $\boldsymbol{X}_{model}$
- The model phase angles should not introduce noise in the Limit State Function as they currently do, in order to apply reliability methods other than CMC and SDARS

For improving the fitting of the load model:

- The distributions of the load model parameters should be fitted to data of jumping individuals representative of crowds in the considered stadiums
- Measurement data should be gathered on crowd loads representative of spectators in Dutch stadiums (or stadiums in the Western world)
- The fitting procedure of the model spectrum parameters should be adjusted to reduce the overestimation of the amplitude spectra
- Correlations in the fitted parameters, specifically between the height and widths of the same peak, should be taken into account in the distributions of the load model parameters

For other possible adjustments to make the methodology less conservative:

- Differences in crowd behaviour at different types of events could be taken into account in the load model, including spectators who are not jumping
- Human-Structure Interaction could be included in the grandstand models, with the crowd represented by SDOF systems, though this likely requires an adjustment to the load model
- For serviceability criteria, more locations could be considered for the failure criterion instead of only the most critical one

For the case study:

- The occurrence of significant vibrations when spectators in the Feyenoord Stadium are jumping at 2 Hz needs to be addressed
- Accelerations should be monitored in the stadium in addition to displacements during certain events, as accelerations are a better measure of the serviceability of the grandstand
- The comfort of spectators should be monitored, in order to obtain a better view of their tolerance towards vibrations

Bibliography

Appelman, S. (2022). *Dynamic Interaction Between Event Deck Structures and a Jumping Crowd* (Master's thesis). Delft University of Technology. http://resolver.tudelft.nl/uuid:e0bada95-bbc1-48a7-b9dd-2992fc483017

Bachmann, H., Ammann, W. J., Deischl, F., Eisenmann, J., Floegl, I., Hirsch, G. H., Klein, G. K., Lande, G. J., Mahrenholtz, O., Natke, H. G., Nussbaumer, H., Pretlove, A. J., Rainer, J. H., Saemann, E.-U., & Steinbeisse, L. (1995). *Vibration Problems in Structures*. Birkhäuser Basel. https://doi.org/10.1007/978-3-0348-9231-5

Blondeel, P., Robbe, P., van hoorickx, C., Lombaert, G., & Vandewalle, S. (2018). Multilevel Monte Carlo for uncertainty quantification in structural engineering. *CoRR*, *abs/1808.10680*. https://doi.org/10.48550/arXiv.1808.10680

Canadian Commission on Building and Fire Codes. (2006). *User's Guide: NBC 2005: Structural Commentaries (Part 4 of Division B)*. (NRCC 48192). https://doi.org/10.4224/40002075

Chen, J., Tan, H., Van Nimmen, K., & Van den Broeck, P. (2019). Data-driven synchronization analysis of a bouncing crowd. *Shock and Vibration*, *2019*. https://doi.org/10.1155/2019/8528763

de Borst, R., & Sluys, B. (2015). *Computational Methods in Non-linear Solid Mechanics*. Delft University of Technology.

Dominik, L. (2023). *The Fink Truss [All YOU Need to Know]*. https://www.structuralbasics.com/fink-truss/ Accessed on 02-10-2023

Ebrahimpour, A., & Sack, R. L. (1989). Modeling Dynamic Occupant Loads. *Journal of Structural Engineering*, *115*(6), 1476–1496. https://doi.org/10.1061/(ASCE)0733-9445(1989)115:6(1476)

Ellis, B. R., & Ji, T. (2004). Loads generated by jumping crowds: Numerical modelling. *Structural Engineer*, *82*(17), 35–40. https://research.manchester.ac.uk/en/publications/loads-generated-by-jumping-crowds-numerical-modelling

Ellis, B. R., Ji, T., & Littler, J. D. (2000). The response of grandstands to dynamic crowd loads. *Proceedings of the Institution of Civil Engineers - Structures and Buildings*, *140*(4), 355–365. https://doi.org/10.1680/stbu.2000.140.4.355

Ellis, B. R., & Ji, T. (1997). HUMAN-STRUCTURE INTERACTION IN VERTICAL VIBRATIONS. *Proceedings of the Institution of Civil Engineers - Structures and Buildings*, *122*(1), 1–9. https://doi.org/10.1680/istbu.1997.29162

Ellis, B. R., & Littler, J. D. (2004a). Response of cantilever grandstands to crowd loads. Part 1: serviceability evaluation. *Proceedings of the Institution of Civil Engineers-Structures and Buildings*, *157*(4), 235–241. https://doi.org/10.1680/stbu.2004.157.4.235

Ellis, B. R., & Littler, J. D. (2004b). Response of cantilever grandstands to crowd loads. Part 2: load estimation. *Proceedings of the Institution of Civil Engineers-Structures and Buildings*, *157*(5), 297–307. https://doi.org/10.1680/stbu.2004.157.5.297

Eurocode Applied. (2017a). *Table of concrete design properties*. https://eurocodeapplied.com/design/en1992/concrete-design-properties Accessed on 23-08-2023

Eurocode Applied. (2017b). *Table of design material properties for structural steel*. https://eurocodeapplied.com/design/en1993/steel-design-properties Accessed on 23-08-2023

Ferreira, D., & Manie, J. *User's Manual – Release 10.6*. 2022. https://dianafea.com/diana-manuals/

Feyenoord. (2017a). *Bezoekersinformatie Feyenoord – Real Sociedad*. https://www.feyenoord.nl/nieuws/nieuwsoverzicht/bezoekersinformatie-feyenoord-real-sociedad-1718 Accessed on 26-09-2023

Feyenoord. (2017b). *Bezoekersinformatie Johan Cruijff Schaal*. https://www.feyenoord.nl/nieuws/nieuwsoverzicht/bezoekersinformatie-johan-cruijff-schaal-1718 Accessed on 07-11-2023

FSV de Feijenoorder. (2018). *Feyenoord, Feyenoord, wat gaan we doen vandaag? Wij gaan winnen, alleen met hoeveel is de vraag! We zullen ze laten beven, ze zullen wat beleven. Feyenoord, Feyenoord, Feyenoord, ole!* https://twitter.com/DeFeijenoorder/status/961689683527917573/photo/1 Accessed on 4-09-2023

Georgiou, L., Racic, V., Brownjohn, J. M., & Elliot, M. T. (2015). Coordination of groups jumping to popular music beats. *Dynamics of Civil Structures, Volume 2: Proceedings of the 33rd IMAC, A Conference and Exposition on Structural Dynamics, 2015*, 283–288.

Ginty, D., Derwent, J., & Ji, T. (2001). The frequency ranges of dance-type loads. *Structural Engineer*, *79*(6), 27–31. https://research.manchester.ac.uk/en/publications/the-frequency-ranges-of-dance-type-loads

Gómez-Déniz, E., Sarabia, J., & Calderín-Ojeda, E. (2021). Bimodal normal distribution: Extensions and applications. *Journal of Computational and Applied Mathematics*, *388*, 113292. https://doi.org/https://doi.org/10.1016/j.cam.2020.113292

Grebowski, K., Rucka, M., & Wilde, K. (2019). Non-destructive testing of a sport tribune under synchronized crowd-induced excitation using vibration analysis. *Materials*, *12*(13), 2148. https://doi.org/10.3390/ma12132148

International Organization for Standardization. (1997). *Mechanical vibration and shock - Evaluation of human exposure to whole-body vibration*. (ISO 2631-1:1997).

International Organization for Standardization. (2007). *Bases for design of structures — Serviceability of buildings and walkways against vibrations*. (ISO 10137:2007). https://connect.nen.nl/Family/Detail/28205?compId=10037&collectionId=0

Jones, C., Reynolds, P., & Pavic, A. (2011). Vibration serviceability of stadia structures subjected to dynamic crowd loads: A literature review. *Journal of Sound and Vibration*, *330*(8), 1531–1566. https://doi.org/10.1016/j.jsv.2010.10.032

Jonkman, S., Steenbergen, R., O.Morales-Nápoles, Vrouwenvelder, A., & Vrijling, J. (2017). *Probabilistic Design: Risk and Reliability Analysis in Civil Engineering - Lecture notes CIE4130*. Delft University of Technology.

Juijn, P. (2013). *Bij benutten ondergrond kost renovatie Kuip maximaal 30 miljoen*. https://www.cob.nl/magazines-brochures-en-nieuws/nieuws/bij-benutten-ondergrond-kost-renovatie-kuip-maximaal-30-miljoen/ Accessed on 13-03-2023

Koper, A., & Kortenaar, M. (2022). *Onderzoek naar de technische oorzaken van het bezwijken van het tribuneelement van het Goffertstadion te Nijmegen* (tech. rep.). HaskoningDHV.

Lourens, E.-M. *System identification and modal testing*. 2021.

Magalhães, F., Caetano, E., & Cunha, Á. (2008). Operational modal analysis and finite element model correlation of the Braga Stadium suspended roof. *Engineering Structures*, *30*(6), 1688–1698. https://doi.org/https://doi.org/10.1016/j.engstruct.2007.11.010

Metrikine, A., & Tsouvalas, A. *Dynamics of Structures - Lecture 8: Modal Analysis of Forced Vibrations of N DOFS with Viscous Damping*. 2022.

NEMO Kennislink. (2008). *Hoe de Kuip Doe Maar weerstaat*. https://www.nemokennislink.nl/publicaties/soliton-in-het-stadion&vensterid=811&cat=259318/ Accessed on 22-09-2023

NOS. (2017). *De Kuip trilt al tachtig jaar*. https://nos.nl/artikel/2165277-de-kuip-trilt-al-tachtig-jaar Accessed on 22-09-2023

NOS. (2021). *Tribune met Vitesse-supporters stort in bij NEC, rellen na afloop*. https://nos.nl/artikel/2402028-tribune-met-vitesse-supporters-stort-in-bij-nec-rellen-na-afloop Accessed on 27-09-2023

NOS. (2023). *PSV halveert per direct capaciteit uitvak Philips Stadion na zorgen constructie*. https://nos.nl/artikel/2464736-psv-halveert-per-direct-capaciteit-uitvak-philips-stadion-na-zorgen-constructie Accessed on 7-03-2023

NumPy. (2022). *Discrete Fourier Transform (numpy.fft)*. https://numpy.org/doc/stable/reference/routines.fft.html Accessed on 23-06-2023

Office for Metropolitan Architecture. *Feyenoord City - Concept Masterplan - Fase 2*. 2016. https://www.commissiemer.nl/projectdocumenten/00003158.pdf

Pavic, A., & Reynolds, P. (2008). Experimental verification of novel 3DOF model for grandstand crowd-structure dynamic interaction. *26th international modal analysis conference (IMAC XXVI)*. https://www.researchgate.net/profile/Paul-Reynolds-21/publication/236029946%5C_Experimental%5C_verification%5C_of%5C_novel%5C_3DOF%5C_model%5C_for%5C_grandstand%5C_crowd-structure%5C_dynamic%5C_interaction/links/0046352da3151cc264000000/Experimental-verification-of-novel-3DOF-model-for-grandstand-crowd-structure-dynamic-interaction.pdf

Reynolds, P., & Pavic, A. (2006). Vibration performance of a large cantilever grandstand during an international football match. *Journal of performance of constructed facilities*, *20*(3), 202–212. https://doi.org/10.1061/(ASCE)0887-3828(2006)20:3(202)

RTL Nieuws. (2019). *Dak van AZ-stadion gedeeltelijk ingestort*. https://www.rtlnieuws.nl/sport/voetbal/artikel/4809756/dak-az-stadion-ingestort

RTV Rijnmond. (2022). *Afblazen bestemmingsplan Feyenoord City is een grote klap voor Rotterdam. Hoe nu verder?* https://www.rijnmond.nl/nieuws/1568894/afblazen-bestemmingsplan-feyenoord-city-is-een-grote-klap-voor-rotterdam-hoe-nu-verder Accessed on 07-11-2023

RTV Rijnmond. (2023). *45 jaar concerten in de Kuip: wat is jouw mooiste herinnering?* https://www.rijnmond.nl/nieuws/1678010/45-jaar-concerten-in-de-kuip-wat-is-jouw-mooiste-herinnering Accessed on 26-09-2023

Rutten, E. R., Bijma, J., & Barendregt, L. (2022). *De Goffert-tribune stortte in, er gebeurde een bijna-ramp en iedereen veegde zijn straatje schoon*. https://www.gelderlander.nl/nijmegen/de-goffert-tribune-stortte-in-er-gebeurde-een-bijna-ramp-en-iedereen-veegde-zijn-straatje-schoon Accessed on 7-03-2023

Santos, F., Cismaşiu, C., Cismaşiu, I., & Bedon, C. (2018). Dynamic characterisation and finite element updating of a RC stadium grandstand. *Buildings*, *8*(10), 141. https://doi.org/10.3390/buildings8100141

SciPy. (2023a). *Scipy.optimize.curve_fit*. https://docs.scipy.org/doc/scipy/reference/generated/scipy.optimize.curve%5C_fit.html Accessed on 22-06-2023

SciPy. (2023b). *Scipy.optimize.stats*. https://docs.scipy.org/doc/scipy/reference/stats.html Accessed on 12-08-2023

SciPy. (2023c). *scipy.signal.windows.hamming*. https://docs.scipy.org/doc/scipy/reference/generated/scipy.signal.windows.hamming.html Accessed on 17-10-2023

Sim, J., Blakeborough, A., Williams, M. S., & Parkhouse, G. (2008). Statistical Model of Crowd Jumping Loads. *Journal of Structural Engineering*, *134*(12), 1852–1861. https://doi.org/10.1061/(ASCE)0733-9445(2008)134:12(1852)

Stichting Koninklijk Nederlands Normalisatie Instituut. (2019a). *General actions – Densities, self-weight, imposed loads for buildings*. (NEN-EN 1991-1-1+C1+C11). https://connect.nen.nl/Family/Detail/28205?compId=10037&collectionId=0

Stichting Koninklijk Nederlands Normalisatie Instituut. (2019b). *Spectator facilities - Part 1: General characteristics for spectator viewing area*. (NEN-EN 13200-1). https://connect.nen.nl/Family/Detail/23033?compId=10037&collectionId=0

The Institution of Structural Engineers. (2008). *Dynamic Performance Requirements for Permanent Grandstands Subject to Crowd Action: Recommendations for Management, Design and Assessment*. Institution of Structural Engineers. https://www.istructe.org/resources/guidance/dynamic-performance-grandstands-crowd-action/

The Stadium Guide. (n.d.). *Stadium disasters*. https://www.stadiumguide.com/timelines/stadium-disasters/# Accessed on 7-03-2023

Tikkanen, A. (2023). *Hillsborough disaster*. https://www.britannica.com/event/Hillsborough-disaster Accessed on 29-09-2023

TNO. *Prob Toolbox 2017*. 2017.

Trompers, A. (2011). *Dode en veertien gewonden bij instorten dak stadion FC Twente*. https://www.bndestem.nl/overig/dode-en-veertien-gewonden-bij-instorten-dak-stadion-fc-twente~aaede2e1/ Accessed on 7-03-2023

Tsouvalas, A. (2020). *Structural Response to Earthquakes*. Delft University of Technology.

van der Meer, F. *Stability of Structures*. 2021.

Vereniging van Aandeelhouders Stadion Feijenoord. (2022). *Historie*. https://web.archive.org/web/20130522095923/http://www.vasf.nl/historie.php Accessed on 15-02-2023, Archived from 22-11-2013

Vinke, R. (2022). *Feyenoord blijft de komende 10 jaar in De Kuip*. https://1908.nl/artikelen/feyenoord-blijft-de-komende-10-jaar-in-de-kuip Accessed on 15-02-2023

Voetbal Rotterdam. (2020). *'Feyenoord kijkt naar tijdelijke huurverlaging De Kuip'*. https://www.voetbalrotterdam.nl/2020/05/feyenoord-kijkt-naar-tijdelijke-huurverlaging-de-kuip/ Accessed on 14-03-2023

Vrouwenvelder, A. *Random vibrations*. 2022.

Waarts, P. H. (2000). *Structural Reliability using Finite Element Analysis* (Doctoral dissertation). Delft Univeristy of Technology.

Weijs, H. (2023). *A Reliability Assessment of Grandstand Elements* (Master's thesis). Delft University of Technology. http://resolver.tudelft.nl/uuid:c2dfcb04-9368-412d-9367-bd8337ed0858

WorldData. (2020). *Average sizes of men and women*. https://www.worlddata.info/average-bodyheight.php

Xiong, J., & Chen, J. (2021). Open Access and Updated Human-Induced Load Data Set. *Journal of Structural Engineering*, *147*(3), 04720003. https://doi.org/10.1061/(ASCE)ST.1943-541X.0002932

A

The Grandstand of the Feyenoord Stadium

This appendix describes the load carrying structure of the Feyenoord Stadium, which is used as a case study for this thesis. The goal of this appendix is to determine, in an exploratory manner, which aspects of the stadium are interesting (and feasible) to model. The focus is on the two characteristic floating 'rings', which have been the defining component of the stadium since its opening. The demountable lower grandstand and cantilever roof structure, both added in 1994, are not structurally connected to the rings, and are thus not covered. First, the global design of the grandstand will be described, followed by a more detailed investigation of the supporting trusses. The possible use for this thesis is also mentioned.

A.1. General description of the structure

Compared to non-overhanging grandstands, cantilevers provide better sight lines and a larger amount of spectators within the same footprint (Reynolds and Pavic, 2006). More subjectively, the crowd being located closer to the pitch also improves the atmosphere of football matches, along with the reflection of noise from fans located beneath the cantilever. The shape of the entire grandstand can be categorized as either one or more continuous 'rings' or ovals around the pitch or as separate, usually straight stands at one or more sides. De Kuip belongs in the former category, though the lower ring has been 'opened' on one side in 1994 to make room for business amenities. Furthermore, both rings are divided into four sectors with a dilatation joint between them, near the corners of the pitch.

The seats are placed on a concrete deck, which can be described as a stack of L-shapes, with rows of seats on alternating horizontal levels, occasionally interrupted by a stair. On the lower tier, this pattern is continuous along the height of the stand, with entrances located at the front and back rows. The upper tier has openings at around half its height, leading to balconies with public amenities. The decks rest on steel beams running parallel to the rows of seats, which are in turn supported on large trusses perpendicular to the beams. Due to the curvature of the stadium, the spacing between these trusses varies somewhat, but it appears to be a few meters. The maximum number of seats between two trusses, at the top of the upper ring, is twelve. Near the middle of the long side of the field, the curvature of the deck is almost zero, so the number of seats should be nearly constant over the height of the grandstand here. Figure A.1 gives an overview of the two rings, and a view of the support structure beneath the first ring.

Two diagrams of the trusses are given in Figure A.2, found in plans for a renovation and for a new stadium (both canceled). The shape can be described as a 'spine' at the back, with two 'arms' in front of it underneath the rings. Note that the left drawing has a typical N-shaped structure in the bottom arm that appears to be missing in the right diagram, which in turn has some small members in the upper part of the spine that are not visible on the left. While differences between the trusses are possible, and some of them could have been altered in the 1994 renovation, the missing members in these drawings appear to be artistic choices by the respective authors. Regardless, both arms have a significant

(a) Front of both rings, from (Voetbal Rotterdam, 2020). The transparent wall on the left is placed above a dilatation joint.

(b) Back of the first ring and trusses (own work)

Figure A.1: Front and back of the main stand of De Kuip

cantilever, with the upper one being over 9 meters. This is among the larger cantilevers found in similar stadiums (Grebowski et al., 2019; Reynolds and Pavic, 2006; Santos et al., 2018). This indicates a low fundamental frequency (Ellis et al., 2000). The lower cantilever appears to be around half the length of the upper one. Both the cantilever and the first span behind it are supported by a beam with a varying profile instead of a truss. This allows the space below this part of the stand to be used for amenities. Considering the load this truss carries in a qualitative sense, it appears the members at the back of the spine will be loaded in tension, and those directly beneath the arms will be compressed.

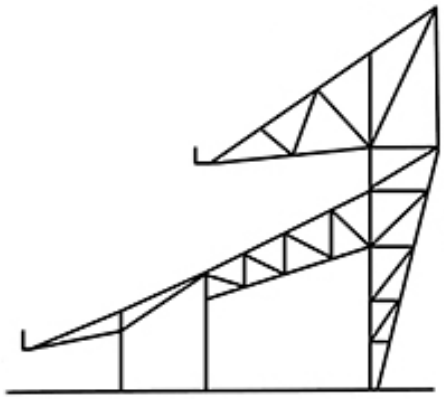

(a) (Juijn, 2013)

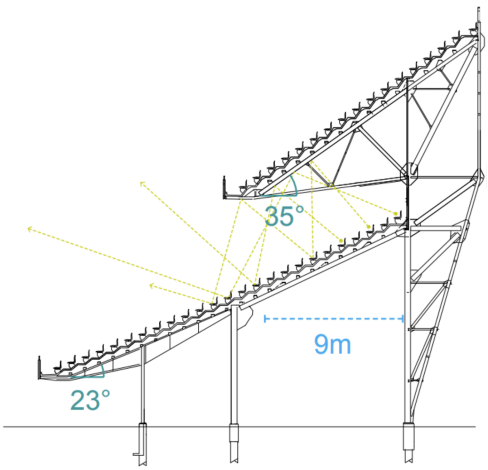

(b) Office for Metropolitan Architecture, 2016

Figure A.2: Two diagrams of the trusses in De Kuip

A.1.1. Use for thesis

The trusses are clearly a vital part of the structure, while being relatively easy to model. The members can likely be modelled using beam or truss elements in two dimensions, which should keep the number of DOFs in an eventual Finite Element model limited limited. While the vibrations of the upper tier are the most notorious, the first cantilever could be interesting too. In any case, the lower part of the truss will play a role in the modal properties, so it should not simply be ignored. Modelling a part of

the concrete deck would be more challenging, as this would require 3D geometry and more complex elements (shells or solids). Due to the nature of reinforced concrete as a material, it would also very likely require nonlinear material behaviour to be taken account of. While making a linear or nonlinear model is not a goal in itself, it has to be recognized that a linear model will be easier to set-up and faster to run than a nonlinear one. It would also allow solving in the frequency domain, which might be interesting given the narrow-banded spectra of rhythmic crowd loads. That said, if second-order effects are to be modelled, which could be significant for slender trusses such as these, geometric nonlinearity would need to be used anyway. If large stresses can appear in the steel members, yielding and plasticity could also play a role.

A.2. Detailed description of the truss

To obtain a more detailed view of the trusses, and to estimate the unknown profiles in the their members, the author has taken a number of photos of the trusses during his visits to the stadium. Several of these are shown in Figures A.4 and A.5. The N-structure in the lower arm is absent at trusses that are connected to a stairwell, so figure A.1b appears to be accurate for these. The profiles used for most of the members fall into one of three categories:

- The vertical members use H-profiles
- The larger diagonal and horizontal members use two U-profiles combined into a H-profile with a small gap.
- Smaller vertical members use L-profiles.

Several members of the second type have been reinforced using plates welded on the flanges of the U-profiles. This not only increases the area and second moment of inertia of the combined profile, but also closes the gap between the two components. The thickness of these reinforcements is hard to estimate due to a thick layer of paint applied over them. The member connecting the tip of the second ring to the spine has an odd profile, see Figure A.5a. It appears to be a H-profile laying on its side, with two additional U-profiles attached to it from halfway across its length.

Most connections in the truss are formed using fin plates and rivets. Such a plate is usually placed in the gap between the two U-profiles of a large, continuous member, like those on the outside of the spine or arms. The web of a smaller diagonal or vertical members is then connected to this plate, meaning it does not make direct contact with the larger member. The moment stiffness of these connections will have a large effect on the modal behaviour of the structure (Santos et al., 2018), but determining this for every connection is not possible. Due to the number of rivets and size of the fin plates, it seems reasonable to expect the connections between the larger members to be quite stiff.

The trusses are connected to each other by small beams and non-structural walls, see Figure A.5b,d,e. The upper walls prevent spectators from walking off the back of the grandstand, and the lower walls surround the amenities of the lower ring. Another wall is placed at the frontmost vertical member, which covers the connection with the varying-height beam. While thin, these walls and members could add additional mass and stiffness to the structure. There are also balconies with public amenities, but these appear to be supported by the stairwells and not the trusses, as the members go through gaps in the concrete floors (Figure A.5f).

Figure A.3 contains an overview of the profile types and the locations of the walls. This includes two members beneath the tip of the cantilever, and another attached to the top of the spine, which are not visible in Figure A.2.

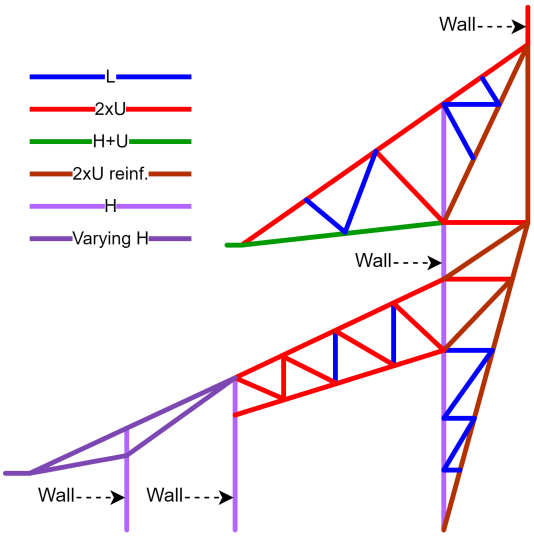

Figure A.3: Overview of profile types and locations of walls in a truss (own work).

A.2.1. Use for thesis

Not enough exact data is available to reconstruct the truss completely, but an estimation can be made. To keep the eventual model simple, only the plane of the truss could be taken into account, resulting in a two-dimensional geometry. Taking the added stiffness of the concrete deck, walls and lateral members into account then becomes difficult, however.

The connections between the members could all be assumed to be either completely rigid or hinged, but neither is very realistic. On the other hand, assuming a moment stiffness for every connection is difficult, so choosing one of these two options is preferable in terms of effort required. Note that, when constructing the truss as a network of nodes and links in modelling software, many ‘connections’ will be partly rigid anyhow, since two of the connected links will be part of a continuous member.

This also depends on the types of elements chosen. Truss elements do not have a rotational DoF and cannot transfer moments, so they are connected by hinges by default. Another option could be to model larger members with beam elements, and smaller ones as truss elements, implicitly assuming the smaller fin-plate connection to be hinged and the larger ones to be rigid. Considering truss structures generally transfer applied load through normal forces, and the size of the fin plates compared to the profiles, this seems less realistic than fully rigid connections.

(a) The connection of the spine to the base

(b) The spine of a truss

(c) An unreinforced and reinforced member

(d) The bottom arm of a truss

(e) The upper arm of a truss. The concrete beneath the ‘armpit’ appears at a few stairwells

(f) The beam supporting the lower cantilever

Figure A.4: A number of photos of the trusses (own work).

(a) The peculiar profile beneath the second ring (brightened)

(b) A connection at the top of the spine

(c) Connection between the N-structure and the beam with the varying profile

(d) The varying profile connecting to a non-structural wall

(e) Walls at the back of the first ring

(f) A member going through a gap in a balcony

Figure A.5: Further photos of the trusses (own work).

B

Creating a Load Model in the frequency domain

This appendix describes the creation of the frequency-domian load model of jumping crowds. The end product of the load model is a Fourier spectrum of the sum of the loads coming from 48 or 60 jumping spectators, which can be described stochastically, as is described in the methodology of the main report. Three approaches are considered to determine this spectrum, and a choice is made between them.

B.1. Approaches and Parameters

The three approaches are:

- Taking random samples from the dataset by (Xiong and Chen, 2021), and applying these directly (after an FFT) on the FE-model - the *Direct* approach
- Parameterising the amplitude spectrum resulting from such samples, ignoring phase differences - the *Amplitude* approach
- Parameterising the complete spectrum (real and imaginary parts), taking account of phase differences - the *Complex* approach

The Direct approach is the easiest to describe: samples are taken from the dataset, summed up, and transformed using the FFT. The resulting spectrum, in complex form, is then directly applied as frequency-dependent load factors in the DIANA input file. The two parameterised approaches are similar to each other: both approximate the spectra as a series of peaks at integer multiples of the base jumping frequency f_{target}, set to 2 Hz in this thesis. Each peak consists of two 'arms' which are described by two parameters: their width w and height H. A parabolic shape is chosen to represent these arms. The left arm of peak k is then given by:

$$P_k(f) = H_{left,i}\left(\frac{(f - f_{peak} + w_{left,i})}{w_{left,i}}\right)^2 \quad \forall f \in [f_{peak} - w_{left,i}, f_{peak}] \tag{B.1}$$

And the right arm:

$$P_k(f) = H_{right,k}\left(\frac{(f - f_{peak} - w_{right,k})}{w_{right,k}}\right)^2 \quad \forall f \in [f_{peak}, f_{peak} + w_{right,k}] \tag{B.2}$$

Where $P_k(f)$ is the value of the absolute spectrum or its real or imaginary component, H is the peak height of the arm and w is its width. The peak frequency f_{peak} is an integer multiple of f_{target}, so $f_{peak} = kf_{target}$ for $k = 1, 2, 3$. For the Amplitude approach, both sides of the peak have the same height, so $H_{right,k} = H_{left,k} = H_k$, while the widths may differ. This means 3 parameters are required

to describe a single peak. In the Complex approach, not only can the value of H differ for both arms of a peak, but separate values for H and w are also needed for the real and imaginary parts. This means 8 parameters are needed for one peak. Figure B.1 shows an example of a peak fitted using the Amplitude approach and the real part of one fitted using the Complex approach.

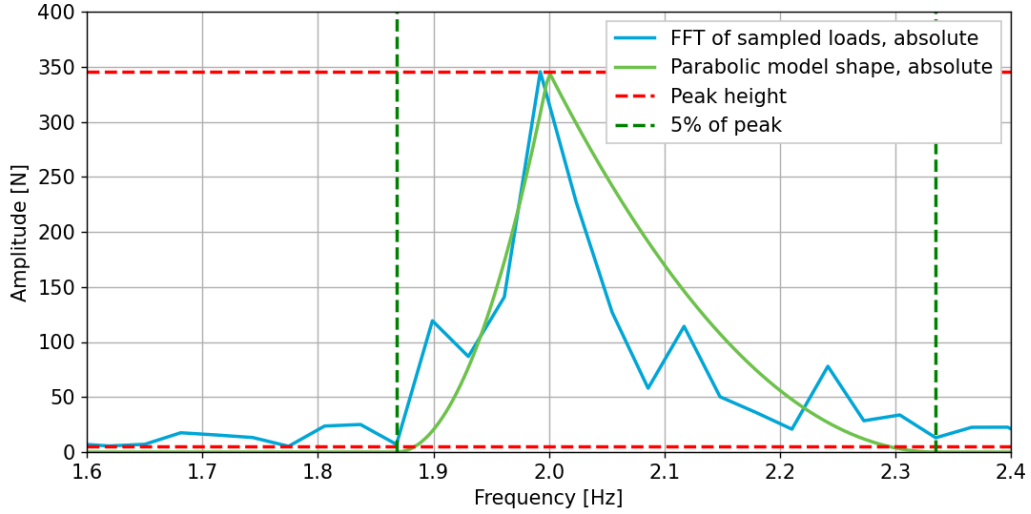

(a) Amplitude approach

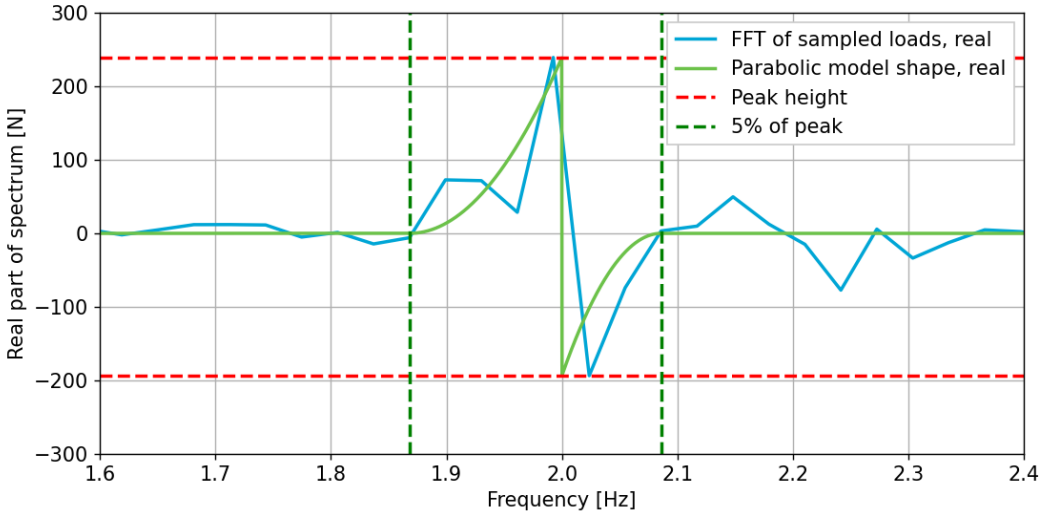

(b) Complex Approach - Real component

Figure B.1: Fitted peaks on sample spectra (both based on the same samples)

Initially, fitting parameters was performed using a nonlinear least-squares (NLLS) optimization in Python (SciPy, 2023a), but this was slow and often led to nonsensical values for the fitted parameters. This is likely due to the relatively coarse frequency resolution and the erratic shape of the spectra, including frequent sign-switching for the Complex approach. A more rough method was used instead, where the values of H and w for every peak are estimated directly from the sample spectrum. This method works best when the parameters can be estimated in an intuitive way, which is the case for the parabolic arm shape. In Equations B.1 and B.2, H is simply the height of the arm at f_{peak}, while w is the distance from f_{peak} at which the arm height $P_k(f)$ is zero, so it can intuitively be estimated by finding a value where the spectrum becomes small.

The heights H are thus estimated by simply taking the maximum value of the spectrum around f_{target} for the Amplitude approach, or the value with the largest magnitude (positive or negative) for the Complex approach. The width w is estimated by finding the frequency at which the sample spectrum value is smaller than 5% of the absolute value of H. This will always be frequencies of the FFT of the sampled load when fitted this way, meaning the 'resolution' of values w can take is quite rough. Figure B.1 shows an example of how this fitting procedure works, and what a peak then looks like. The estimated values are indicated by dotted lines. This method is much faster and more stable than uisng NLLS.

Other arm shapes were also considered, and a comparison between three options is given in Figure B.2. One of the alternatives is an asymptotic shape, which appears to approximate the shape of the arms of the peak better than the parabolic shape for some sample spectra, but it overestimates the peak height. Fitting the parameters with the rough method is also less intuitive, while the nonlinear least squares method leads to more numerical problems and was even slower. Another alternative is a Gaussian shape, which tends to underestimate the peaks and tails of the peaks when fitted using NLLS. It also has the same numerical problems as the asymptotic shape, which seem to be endemic for models with many parameters fitted on erratic data. While other shapes could potentially result in a better approximation of the spectra, it is decided to continue with the parabolic shape in the interest of time.

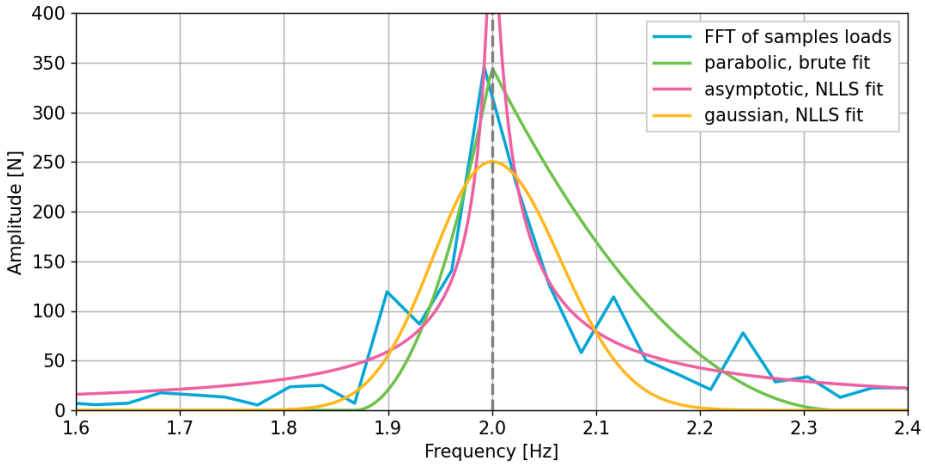

Figure B.2: Comparison of arm shapes for the Amplitude approach

In addition to the peaks, the mean value of the load F_{mean} is applied as an additional parameter. This value is simply inserted as the value of the spectrum at $f = 0$ for the Amplitude approach, and as the real component at the same location for the Complex approach. So, to describe K peaks, the Amplitude approach requires $3K + 1$ parameters, while the complex approach requires $8K + 1$. For all these parameters, a distribution can be determined by repeatedly drawing samples from the dataset and constructing a sample load spectrum, as in the Direct approach, and fitting the parameter values that approximate the shape of this spectrum. By recording the fitted values of the parameters for every sample spectrum, a distribution for each parameter can be determined, as well as possible correlations between the parameter values. Strongly correlated parameters could combined into one stochastic inputs, reducing the number of variables in the limit state function. How well this fitting procedure works is part of the criteria used to decide between the three different approaches, which is done in the next section.

B.2. Selection

The criteria used to select an approach are:

- Low number of parameters needed to describe them
- Able to fit a distribution to the resulting fits of the parameters
- Usability of the resulting Limit State Function
- Flexibility in frequencies that can be calculated
- Approximation of the shape of the 'True' spectra
- Approximation of the variance within the 'True' spectra

The Direct approach is clearly the best when considering the last two criteria, though not perfect considering the frequency resolution is not infinitely fine. It completely fails on the first four, however. The number of spectators modelled is 492, and the number of usable records is 204. Aside from requiring repeated samples, this means 492 discrete stochastic variables are needed to described the load, each with 204 different realizations with equal opportunity. The only distribution that could be fit on this is a uniform distribution, where a realization within a certain bound would correspond to a certain record. These records are also not sorted by their 'resulting' RMS vibration, and doing so is not feasible, as this ordering could be influenced by the location where it is applied just as well as the the load record itself. This means the resulting Limit State function using this approach would have at least 492 different variables, and would contain many erratic jumps along each of these many dimensions. Furthermore, the frequency resolution used when applying the loads to the FE model would have to be the same as that of the original records, or an integer multiple, otherwise the spectra would have to be interpolated for frequencies not present in the FFT of the records. Zero-padded records could be used to increase the number of frequencies in the FFT, but this does not truly result in a better frequency resolution.

The two parameterised approaches do not suffer these problems. For two realisations of the spectrum and three peaks, the Amplitude approach requires 20 stochastic variables (SV's), and the Complex approach requires 50 (though F_{mean} can be skipped when only the RMS acceleration is considered for the response, resulting in 18 and 48 realisations SV's, respectively). This is still a significant amount, but much less than the 492 for the Direct method. Furthermore, the distributions of these stochastic variables can be determined from repeatedly fitting the parameterized spectra on sampled spectra, as mentioned. If these distributions can be approximated by well-known distributions from literature (e.g. normal, log-normal), no discrete stochastic values are needed, and the Limit State-function will be much more usable compared to the Direct approach. Finally, the function describing the spectrum can be evaluated at any value of f, so the frequency resolution can be freely chosen. In fact, most plots in this appendix use a very high frequency resolution to display smooth lines, but the resolution used in the final analyses can be tuned to find a compromise between accuracy and runtime of the FE-model. This does require the FFT to have the same units as the original signal to prevent scaling issues, which is done by setting the normalization option in NumPy to 'backward' (NumPy, 2022).

B.2.1. Variance in load

From now on, the Direct approach is disregarded for use in the final Limit State function. It can still play a role in choosing between the two parameterised models, however, as the fits of both are based on samples taken as in the Direct approach. First, considering the variance within the 'True' spectra, the following procedure is followed: 1000 sample spectra are drawn, and for each the parameters are fitted on the first three peaks to create 1000 parameterised spectra. The sample spectra are then plotted over each other with a large transparency, which visualizes their variance: the darker an area in the resulting plot, the more spectra overlap there. Over this plot, percentiles (1, 5, 50, 95, 99) of the parameterized spectra are plotted. These have been generated using a much higher frequency resolution than the underlying sample spectra, and the percentiles are calculated for each frequency. Assuming the distribution of the 'True' spectra is symmetric, the upper and lower percentiles of the parameterised spectra should form an envelope around the shaded area, while the 50th percentile should follow the darkest area of the plot. The result is given in Figure B.3 and B.4.

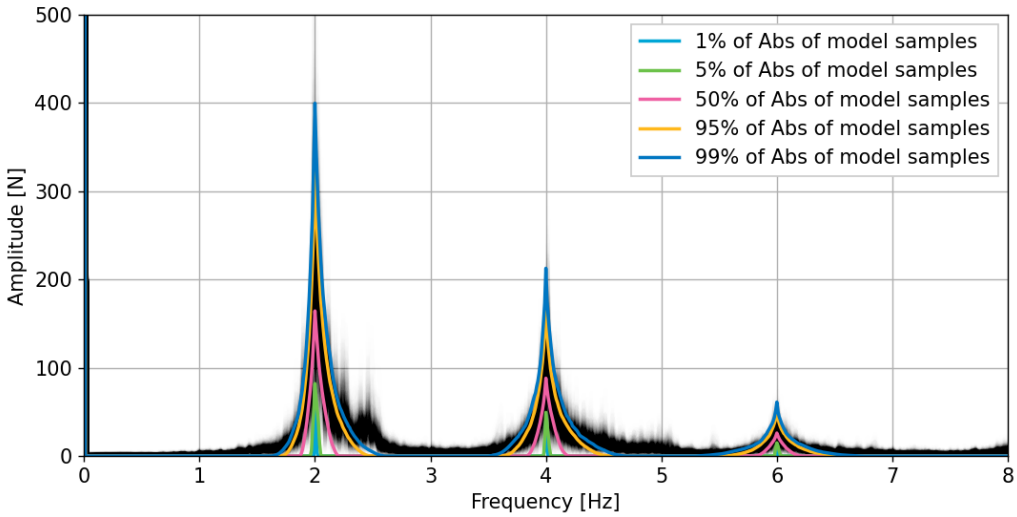

Figure B.3: Layered Plot comparing the variance in direct sampling and parameterized spectra for the Amplitude approach

With the Amplitude approach, the upper percentiles form a good upper bound near the center of the peaks, but less so around the tails. Both the lower percentiles and median appear to be too low, though this is hard to tell around the peaks. Around the tails, it is clearly visible that the 50th percentile lies beneath the darkest part of the layered spectra, and there is a large gap between the shaded area and the lower bounds. This is likely due to the rough fitting approach underestimating the widths of the peaks, as previously mentioned. The effect appears to be worse for the right arms of the peaks compared to the left, and worse for the first two peaks compared to the third.

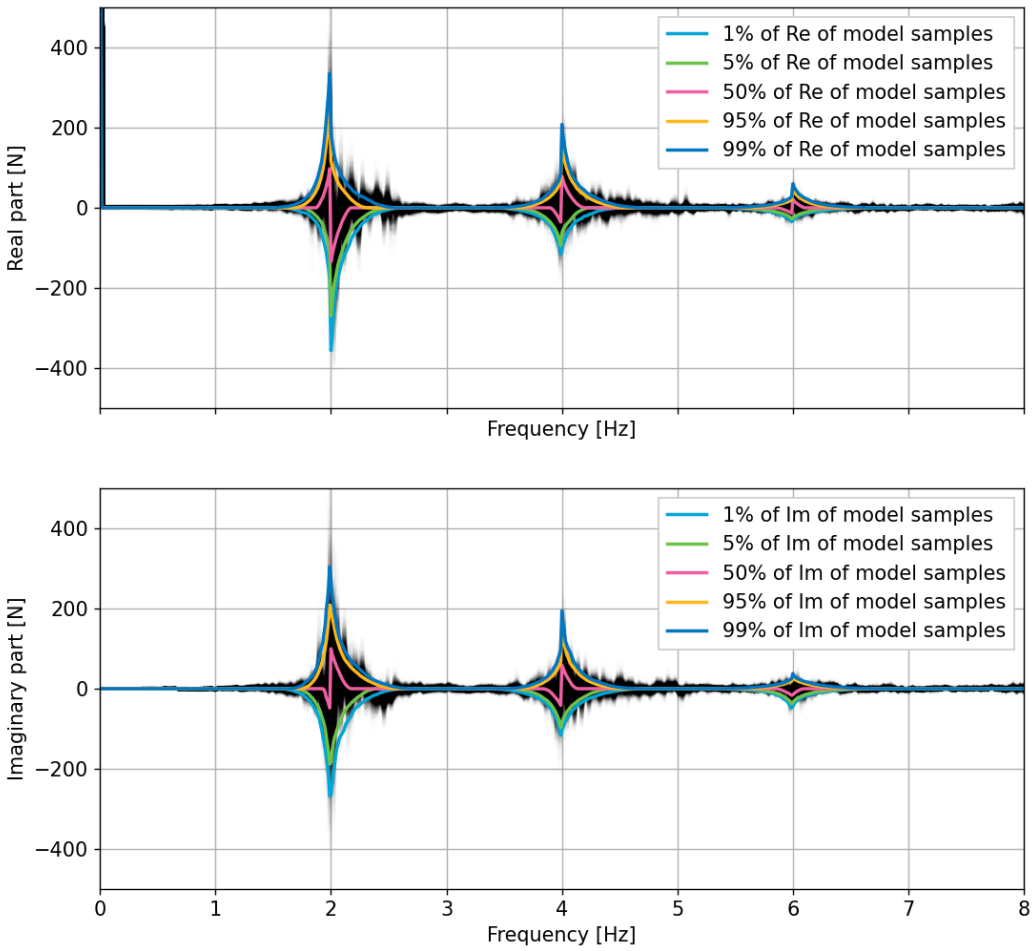

Figure B.4: Layered Plot comparing the variance in direct sampling and parameterized spectra for the Complex approach

With the Complex approach, the darkest part of the layered plot is much wider, and the median falls neatly within it. This is due to the peaks taking both positive and negative values, though for every arm one sign clearly occurs more often than the other. This suggests peak values close to zero do not occur very often. The distribution of the peak parameters could then have two peaks itself, which would be difficult to describe using well-known distributions. The upper bounds and lower bounds create a reasonably accurate envelope for both the real and imaginary parts of the spectra. The erratic jumps are worse in the complex representation of the spectrum, again often switching signs, causing more ‘gaps’ to appear between the bounds. There does not appear to be a pattern between the peak signs of the real and imaginary parts across the peaks. The signs of the mean are flipped for the first peak, but not for the second peak, and only on one side for the third. The widths are generally larger for the Complex approach compared to the Amplitude approach. Overall, while neither approach is perfect, the Complex approach generally captures the variance in the ‘True’ spectra better than the Amplitude approach.

B.2.2. Distribution of parameters

The second comparison covers the distributions of the parameters that describe the parameterised spectra. This comparison is performed by, once again, drawing a large number of sample spectra (10,000 in this case) and plotting histograms and covariance matrices of the resulting fitted parameter values. This is done considering the first three peaks, and thus 10 parameters for the Amplitude approach and 25 for the Complex approach. Displaying all of the resulting histograms is not useful, so a select few are presented here, along with fitted distributions.

First, the mean value of the load signal, or rather the real/absolute value at $f = 0$ in the spectrum, shown in Figure B.5. This value is identical for both parameterised approaches, and its distribution clearly resembles a normal distribution. This parameter can thus be very easily described by a stochastic input and then implemented in a reliability analysis.

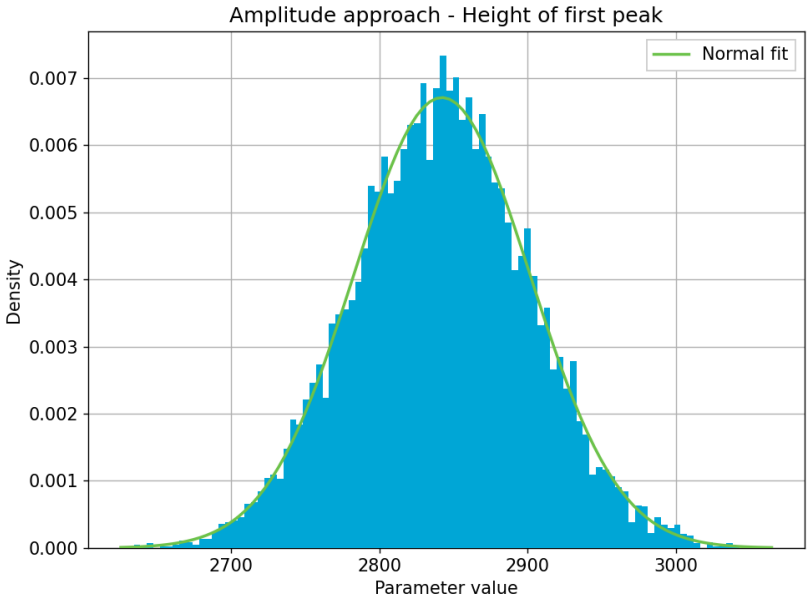

Figure B.5: Distribution of the mean of the load spectra

Next, the height of the first peak in the Amplitude approach, shown in Figure B.6. This parameter, as well as the height of subsequent peaks, appears to follow a lognormal distribution. This can also easily be implemented, possibly by using the natural logarithm of the actual value (which is then normally distributed and can be easily transformed to standard-normal space). This distribution is not symmetric, which can explain why the 50th percentile in Figure B.3 does not follow the darkest part of the layered plot.

Then, the left width of the first peak in the Amplitude approach, shown in Figure B.7. As mentioned previously, the values this parameter can take depend on the frequency resolution of the sample spectra. This means its histogram appears as a discrete random variable, (emphasised in the figure by spacing out the bars). Fitting a continuous distribution on this data is then less accurate, as the fitted data is effectively rounded up or down to a handful of possible realizations. A lognormal distribution still appears as a good candidate, though its harder to judge its accuracy. The values for the right width of the first peak and subsequent peaks are similar.

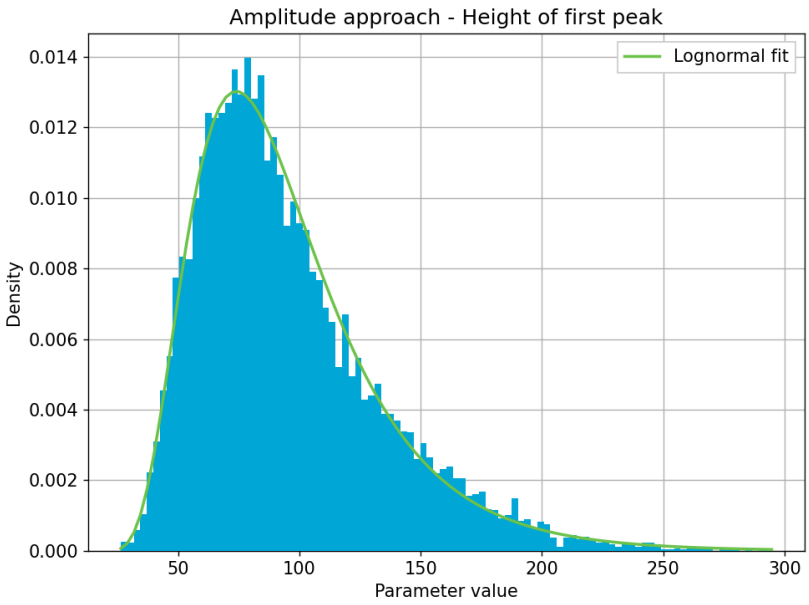

Figure B.6: Distribution of the height of the first peak of the absolute load spectra

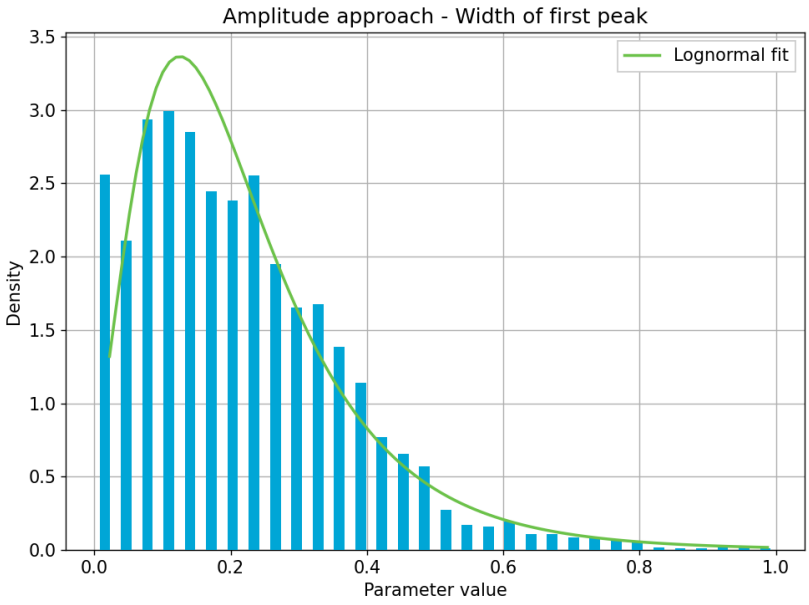

Figure B.7: Distribution of the left width of the first peak of the absolute load spectra

On to the parameters of the Complex approach. The height of the right side of the first peak in the real part is shown in Figure B.8. As expected, both positive and negative values occur, but no values close to zero, leading to a bimodal distribution. A lognormal distribution, as in the Amplitude equivalent values, clearly does not describe the histogram accurately. A bimodal normal distribution has been found in literature (Gómez-Déniz et al., 2021) and fitted, but also does not yield an accurate result. Implementing a custom distribution like this in SciPy is doable, and has been done to fit it here, but performing a reliability calculation with it will be difficult. The handful of other bimodal distributions implemented in SciPy by default also do not yield any usable result, if the fitting succeeds at all (and it often does not). Subsequent peaks, and peaks in the imaginary parts, show the same pattern. Generally, the distribution is asymmetrical, which could be expected looking at Figure B.4 and its non-zero means.

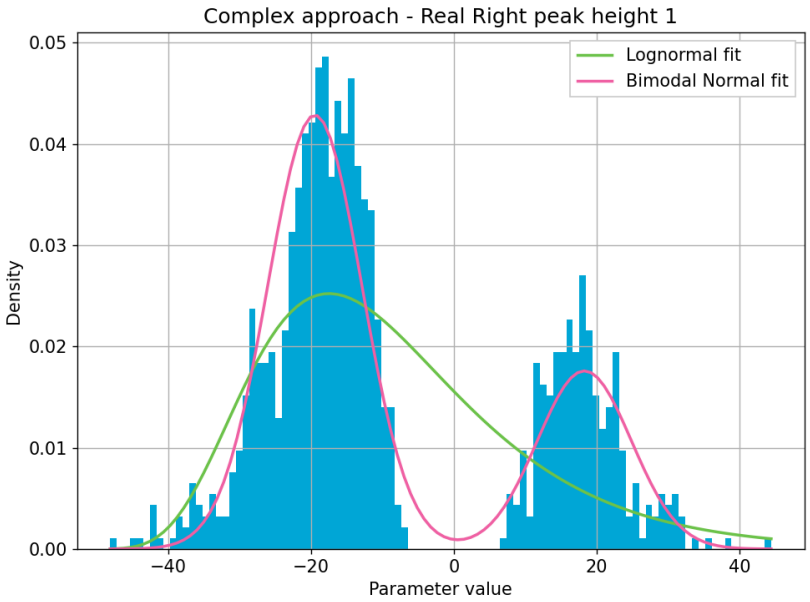

Figure B.8: Distribution of the height of the first peak of the real part of the load spectra

The width of the peaks in the Complex domain, as in Figure B.9, show the same as the widths in the Amplitude approach, with worse fits. This also corresponds to Figure B.4.

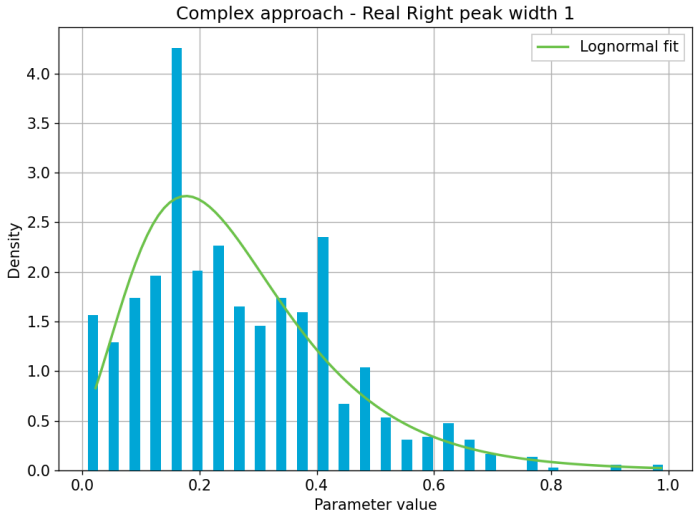

Figure B.9: Distribution of the left width of the first peak of the imaginary part of the load spectra

Finally, Figures B.10 and B.11 show the correlations between the parameters for the two approaches. The color of every cell in these grids represents the Pearson correlation coefficient between the corresponding parameters within the 10,000 performed fits.

In the Amplitude approach, the heights of the first and third peaks are somewhat positively correlated with the mean load, and the height of the third peak with the other heights (around 0.20 for both). The widths of every peak are negatively correlated to the corresponding height (around -0.25 to -0.3). In other words, tall peaks tend to be thinner, which would correspond to the crowd being more able to follow the target jumping frequency. No other noteworthy correlations occur in this approach.

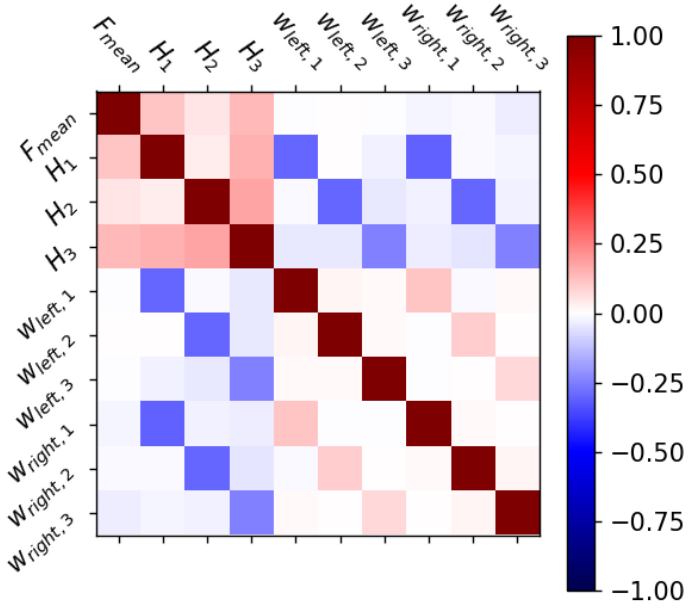

Figure B.10: Correlation matrix for the 10 parameters of the Amplitude approach with 3 peaks. The first letter in the labels represents the left or right side of the peaks

In the Complex approach, a strong negative correlation appears between the left and right peak values in both the real and imaginary parts (-0.62 and -0.66 respectively). A large positive peak on one side of f_{peak} tends to correspond to a large negative peak on the other side. Other positive and negative correlations appear between the peak heights appear as well, but it is unclear whether these are caused by these 'jumps' in sign or whether the absolute value of the peaks are also correlated. These two plots also clearly show the large difference in the number of variables between the Amplitude and Complex approaches.

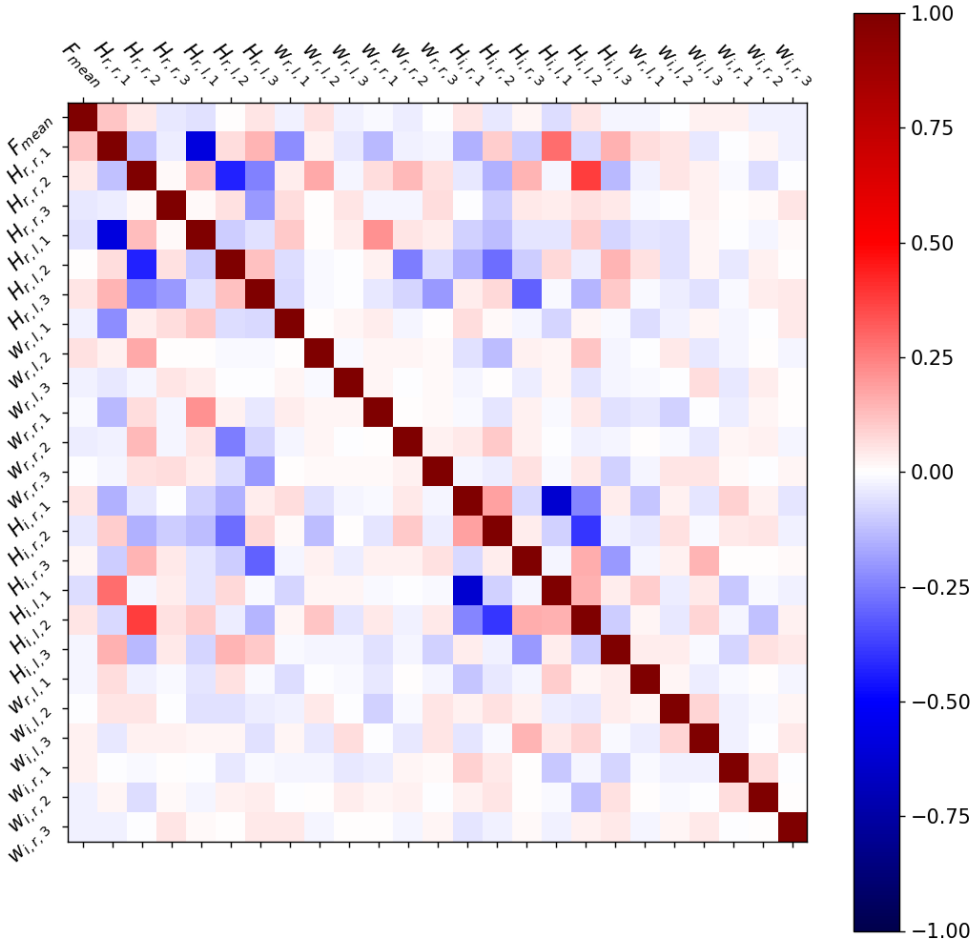

Figure B.11: Correlation matrix for the 25 parameters of the Amplitude approach with 3 peaks. The first letter in the labels represents the real or imaginary part, the second letter the left or right side of a peak

B.2.3. Decision

For the first two criteria, a low number of variables and the ability to fit a distribution to them, the Amplitude approach clearly wins out against the Complex approach. The third and fourth criterion do not really make a difference between the two, but they do disqualify the Direct approach. In terms of capturing the shape and variance of the true spectra, the Complex approach is better, though still far from perfect. For capturing the variance in the response, there is not much difference between the two. Overall, the Direct approach is not usable, and there is no clear winner between the Amplitude and Complex approach at first glance. However, the Amplitude approach being easier to set-up makes performing a reliability analysis easier, too. So, the final choice lands on the Amplitude approach.